

Homologous Recombination Within a Chromatin Environment

DISSERTATION DER FAKULTÄT FÜR BIOLOGIE
DER LUDWIG-MAXIMILIANS-UNIVERSITÄT MÜNCHEN



vorgelegt von

Claudio Amadeo Lademann, M.Sc. ETH Biologie

Juli 2016

EIDESSTATTLICHE ERKLÄRUNG

Hiermit erkläre ich an Eides statt, dass ich die vorliegende Dissertation selbstständig und ohne unerlaubte Hilfe angefertigt habe. Ich habe weder anderweitig versucht, eine Dissertation einzureichen oder eine Doktorprüfung durchzuführen, noch habe ich diese Dissertation oder Teile derselben einer anderen Prüfungskommission vorgelegt.

München, 24. 11. 2016

Claudio Lademann

Promotionsgesuch eingereicht am: 28.07.2016

Datum der mündlichen Prüfung: 16.11.2016

Erster Gutachter: Prof. Dr. Stefan Jentsch

Zweiter Gutachter: Prof. Dr. Peter Becker

Die vorliegende Arbeit wurde zwischen August 2011 und Juli 2016 unter der Anleitung von Prof. Dr. Stefan Jentsch am Max-Planck-Institut für Biochemie in Martinsried durchgeführt.

Teile dieser Arbeit sind in den folgenden Publikationen veröffentlicht:

Renkawitz J*, **Lademann CA***, Jentsch S. Mechanisms and principles of homology search during recombination. *Nat Rev Mol Cell Biol.* 2014 Jun;15(6):369-83.

*: equal contribution

Renkawitz J, **Lademann CA**, Jentsch S. γ H2AX spreading linked to homology search. *Cell Cycle.* 2013 Aug 15;12(16):2526-7.

Renkawitz J, **Lademann CA**, Kalocsay M, Jentsch S. Monitoring homology search during DNA double-strand break repair in vivo. *Mol Cell.* 2013 Apr 25;50(2):261-72.

Summary

DNA repair is essential for life. It secures the correct inheritance of genetic information and prevents premature aging and cancer development. The only high-fidelity pathway that deals with the most toxic of all DNA lesions – double-strand breaks – is homologous recombination. Herein, the usage of an undamaged homologous donor as a template for repair allows the accurate restoration of the genetic information. Compared to the local processing of other DNA lesions, this sophisticated mechanism yet comes at the cost of wide-ranging DNA transactions. Consequently, it involves not only a plethora of nucleases and other DNA repair proteins, but also requires a variety of factors that allow them to access the DNA within a chromatin environment. Despite significant progress regarding our knowledge on the involvement of chromatin remodeling during homologous recombination in the recent years, mechanistic insights into discrete functions of related players remain rare.

In this study, I aimed to identify novel requirements for chromatin remodeling during homologous recombination. Particularly, I was interested into the question whether homology search conducted by the Rad51 nucleoprotein filament is accompanied by chromatin changes while probing vast amounts of heterologous DNA. Combining a defined system of site-specific double-strand breaks in the yeast *S. cerevisiae* together with distinct localization analysis of DNA repair and chromatin factors by ChIP, I found novel functions of well-known members of the Snf2/Swi2 family of chromatin remodeling enzymes during homologous recombination. I identified the Rad54 family proteins Rad54 and Rdh54 as the first factors that assist the Rad51 recombinase directly in the homology search process. While the mechanism underlying this function remains to be elucidated, both proteins help to indirectly promote a phosphorylation-dependent large-scale remodeling of histones H2A and H2B at sites of homology search. Investigation of canonical nucleosome remodeling machineries then uncovered an unexpected and intriguing function of the INO80 complex as the first chromatin remodeler directly assisting Rad51 loading onto ssDNA. This is achieved by removal of histone H2A.Z, and it is this histone variant, rather than the canonical nucleosome per se, which accumulates at double-strand breaks and specifically interferes with Rad51 filament formation in the absence of INO80. Removal of H2A.Z consequently rescues Rad51 loading as well as homologous recombination in INO80 deficient cells.

The results presented in this study implicate novel requirements and stages for chromatin remodeling during homologous recombination and add further possible layers of regulation to this pivotal and widely conserved DNA repair pathway.

Outline

1	INTRODUCTION.....	1
1.1	The impact of DNA damage.....	1
1.2	DNA double-strand breaks and their repair.....	3
1.2.1	Causes and consequences of DSBs.....	3
1.2.2	DSB repair by non-homologous end joining.....	3
1.2.3	DSB repair by homologous recombination.....	5
1.2.3.1	Regulation of Rad51 filaments.....	7
1.2.3.2	Homology search.....	9
1.3	Chromatin and its role in DSB repair.....	12
1.3.1	Chromatin structure and function.....	12
1.3.2	Histone variants and histone modifications.....	13
1.3.3	ATP-dependent chromatin remodelers and histone chaperones.....	16
2	AIMS OF THE STUDY.....	20
3	RESULTS.....	21
3.1	Homology search requires Rad54 and Rdh54 proteins and induces large-scale remodeling of histones H2A and H2B.....	21
3.1.1	An assay to monitor site-specific recombination in real-time.....	21
3.1.2	Recombination efficiency correlates with homology search signals and is determined by the nuclear architecture.....	23
3.1.3	Rad54 and Rdh54 are important regulators of the homology search process.....	25
3.1.4	Sites of homology search display changes in chromatin structure.....	29
3.1.5	Rad54 and Rdh54 indirectly influence the remodeling of histones H2A and H2B at sites of homology search.....	33
3.1.6	Homology search does not require phosphorylation-induced remodeling of histones H2A and H2B.....	36
3.2	INO80 promotes Rad51 filament formation and recombination by removal of the histone variant H2A.Z.....	38
3.2.1	The INO80 chromatin remodeler is required for Rad51 filament formation.....	38
3.2.2	Defective Rad51 recruitment in INO80-deficient cells is independent of DNA end resection or recombination mediators.....	40
3.2.3	INO80 regulates H2A.Z at a DSB.....	43

3.2.4	Removal of H2A.Z rescues Rad51 filament formation and recombination in the absence of a functional INO80 complex.....	45
3.2.5	H2A.Z is required for centromere-linked recombination.....	49
4	DISCUSSION.....	51
4.1	Homologous recombination in a three-dimensional and chromatinized environment.....	51
4.2	Rad54 and Rdh54 function during homology search.....	53
4.3	Chromatin remodeling at sites of homology search.....	56
4.4	The histone variant H2A.Z inhibits Rad51 filament formation.....	58
4.5	An INO80-H2A.Z axis regulating recombination activity.....	62
5	MATERIALS AND METHODS.....	65
5.1	Microbiology.....	65
5.1.1	<i>Escherichia coli</i> (<i>E. coli</i>) techniques.....	65
5.1.2	<i>Saccharomyces cerevisiae</i> (<i>S. cerevisiae</i>) techniques.....	66
5.2	Molecular biology techniques.....	74
5.2.1	DNA isolation, purification and sequencing.....	74
5.2.2	DNA amplification by polymerase chain reaction (PCR).....	75
5.2.3	Molecular cloning.....	78
5.3	Biochemical and cell biological techniques.....	80
5.3.1	Protein techniques.....	80
5.3.2	Chromatin techniques.....	83
5.4	Bioinformatics.....	87
5.4.1	ChIP-chip analysis.....	87
5.4.2	ChIP-seq analysis.....	87
5.4.3	Statistical analysis.....	88
5.4.4	Online resources and computer programs.....	88
6	REFERENCES.....	90
7	ABBREVIATIONS.....	103
8	ACKNOWLEDGEMENT.....	105
9	CURRICULUM VITAE.....	106

1 INTRODUCTION

1.1 The impact of DNA damage

“We totally missed the possible role of ... [DNA] repair although ... I later came to realise that DNA is so precious that probably many distinct repair mechanisms would exist.”

Francis Crick, writing in Nature, 1974¹

DNA is the central unit of life. It carries the genetic information and with it the construction plan for generating proteins, cellular structures and eventually whole organisms. Faithful duplication of a genome during DNA replication allows the transmission of this vital information to daughter cells, and enables the inheritance of genetic trademarks over generations.

Reflecting its essential function, DNA was thought to be an inherently stable entity and it came as a surprise that this is in fact not the case. The macromolecule not only faces a considerable intrinsic instability due to spontaneous hydrolysis, but is also under constant attack of reactive physical and chemical agents from outside and inside the cell²⁻⁴ (Figure 1 A). Altogether, this adds up to a total of 100 000 changes per day at the level of a human genome, and this number can double upon prolonged exposure to sunlight. Although mutagenesis drives evolution, high doses of DNA damage threaten genomic integrity, contribute to premature aging and in vertebrates also to the development of cancer² (Figure 1 B). Thus, it goes without saying that DNA damage repair mechanisms must exist to counteract this problem. Over the past 50 years, a variety of sophisticated pathways have been identified to deal with an even greater variety of DNA lesions⁵. Base damages, such as oxidation, alkylation or deamination, intra- and interstrand crosslinks, DNA-protein crosslinks as well as different kinds of DNA strand breaks are just some examples in this regard. Reflecting the central role of DNA over all kingdoms of life, it is a logical consequence that many of the corresponding repair pathways, such as base-excision repair, mismatch repair, nucleotide-excision repair and homologous recombination are highly conserved from bacteria to humans⁶⁻⁹.

Integrating these activities into a sophisticated signaling cascade collectively referred to as the DNA damage response (DDR) ensures the proper coordination of DNA repair with ongoing cellular physiology and eventually protects cells from death, and organisms from the development of diseases¹⁰.

INTRODUCTION

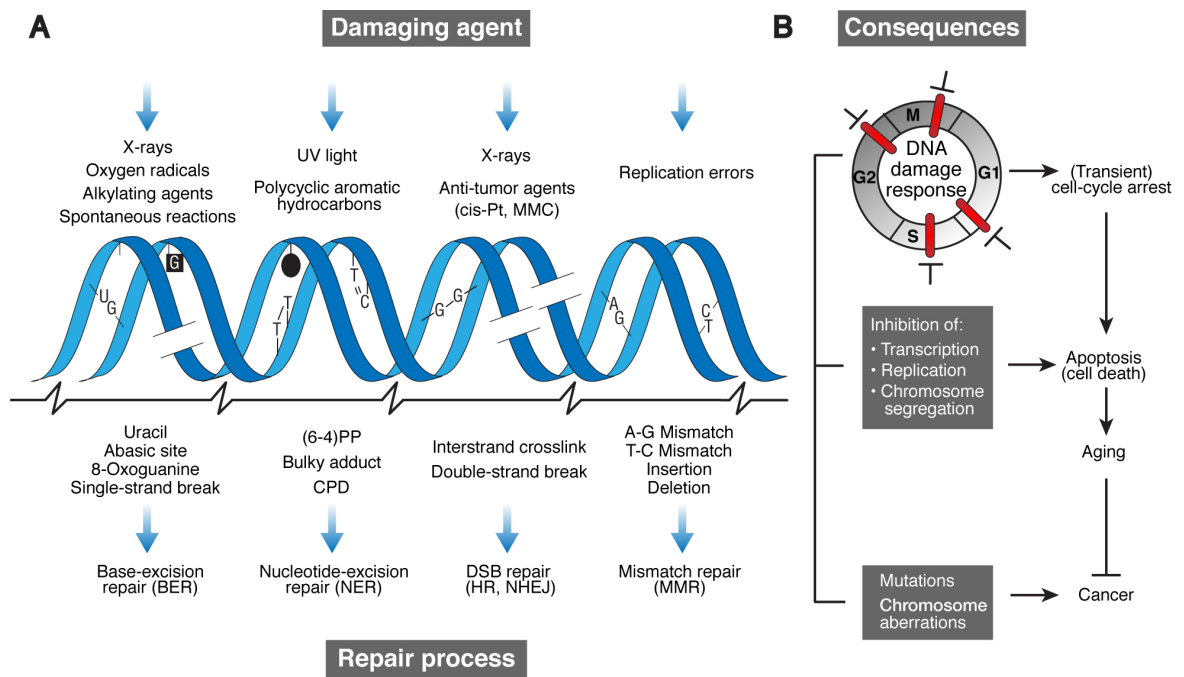


Figure 1 | DNA damage, repair and consequences

(A) A variety of endogenous and exogenous stimuli as well as spontaneous reactions trigger DNA damage. Common alterations comprise base modifications, such as guanine oxidation (generating 8-Oxoguanine) or cytosine deamination (generating uracil), bulky adducts, such as UV-light induced cyclobutane pyrimidine dimers (CPD) and DNA strand breaks (single- and double-strand breaks). Different kinds of lesions are repaired by specialized pathways, which are highly conserved throughout evolution. **(B)** DNA damage activates a signaling cascade known as the DNA damage response that couples cell cycle progression to damage repair. The long-term consequences of DNA damage are essentially twofold. Constant interference with essential processes such as transcription or replication triggers cell death and eventually contributes to aging. Surviving cells are subject to permanent genetic changes, such as point mutations and chromosomal aberrations, which support the development of cancer. Adapted from reference 11.

1.2 DNA double-strand breaks and their repair

1.2.1 Causes and consequences of DSBs

A single nick in the phosphodiester backbone of one DNA strand is referred to as a single-strand break (SSB). SSBs can be caused by exogenous or endogenous sources, such as ionizing radiation or reactive oxygen and nitrogen species, respectively. In addition, they are induced as reaction intermediates by topoisomerases and also during the repair of base damages as well as DNA interstrand crosslinks¹². When two closely spaced SSBs are formed in complementary DNA strands, or when a replication fork encounters a nicked template, a double-strand break (DSB) is generated^{13,14}. Overall, about 1 % of the SSBs in a cell are converted to DSBs, resulting in a number of one DSB per 100 000 kb per cell cycle^{12,13}. Despite their comparably rare occurrence, DSBs are particularly harmful lesions and already a single persisting DSB blocks DNA replication and triggers a constant cell cycle arrest^{15,16}. Not surprisingly, it is also the toxicity of these lesions that is exploited during cancer therapy by radio- or chemotherapeutic agents¹⁷.

Importantly, DSBs are not only accidentally occurring lesions that bring harm to the cell, but are intentionally generated by various organisms to allow genetic rearrangements in essential cellular programs. The most fundamental of these processes is the case of meiosis, where DSBs induced by the enzyme Spo11 trigger genetic exchange in sexually reproducing organisms¹⁸. In yeast cells, the homothallic switching (HO) endonuclease induces a single DSB that allows a mating-type switch to initiate sexual reproduction¹⁹ and enzymatic DSB generation in vertebrates triggers the diversification of the antibody portfolio in B-lymphocytes²⁰.

It is their strong cytotoxic potential on the one hand and their nature as the origin of genetic variation on the other hand that led to the evolution of a unique toolbox of repair pathways that can deal with a broad spectrum of DSBs (Figure 2 and Figure 3). In the following, I will further outline the mechanistic bases of these pathways. As all of them are well conserved among eukaryotes, information will be generally given for yeast proteins. Mammalian proteins will be indicated separately only if not direct homologs.

1.2.2 DSB repair by non-homologous end joining

During non-homologous end joining (NHEJ), the broken ends of a DSB are re-joined by the activity of DNA ligases (Figure 2 A). The pathway is principally applicable in every organism and works independent of the cell cycle status^{21,22}. NHEJ plays a very prominent

INTRODUCTION

role in mammals, while it is less important in yeast cells. This is at least in part due to the fast cell cycle of yeasts, which spend only little time in G1 and can often use a different pathway for repair (see section 1.2.3). The major advantage of NHEJ is its strong flexibility that allows to seal almost any kind of DSB with two available broken ends²¹. Initially, the trimeric Mre11-Rad50-Xrs2 (MRX) complex and the ring-shaped Ku70/Ku80 heterodimer (Ku complex) recognize and sense the lesion^{23-27, *}. Members of both complexes then position DNA ligase IV and its cofactor Lif1 (XRCC4 in mammals) at the break, followed by the critical alignment of the free DNA ends to initiate ligation²⁸⁻³⁰. Recent data from vertebrate cell extracts suggest that this alignment is a two-step process, with initial long-range tethering by Ku70/80 followed by detailed alignment via DNA ligase IV³¹. At “dirty” ends with incompatible overhangs, ligation cannot proceed directly. Here, processing enzymes and gap-filling polymerases such as Fen1 (ARTEMIS in mammals) and Pol4 (Pol μ and Pol λ in mammals) are recruited, respectively to catalyze necessary end modifications³²⁻³⁴. Although ligation often results in accurate repair, it is exactly the flexibility to modify the free ends that makes NHEJ intrinsically error-prone for small insertions and deletions²¹.

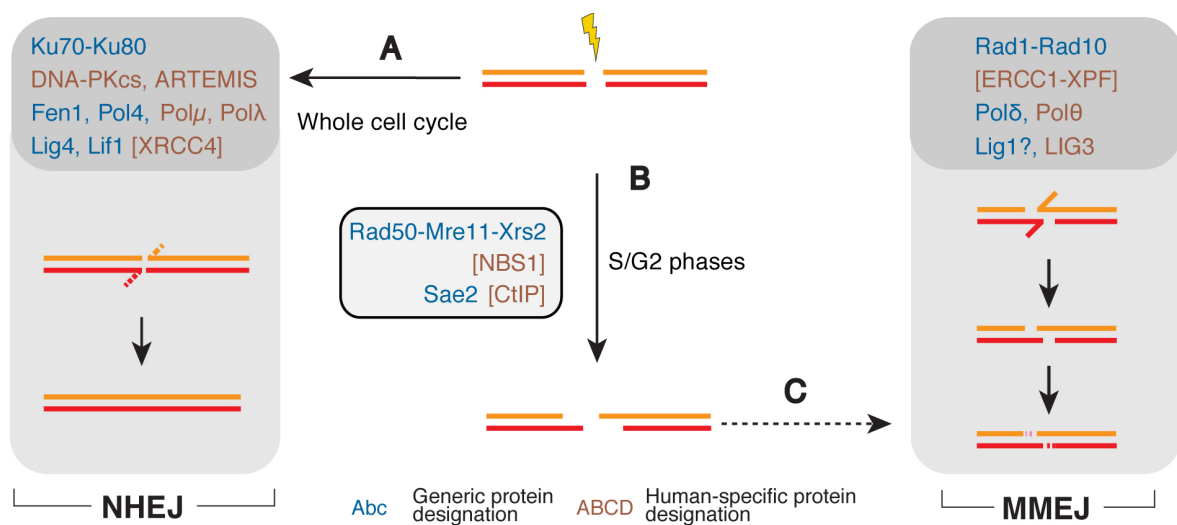


Figure 2 | Double strand-break repair by ligation-based mechanisms

(A) Non-homologous end joining (NHEJ) is a major DSB repair pathway. DSBs are bound by the Ku70/Ku80 proteins (including DNA-PKcs in mammals). Together with DNA Ligase IV (Lig4) and its cofactor Lif1/XRCC4, the broken ends are positioned for ligation. Potential incompatible overhangs are clipped off by nucleases such as Fen1/ARTEMIS and gaps filled in by DNA polymerases IV/ μ prior to ligation. **(B)** In S/G2 phases of the cell cycle, Ku70/80 binding is counteracted by DNA end resection enzymes. Revelation of microhomologies allows their alignment for end positioning. Overhangs are clipped off by Rad1-Rad10/ERCC1-XPF nucleases and gaps filled in by DNA polymerases δ/θ . Ligation via Lig1/LIG3 eventually results in mutagenic repair, making microhomology-mediated end joining (MMEJ) an unfavored backup pathway for DSB repair (indicated by dashed arrow).

* In mammalian cells, the MRN complex (homologous to MRX) is dispensable for NHEJ and instead Ku70/80 binds the DNA-PKcs protein kinase to form the DNA-PK holoenzyme.

In addition to this classical NHEJ, breaks can also be re-ligated in a process called microhomology-mediated end joining (MMEJ)³⁵ (Figure 2 B). In contrast to NHEJ, MMEJ requires initial degradation (resection) of the 5' end at each side of the DSB. This process is driven by the nuclease activity of Mre11 in conjunction with the Sae2 protein³⁶ and allows the revelation of microhomologies at the different sides of the break. As little as 6 nt (in mammals even only 1 nt) are then enough to align the broken ends and initiate repair. Heterologous 3' flaps are subsequently removed by the Rad1-Rad10 (XPF-ERCC1 in mammals) nuclease, the gaps filled in by the replicative polymerase δ (Pol θ in mammals)^{37,38} and ligation likely performed by DNA ligase I (DNA ligase III in mammals)³⁵. Due to the substantial deletions that MMEJ can introduce, it is generally considered as a backup pathway when the two major repair pathways, namely NHEJ and homologous recombination, cannot be applied.

1.2.3 DSB repair by homologous recombination

Homologous recombination (HR) uses an undamaged homologous DNA sequence as a donor template for repair^{9,39} (Figure 3). Because this donor sequence is usually the exact copy of the broken DNA strand generated during DNA replication, information that got lost during DSB generation is faithfully restored via this pathway. Thus, there are two main principles that discriminate DSB repair by HR from repair by classical NHEJ. First, HR is a generally error-free process. Second, its applicability is in principle limited to the S and G2 phases of the cell cycle, when a desired donor template is available. The ability of accurate repair makes HR an important pathway in all living organisms and underlying defects result in strong sensitivities to DSBs and account for the vast number of heritable breast and ovarian cancer in humans⁴⁰.

The decision to commence HR is largely coupled to the initiative end resection step of the pathway. Due to the CDK-regulated activity of Sae2, this process can only be triggered in the desired cell-cycle phases⁴¹. Following the Mre11/Sae2-mediated short-range degradation of the first few hundred base pairs, a different set of enzymes further extends ssDNA generation. This long-range resection is either driven by the exonuclease Exo1, or the helicase-containing Sgs1-Top3-Rmi1 complex (STR; BLM-TOPO3 α -RMI1-RMI2 in mammals) in conjunction with the endonuclease Dna2^{42,43}. Exposure of ssDNA leads to the immediate recruitment of the heterotrimeric, high-affinity ssDNA binding protein RPA that removes secondary structures and also acts to inhibit illegitimate MMEJ⁴⁴. Recombination mediators (see section 1.2.3.1) subsequently drive the exchange

INTRODUCTION

of RPA for the recombinase Rad51. This generates a highly coordinated right-handed nucleoprotein filament, commonly known as the presynaptic filament, which is the central entity of the HR pathway^{45,46}. This functional unit then undergoes the search for a homologous template and eventually invades the donor, thereby forming the characteristic microscopic D-loop structure with one displaced donor strand^{39,47}. The Rad54 protein stabilizes the D-loop and initiates removal of Rad51 from the heteroduplex to allow subsequent priming of DNA synthesis from the invading strand by DNA polymerase δ ⁴⁸. At this stage, the extended D-loop marks the branching point for a number of HR sub-pathways, of which one will be chosen depending on the cellular context³⁹. In mitotic cells, seamless repair is guaranteed by synthesis-dependent strand annealing (SDSA) (Figure 3 B). Following D-loop extension, the heteroduplex DNA is reversed to allow annealing of the newly synthesized strand with the resected strand of the second DSB end. In contrast, the utilization of the Dmc1 recombinase in meiotic cells favors capturing of the second DSB end inside the D-loop. This results in the formation of a double Holliday junction (dHJ), representing the classical DSB repair model (DSBR) (Figure 3 C). Endonucleases such as Mus81-Mms4, Yen1 or Slx1-Slx4 are capable to trigger genetic exchange by resolving such structures in a crossover or non-crossover fashion⁴⁹. Despite the fact that dHJs can form in mitotic cells at low frequency, crossover formation here is strongly suppressed by their dissolution via the STR complex⁵⁰. Finally, a third variation of HR is able to deal with one-ended DSB, which among others form at replication forks, particularly when no second fork directly approaches from the opposite direction⁵¹. In this case, the free end in the D-loop will be replicated in a mutagenesis-prone, conservative mode known as break-induced replication (BIR) that involves the DNA helicase Pif1⁵² (Figure 3 D).

In addition to the Rad51-mediated recombination pathways, DSBs can also be repaired in a Rad51-independent, but homology-directed manner³⁹. This single-strand annealing (SSA) is somewhat reminiscent of the MMEJ pathway. However it involves re-annealing of RPA-coated ssDNA between larger repeats using the strand-annealing activity of Rad52 (Figure 3 E). Similar to MMEJ, SSA results in extensive deletions by processing of the 3' flaps via Rad1-Rad10 and the mismatch repair proteins Msh2-Msh3. The requirement of SSA inside cells is unclear, though it might be useful for repairing DSBs within highly repetitive DNA.

INTRODUCTION

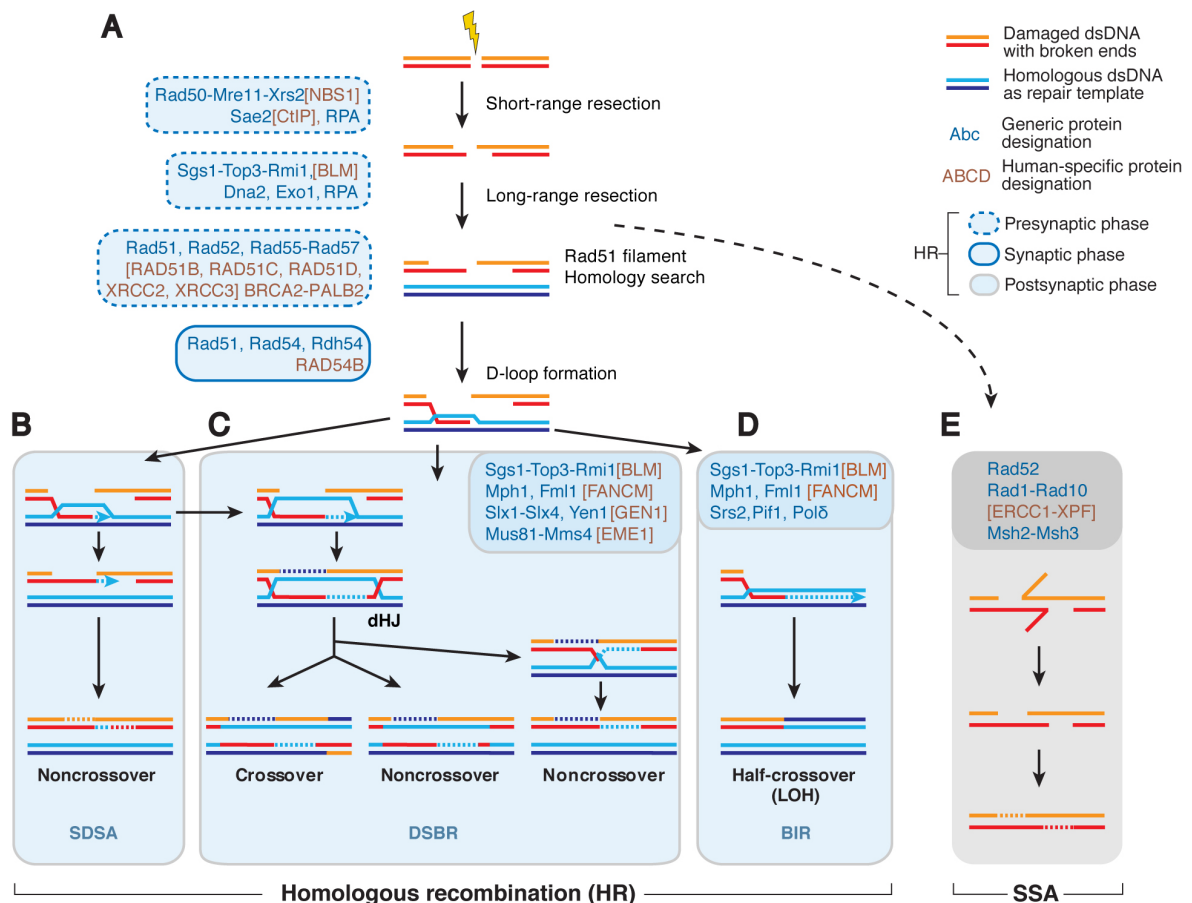


Figure 3 | Double-strand break repair by recombination-based mechanisms

(A) Homologous recombination (HR) is the preferred DSB repair pathway in S/G2 phases of the cell cycle. Here, DSBs can be subject to DNA end resection. Short-range resection initiation and long-range extension beyond a few hundred base pairs is covered by different sets of enzymes. Emerging ssDNA is covered by RPA, and mediator proteins help to replace this factor for Rad51. The Rad51 filament performs the homology search and invades the homologous donor template. The resulting D-loop is the branch point for different HR sub-pathways. **(B)** Mitotic DSBs channel into synthesis-dependent strand annealing (SDSA), where the D-loop is reverted to avoid crossovers. **(C)** Meiotic DSBs result in double Holliday junction (dHJ) formation. Nucleases cleave these structures to mediate crossover or non-crossover outcomes. **(D)** One-ended DSBs emerging at replication forks are repaired by break-induced replication (BIR), which leads to loss of heterozygosity (LOH). **(E)** Homologies on opposing sides of the break can be recombined in a Rad51-independent manner using the strand annealing activity of Rad52. Large overhangs are clipped off by the Rad1-Rad10/ERCC1-XPF nucleases. Single-strand annealing (SSA) is a highly mutagenic backup pathway of unclear relevance (indicated by dashed arrow). Adapted from reference 39.

1.2.3.1 Regulation of Rad51 filaments

The presynaptic filament is the central structure of the HR pathway with the potential to exchange DNA strands from different origins (Figure 4 A). Inappropriate DNA rearrangements can have hazardous consequences and consequently the formation of this functional unit is a tightly regulated process. The existence of tipping points at which structures are established or reversed ensures quality control, and this is achieved by a number of HR accessory proteins generally referred to as recombination mediators^{53,54} (Figure 4 B).

INTRODUCTION

The core recombination mediator, the Rad52 (BRCA2 in mammals) protein, functions to counteract the inhibitory effect of RPA on Rad51 loading onto ssDNA. Rad52 binds both RPA and Rad51, targets Rad51 to ssDNA and is essential for Rad51 recruitment to damage sites^{45,46,55-57}. The central role of Rad52 in this process is underscored by in vitro experiments, where it alone is sufficient to overcome the RPA barrier. In addition to Rad52, Rad51 filament formation is promoted by a number of Rad51 paralogs. These proteins bear readily detectable sequence similarities to Rad51 and structurally share the common RecA-like fold with it⁵⁴. Despite these similarities, Rad51 paralogs do neither form extensive nucleoprotein filaments on their own nor do they have the ability to catalyze DNA strand exchange. The best studied of these proteins are Rad55 and Rad57, which form a stable heterodimer. This complex stimulates Rad51 loading onto RPA-coated ssDNA in vitro, and assists in Rad51 recruitment to DNA damage sites in vivo⁵⁶⁻⁵⁸. In addition to the promotion of initial Rad51 loading, it was shown that Rad55-Rad57 also steadily stabilizes the presynaptic filament and thereby protects it from degradation by a negative mediator, the Srs2 helicase⁵⁹. Two other Rad51 paralogs, Csm2 and Psy3, interact with the Shu1 and Shu2 proteins and this complex synergizes with Rad55-Rad57 in both in vitro filament formation and in vivo filament stabilization⁶⁰⁻⁶². Especially in metazoans, it is less clear how Rad51 paralogs stimulate strand exchange. A recent study in *Caenorhabditis elegans* yet identified an ability of these proteins to physically remodel the Rad51 filament to a more “open” conformation that primes it for DNA strand exchange⁶³.

In contrast to the discussed positive mediators, a number of DNA helicases can disrupt Rad51 filaments and thereby act as negative mediators, as in the case of the above-mentioned Srs2[†],⁶⁴⁻⁶⁶. This activity is especially important to protect cells from illegitimate recombination at replication forks, where Srs2 is directly recruited via the SUMOylated sliding clamp PCNA⁶⁷. While Srs2 counteracts recombination initiation, Rad54 family proteins critically regulate Rad51 filaments at the synaptic stage⁶⁸. While the removal of Rad51 from heteroduplex DNA is essential to eventually complete recombination, it is suppressed during S-phase in a Rad54-phosphorylation dependent manner to avoid replication fork collapse⁶⁹. Generally, not only phosphorylation, but a number of other post-translational modifications (PTMs) are involved in the regulation of HR, including ubiquitylation and SUMOylation³⁹. While they play major roles in DSB signaling and the cell-cycle dependent initiation of DNA end resection (see also section

[†] There is no direct homolog of Srs2 in higher eukaryotes, but the human RECQ5 helicase seems to fulfill similar functions⁶⁴.

1.3.2), there are also direct contributions to presynaptic filament formation. An intriguing role in this regard plays SUMO, which fosters protein-protein interactions among a number of recombination mediators as well as RPA and this “SUMO-glue” thereby contributes to Rad51 loading at a DSB⁷⁰.

1.2.3.2 Homology search

Subsequently to its formation, the presynaptic filament undergoes the search for the homologous donor sequence⁷¹ (Figure 4 C). For this process, three different criteria have to be met: establishment of spatial proximity with the target DNA, probing this DNA for homology, and recognizing the homologous sequence.

There is much information on the probing of non-homologous DNA and recognition of homologous DNA from in vitro experiments, in which the proximity problem is negligible due to free molecular diffusion. Under such conditions, homology probing and recognition are clearly intrinsic abilities of DNA recombinase proteins and no other mediators are required⁷¹. This is due to the presence of two different DNA binding sites in these proteins that enables holding the single-stranded resected DNA in one place while stochastically probing a short stretch of target DNA with the other site^{72,73}. Because the affinity of the secondary binding site to ssDNA is yet too weak to initiate this process on its own, it in vitro relies on pre-existing ssDNA bubbles, generated by spontaneous DNA breathing or DNA supercoiling⁷⁴⁻⁷⁶. The search reaction is generally accelerated by filament sliding in a range up to 300 bp, and by intersegmental contact sampling, the probing of multiple regions at different sites of the filament^{77,78} (Figure 4 C). Contacts with target DNA are extremely short-lived and kinetically unstable unless a microhomology of at least 8 bp is encountered^{75,79}. It thereby is the physical distance between the two DNA binding sites that energetically dictates this minimal recognition motif and hence enables a confinement of the search to sites with a high probability of being indeed the homologous target. If this is the case, strand exchange is kinetically favored due to the non-uniform extension of the presynaptic filament, and immediately proceeds in steps of 3 nt^{79,80}.

In contrast to the in vitro situation, only little is known about the principles how presynaptic filament and homologous DNA gain initial proximity in the context of whole chromosomes and the nuclear environment. It was long thought that homology search in yeast proceeds genome-wide with equal efficiency⁸¹⁻⁸⁵, in contrast to mammalian cells, where recombination between non-homologous chromosomes is generally poor⁸⁶. Suggested reasons for this discrepancy were the less well-defined chromosomal

INTRODUCTION

architecture in yeast, with chromosomal territories showing quite robust intermingling⁸⁷, and the smaller nuclear size in general. Nevertheless, yeast does possess a number of nuclear landmarks, of which three are enough to predict the overall nuclear architecture^{88,89}: first, the nucleolus, a crescent-shaped structure close to the nuclear periphery, second, telomeres, which are tethered to the nuclear envelope, third, centromeres, which are tethered to the spindle pole body and occupy a position opposite to the nucleolus. Using centromere clustering as an example, our recent work identified that also in yeast homology search is generally the more efficient, the smaller the predicted spatial distance of the target DNA to the DSB is⁴⁷ (Figure 4 C). Although the proof that this applies for the total efficiency of HR as well remains to be made, this finding suggests important conclusions for the process of recombination⁷¹. First, the guidance of homology search by the nuclear architecture automatically shifts the bias to the choice of the preferred donor template, due to the naturally close proximity mediated by sister-chromatid cohesion and alignment of homologous chromosomes⁹⁰⁻⁹². Second, it still allows the exploration of a reasonable nuclear area to eventually complete recombination in cases a *bona fide* donor cannot be found immediately. Indeed, such non-allelic or ectopic HR events can occur naturally between repetitive elements dispersed throughout the chromosomes, and contribute to genome evolution^{93,94}.

It is interesting that these principles apply in a context where the mobility of DNA at DSBs is massively changed compared to a non-broken state, and with it likely the nuclear architecture as well⁹⁵⁻⁹⁹. At least in the large nuclei of mammalian cells, these long-range movements seem to directly contribute to NHEJ between distant DSBs¹⁰⁰. In contrast, there has been much debate and confusion about whether this accounts for repair by HR and thus the homology search as well¹⁰¹. The reliance on core recombination factors such as Rad51 and Rad54, as well as DDR kinases suggested an initial role in DNA repair⁹⁶. Nevertheless, this model has recently been challenged by showing that the critical kinase target that promotes mobility in yeast is the kinetochore protein Cep3¹⁰². Ablation of its phosphorylation-site specifically decreased DSB mobility, but not HR efficiency. Instead, phospho-Cep3-induced centromere detachment from the spindle pole body enforces the DDR-induced cell cycle arrest by triggering the spindle assembly checkpoint.

Overall, the nature of a successful *in vivo* homology search, whether it is a rather passive process or requires accessory factors supporting the Rad51 filament, remains to be elucidated. This does not only hold true with regards to the global nuclear architecture, but especially also when looking at the local DNA packaging into chromatin.

INTRODUCTION

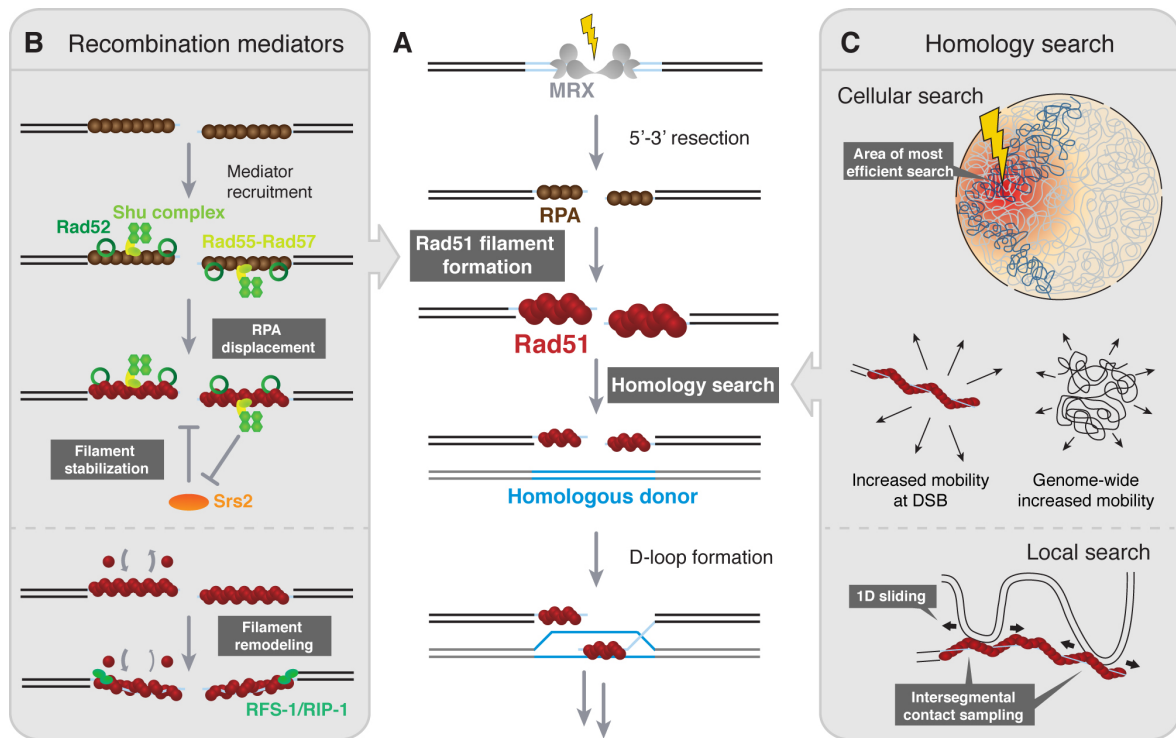


Figure 4 | Rad51 filament formation and homology search

(A) The central entity of the HR pathway is the Rad51 filament. It is able to identify the homologous donor sequence during the homology search and to prime the repair process. **(B)** Formation of the Rad51 filament is highly regulated. Binding of replication protein A (RPA) to ssDNA protects DSB ends, e.g. against realignments driving error-prone MMEJ. Recombination mediator proteins overcome the RPA barrier by interacting with both RPA and Rad51 and coordinately exchange both proteins for each other. Most important in this regard is Rad52 (BRCA2 in mammals). Rad55-Rad57 and the heterotetrameric Shu complex additionally stabilize the filament against anti-recombination mediators, such as Srs2. Metazoan mediators such as RFS-1/RIP-1 remodel the filament for proper strand exchange capacity. **(C)** Homology search is a two-step process. Rad51 filament and target DNA have to gain initial spatial proximity. The efficiency of this cellular homology search correlates with the 3D physical distance between DSB and target DNA. DSB-induced chromatin mobility might actively contribute to this process as well. Once in close contact, local homology search involves accelerating mechanisms such as filament sliding and intersegmental contact sampling. It is unclear, which proteins other than Rad51 directly contribute to the homology search process. Part (C) adapted from reference 71.

1.3 Chromatin and its role in DSB repair

1.3.1 Chromatin structure and function

In *E. coli*, the length of DNA exceeds the one of the cell about 10 fold. For a human cell however, this ratio is about 20 000 times larger. The packing of the genetic information within the confines of a small nucleus consequently constitutes a major challenge, which is further complicated by the strong electrostatic repulsion between the negatively charged phosphates of the DNA backbone. Thus, with the cellular compartmentalization and ever increasing complexity of their genomes, eukaryotic organisms inevitably had to co-evolve sophisticated packaging mechanisms to squeeze the DNA inside their nuclei[‡]. The solution comes with the generation of chromatin, in which highly conserved, basic histone proteins bind the DNA and neutralize the negative charges¹⁰⁴. While the impact of this chromatinization culminates during cell division in light-microscopically visible structures known as chromosomes, it all builds on simple bricks – the nucleosomes¹⁰⁵.

In a nucleosome, 147 bp of DNA make 1.65 superhelical turns to wrap around an octameric histone assembly comprising each two molecules of H2A, H2B, H3 and H4¹⁰⁶. The obligate heterodimerization of H2A with H2B and H3 with H4 thereby directs the nucleosome assembly. The central ~80 bp of DNA are bound by a more stable (H3-H4)₂ tetramer, to which two H2A-H2B dimers dock at each two contact points, organizing the peripheral base pairs on every side¹⁰⁷. Interactions between the whole histone octamer and DNA are importantly not DNA base-specific, although sequences that facilitate DNA bending are preferential binding sites¹⁰⁴. Just like beads on a string, individual nucleosomes are separated by an organism-dependent variable length of linker DNA between 10-80 bp and together with linker histones[§] and non-histone proteins, this repeating unit self-organizes into higher-order structures of increasing complexity¹⁰⁹.

The inherent stability of the chromatin structure can cause problems in cases where other proteins require access to the DNA, such as during gene transcription, DNA replication and DNA repair. Already 25 years ago, this has led to the proposal of the famous “access-repair-restore” model¹¹⁰. Herein, initial opening of the chromatin is critical to allow lesion processing by the dedicated repair enzymes, followed by careful restoration of the structure after completion of repair. On top of being a pure obstacle, chromatin further fulfills a number of additional regulatory and signaling functions in DNA repair^{111,112}. It thereby is the combination of a few basic principles that integrate and

[‡] Rudimentary chromatinization is present in some Archea, likely for regulatory and not packaging reasons¹⁰³.

[§] In yeast, linker histone H1 seems not required for higher-order folding per se¹⁰⁸.

coordinate chromatin changes and signaling not only in response to DNA damage: first, histone variant proteins and histone modifications, which intrinsically alter the properties of chromatin and second, ATP-dependent-chromatin remodeling enzymes and histone chaperones, modifying the chromatin structure by re-organizing nucleosomes from the outside.

1.3.2 Histone variants and histone modifications

In addition to the four canonical histone proteins, cells have evolved a range of histone variants. Unlike archetypical histones, their expression is independent of the cell-cycle stage, which allows local and on-demand integration into nucleosomes in a replication-independent manner. Most of these proteins have been described as replacements for H2A and H3, opposed by a limited number of vertebrate-specific H2B variants and a largely invariant H4 core histone¹¹³. In higher eukaryotes, processes such as spermatogenesis or neuronal homeostasis are regulated by the tissue-specific expression of specialized variant histones. In contrast to that, other variants are well conserved among eukarya, reflecting their important roles in very basic cellular processes. Among the best examples are the centromere-specific H3 variant CenH3, which coordinates kinetochore assembly from yeast to humans, or the H2A variant H2A.Z, which plays major roles in transcription, chromosome segregation as well as during DNA repair¹¹⁴.

The specific functionality of H2A.Z is best exemplified by the fact that e.g. the *S. cerevisiae* H2A.Z shows higher conservation between species than to its canonical counterpart itself¹¹⁵. Hence, H2A.Z evolved early in evolution and fulfills roles that cannot be taken over by canonical H2A. This is reflected by the embryonic lethality of H2A.Z knockout mice and the strong sensitization of yeast cells lacking this specific variant to a number of cellular stresses^{116,117}. H2A.Z shares about 60 % amino acid identity with H2A, displaying important differences in the C-terminus that contains an alternative docking domain and an extended specific acidic patch¹¹⁸. These differences not only allow H2A.Zs incorporation into the chromatin by interaction with the Swc2 subunit of the chromatin remodeler SWR1¹¹⁹ (see section 1.3.3), but also enable specific protein-protein interactions^{120,121}. The crystal structure of a H2A.Z containing nucleosome does not differ much from the canonical nucleosome, but suggests a subtle destabilization of interactions between the H2A.Z-H2B dimers and the (H3-H4)₂ tetramer¹²². Hence, incorporation of H2A.Z is generally correlated with a more open chromatin structure and this might also explain its cellular functions. Importantly, the distribution of the 10 % of nucleosomes

INTRODUCTION

containing H2A.Z throughout the genome is not random¹²³. Its incorporation mainly at RNAPII promoters flanking the nucleosome free region at transcriptional start sites is suggested to promote transcriptional activation, especially at promoters of inducible genes¹¹⁸. Following DNA damage, H2A.Z is transiently incorporated next to DSBs and regulates DNA repair outcome as well as the DDR¹²⁴⁻¹²⁶. Interestingly, there is evidence for both a contribution of the histone variant to DNA end resection, as well as to the recruitment of the Ku complex^{125,127,128}. Because repair by HR and NHEJ is accordingly down-regulated in absence of H2A.Z, cells up-regulate mutagenic MMEJ as a compensation pathway under these conditions¹²⁴. Thus, H2A.Z incorporation seems to establish a relaxed chromatin structure that is generally primed for canonical DSB repair, upstream of the decision which pathway to take¹²⁴. In addition to directly contributing to DNA repair, H2A.Z together with SWR1 mediates a change in the subcellular localization of DSBs^{125,129}. Generally, this event seems to suppress unwanted recombination events and if it is abolished, increased recombination levels have been observed^{129,130}. At the bottom line, it is likely the combination of its roles in both promoting and balancing DNA repair capacity that leads to the strong sensitivity of cells lacking H2A.Z when challenged with DNA damaging agents or replication stress.

A second H2A variant with major implications in DSB repair is H2AX. This version differs from the core histone in a C-terminal extension bearing the conserved amino acid sequence SQ(E/D) ϕ (with ϕ denoting a hydrophobic residue)¹³¹. Notably, there seems to be a potential link between the prevalence of H2AX and the efficiency of HR in different organisms. Both in *C. elegans* and humans, in which this variant is absent or present in only 10 % of all nucleosomes, respectively, HR activity is rather poor. Conversely, in yeast cells the *bona fide* presence of the SQ(E/D) ϕ motif in the canonical H2A (which is thus H2AX-like) goes along with an extraordinarily high HR activity¹¹⁵. Interestingly, in *D. melanogaster*, the H2AX C-terminal tail is linked to an H2A.Z globular domain. This so called H2A.V constitutes the only H2A variant in this organism and as for both variants in other clades, one of its major functions is the proper sensing of DNA damage¹³².

The central role of H2AX in DNA repair is thereby not mediated by intrinsic properties of the histone variant itself, but rather by the DNA damage-induced serine phosphorylation of the SQ(E/D) ϕ motif. This event is catalyzed by the upstream DDR kinases of the phosphatidylinositol-3-OH-kinase-like family of protein kinases (PIKKs). All three of them are involved in this phosphorylation event, dependent on their recruitment to the DSB: Mec1 (ATR in mammals) via ssDNA, Tel1 (ATM in mammals) via the MRX complex, and the metazoan specific DNA-PKcs, via the Ku complex¹³³ (Figure 5 A and B).

INTRODUCTION

The resulting γ H2AX is generally known to be the earliest of all chromatin modifications^{**}, which arises within seconds to minutes after DSB generation and spreads up to hundreds of kilobases in yeast and even megabases in mammals away from a single DSB^{47,135}. Interestingly, our recent work showed that a reason for the large-scale distribution of γ H2AX is its direct linkage to the homology search process, with the inducer kinases possibly hitchhiking the presynaptic filament¹³⁶. Yet, the needs for such a large-scale chromatin modification as well as its full consequences are still partially unclear. In mammals, the main γ H2AX adaptor is the BRCT domain containing protein MDC1, which among others fosters MRN binding to DSBs and also recruits the ubiquitin ligase RNF8 – proteins required locally at the repair site^{137,138}. In accordance, H2AX knockout mice display repair defects, which also result in reduced immunoglobulin isotypes and increased cancer susceptibility¹³⁹. Yeast cells instead do not show severe growth defects in absence of γ H2AX, but the corresponding strains display reduced levels of NHEJ rather than HR¹⁴⁰. While this seems to be at odds with the above-mentioned hypothesis that the presence of H2AX correlates with the efficiency of recombination, γ H2AX also contributes to a DSB-induced recruitment of the cohesin complex^{141,142}. The reinforced alignment of homologous sequences thereby might facilitate the usage of the correct homologous donor during post-replicative DSB repair, which is one of the best examples of why the chromatin would need to be modified over such large domains. Yeast lacks general γ H2AX adaptors such as MDC1, and recent results challenge the early findings that the phosphorylation is directly recognized by chromatin modifiers such as the NuA4 complex^{143,144}. In further contrast to the situation in mammalian cells, γ H2AX in yeast is largely not required to induce cell-cycle arrest, but conversely for the escape from the latter following pro-longed DNA damage persistence¹²⁶.

Also ubiquitin- and SUMO-modified histones mediate important protein-protein interactions in the response to DSBs. One example in this regard is the C-terminal SUMOylation of the variant H2A.Z. In yeast, this modification mediates the above-mentioned re-localization of DSBs to the nuclear periphery, by mediating an interaction with the inner-nuclear membrane protein Mps3¹²⁵. Histone ubiquitylation instead plays a major role in the response to DSBs specifically in mammalian cells. The ubiquitin ligase RNF8 together with UBC13 is recruited to DSBs and ubiquitylates the linker histone H1, which in turn recruits RNF168 that subsequently ubiquitylates H2A-like histones^{145,146}. This signaling cascade helps recruiting DSB-associated factors such as BRCA1 and 53BP1,

^{**} Recently, liquid demixing induced by PARylation was reported to occur prior to phosphorylation events at DSBs, though its functionality remains unclear¹³⁴.

which promote HR or NHEJ, respectively, and thus once again, renders an environment generally permissive for suited DNA repair.

Apart from acting as recruitment platforms for other factors, histone modifications also have the ability to intrinsically alter nucleosome properties. This is best exemplified by the presence of acetylation marks, which neutralize the positive charges of the modified lysines and thereby e.g. help unfolding chromatin at active promoters¹⁴⁷. Also during DSB repair, the acetylation of histone H2A and H4, catalyzed by the NuA4 complex, contributes to an open chromatin structure that primes the break site for subsequent repair^{143,148}. At least in mammalian cells, acetylation of H4 requires the initial incorporation of H2A.Z¹²⁴. The human homologue of the NuA4 complex thereby not only contains acetyltransferase, but also H2A.Z-exchange activity, giving an intriguing example how different chromatin transactions are coordinated for the common goal of DNA repair¹⁴⁶.

1.3.3 ATP-dependent chromatin remodelers and histone chaperones

Chromatin remodeling enzymes use the energy of ATP hydrolysis to move, eject or restructure nucleosomes on DNA and thus are the classical machineries that make chromatinized DNA elements accessible to other factors¹⁴⁹. Based on the amino acid sequence, all of these enzymes share a conserved Snf2-type ATPase domain and together they constitute the large Snf2/Swi2 family within the SF2 superfamily of helicase-like enzymes^{150,151}. Importantly and in contrast to classical helicases, these enzymes do not separate DNA strands, but instead use their ATP-dependent motor domain to track along dsDNA and thereby break protein-DNA contacts. Classical nucleosome remodelers often come as multi-subunit molecular assemblies, which empowers them with certain key characteristics: a high affinity for the nucleosome itself, the ability to recognize different histone modifications, the regulation of their ATPase activity and numerous interaction sites for other chromatin proteins¹⁴⁹. The combination of these features allows each remodeler to act in a variety of cellular processes, which is reflected by the growth defects or complete inviability under otherwise normal growth conditions if their activity is lacking. However, also single enzymes, often acting as homodimers or –oligomers, are known to alter chromatin structure and this remodeling is further not limited to nucleosomal proteins. Examples in this regard are Mot1 or Rad54, which remove the TATA-binding protein or the Rad51 recombinase from DNA, respectively⁶⁸.

INTRODUCTION

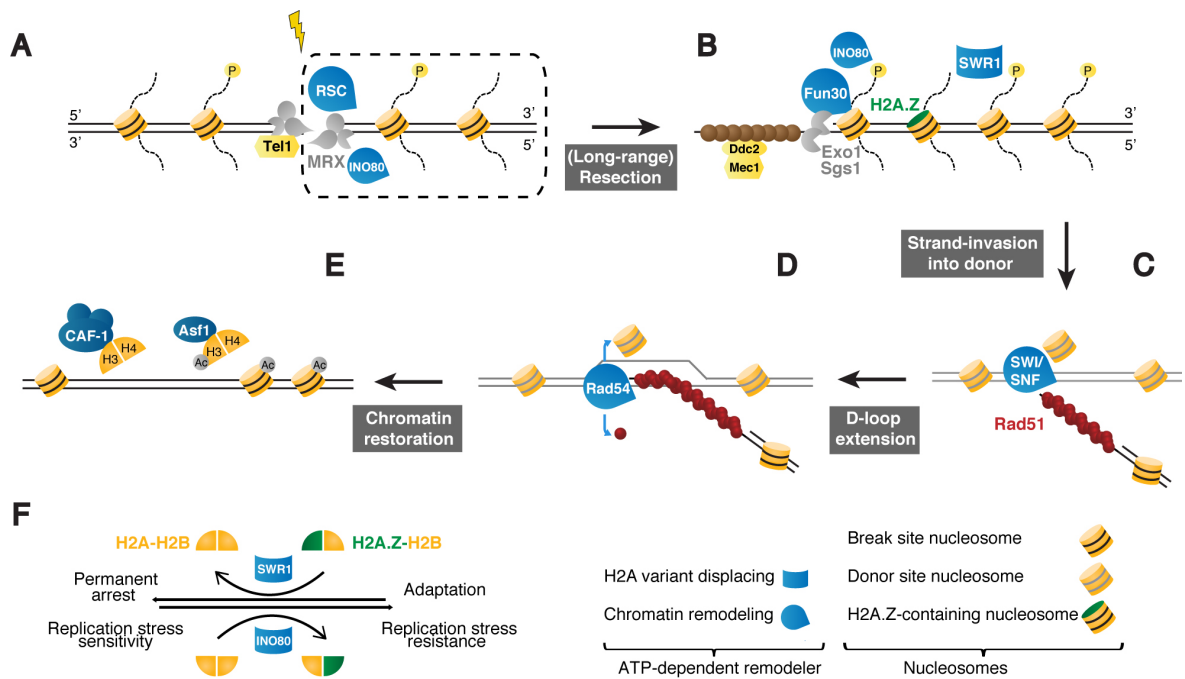


Figure 5 | Chromatin remodeling during homologous recombination

(A) One of the earliest responses at DSBs is the recruitment of checkpoint kinases, such as Tel1 (ATM in mammals), that phosphorylate histone H2A(X) and induce damage signaling. Resection initiation by the MRX complex requires the activity of the RSC chromatin remodeler. **(B)** Long-range resection is driven by chromatin remodeling of Fun30 and supported by the SWR1-mediated incorporation of the histone variant H2A.Z. Recruitment of Mec1-Ddc2 (ATR-ATRIP in mammals) to RPA-coated ssDNA further enhances checkpoint signaling. INO80 plays a minor backup function during the resection process. **(C)** Following the assembly of the Rad51 filament, SWI/SNF-mediated nucleosome remodeling is required for strand invasion at least at heterochromatic donors. **(D)** Once strand invasion occurred, Rad54 drives DNA synthesis by removing nucleosomes ahead of the invading strand and disassembling Rad51 from dsDNA. **(E)** Following the completion of repair, histone chaperones such as Asf1 and CAF1 coordinate the reassembly of histones. This requires acetylation of H3 at lysine 56. **(F)** The antagonism of SWR1 and INO80 remodelers with respect to the chromatin binding of H2A.Z emerges as a regulator of genome stability. Removal of H2A.Z by INO80 secures checkpoint adaptation and survival after replication stress. It is unclear whether INO80s variant displacement activity is also required during HR.

While local nucleosomes can also hinder DSB repair by NHEJ, the chromatin access problem becomes particularly apparent in case of HR. Here, DNA processing goes far beyond the initial lesion and additionally involves external sites at the donor template. As a consequence, members of the Snf2-, Swr1- and Rad54-like subfamily groups of remodelers are particularly important for this pathway and generally for resistance against DNA damage^{68,150,152}. While this accounts for both lower and higher eukaryotes, mechanistic studies mainly derived from yeast cells begin to unravel the diverse functions of these remodelers in the different steps of HR. It is generally appreciated that nucleosomes are lost during the process of DNA end resection. The RSC and to a lesser extend also the INO80 chromatin remodeling complex have been shown to reduce the nucleosome occupancy directly next to the break site and in turn foster the recruitment of initial processing factors such as the MRX complex^{127,153} (Figure 5 A). Instead, long-range

INTRODUCTION

resection and the recruitment of the corresponding enzymes largely depend on the activity of the Fun30 remodeling enzyme¹⁵⁴⁻¹⁵⁶ (Figure 5 B). Also the SWR1 complex was reported to contribute to DSB repair by promoting end resection (Figure 5 B), although others placed it in the NHEJ pathway^{125,127,128}. As this complex does not remove or slide nucleosomes, but specifically catalyzes the exchange of H2A-H2B for H2A.Z-H2B dimers¹¹⁷, the H2A.Z-mediated chromatin changes described above (see section 1.3.2) might well unite these apparently inconsistent findings. Following resection, the next chromatin barrier waits at the donor template. Although the Rad51-filament alone is sufficient to capture a nucleosomal donor on a chromatinized template in vitro, both the SWI/SNF and the INO80 complexes have been suggested to be involved in nucleosome displacement at the donor site in vivo, thus facilitating strand invasion¹⁵⁷⁻¹⁵⁹ (Figure 5 C). Downstream of synapsis, Rad54 is further implicated in the sliding and removal of nucleosomes inside the donor, probably facilitating subsequent strand exchange¹⁶⁰ (Figure 5 D). Importantly, all of the above studies were undertaken by using the yeast mating-type system as a model for recombination, where the donor loci are buried in dense heterochromatin structures. Especially in light of the fact that also during in vitro recombination with heterochromatinized templates Rad51 needs assistance of SWI/SNF¹⁶¹, it remains unclear to which extent donor remodeling applies in cases of canonical nucleosome structures as well. Finally, in addition to its role in initial DNA end resection, the RSC complex seems to fulfill a second, post-synaptic step during repair that facilitates the final ligation of the already extended invading DSB ends¹⁵⁹.

The SWR1 and INO80 remodelers harbor a unique long insertion in the Snf2-ATPase domain of their catalytic subunits, which groups them into a separate remodeler class¹⁶². Although INO80 has long been known to remodel canonical nucleosomes¹⁶³, recent data indicate also a closer functional overlap with the SWR1 complex. However, instead of integrating H2A.Z-H2B dimers into nucleosomes, INO80 catalyzes their removal from chromatin¹⁶⁴. Remarkably, emerging evidence suggests that this functional antagonism between the two remodelers helps to secure genome stability (Figure 5 F). First, this process triggers an adaptation to the DNA damage checkpoint, by restoring γ H2AX levels¹²⁶ (see section 1.3.2). Although the benefit of this process remains unclear, it might give cells additional time to repair a DSB in the next cell division. Second and more importantly, H2A.Z removal by INO80 is critical for survival upon DNA replication stress, albeit the mechanism behind this important function remains entirely enigmatic¹⁶⁴. It is thus an interesting possibility that the counteraction of SWR1 by INO80 might also be required directly for DSB repair.

INTRODUCTION

Histone chaperones are the proteins that generally govern an ordered nucleosome build-up, shielding the positive histone charges and protecting them from non-specific interactions with the negatively charged DNA¹⁰⁷. Different chaperones thereby target different sub-complexes of the nucleosome. The FACT complex as well as Nap1 are important H2A-H2B chaperones, whereas Asf1 and CAF1 play major roles in regulating H3-H4 removal and deposition. Histone chaperones are inevitable during DNA replication, where they mediate both the coordinated disassembly and reassembly of nucleosomes ahead and behind of the replication fork, respectively. In contrast to replication, the role of these proteins during DSB repair so far seems to be restricted to the nucleosome reassembly after the repair event¹⁰⁷, where they “clean up” the disorder left behind by the action of the numerous chromatin remodelers. Herein, Asf1 first indirectly promotes the acetylation of histone H3 at lysine 56, a critical event for delivery of novel H3-H4 entities to CAF1, which subsequently inserts these building block into the chromatin^{165,166} (Figure 5 E). Importantly, the activity of histone chaperones is also required to shut down the DNA damage checkpoint. On the one hand, the defective nucleosome delivery in the absence of Asf1 and CAF1 itself sustains a constant cell cycle arrest by a yet unclear mechanism^{166,167}. On the other hand, the FACT complex at least in mammals is critical for the removal of γ H2AX from chromatin¹⁶⁸. There are also other variant specific chaperones, and most interesting with regards to DNA damage are those targeting H2A.Z. In yeast, Chz1 acts in conjunction with SWR1 to deposit this H2A variant, while mammalian cells possess a chaperone that specifically mediates H2A.Z removal from chromatin^{169,170}. Only very recently it was shown that this protein called ANP32E catalyzes the dynamic turnover of DSB-incorporated H2A.Z, which is required for chromatin relaxation around the break site and sufficient NHEJ¹⁷¹.

Collectively, chromatin remodelers and histone chaperones play essential roles in DSB repair and especially during HR. While chaperones mainly restore chromatin after repair has been completed, nucleosome alterations by remodeling enzymes are inevitable already for lesion processing. A picture emerges in which a number of ATP-dependent machineries fulfill various functions along the complicated HR pathway and we are just at the beginning to understand the whole impact of their activities.

2 AIMS OF THE STUDY

HR is the most accurate pathway to repair the most toxic of all DNA damages – DSBs. Despite decades of research and seminal achievements by many different laboratories, central aspects of HR remain poorly understood. Especially our understanding of the impact of the associated chromatin remodeling is still poor, and mechanistic explanations for a variety of involved chromatin factors are at best vague.

This study aims to address the fundamental question whether chromatin remodeling is required during the search for a homologous donor sequence during HR. In contrast to any step during any other DNA repair pathway, homology search affects vast amounts of undamaged DNA, demanding special attention and careful control in cases of underlying chromatin changes.

Using the power of genetics in the model organism *S. cerevisiae* combined with chromatin immunoprecipitation (ChIP) of DNA repair proteins, I will discriminate between the roles of chromatin remodeling factors in distinct steps of HR. An important milestone towards this goal is the verification of Rad51 ChIP as a measure of homology search. To this end, I plan to establish a flexible assay to easily monitor HR between any two loci in a genome, which allows the correlation of previously measured intensities of homology search with the total efficiency of HR.

3 RESULTS

3.1 Homology search requires Rad54 and Rdh54 proteins and induces large-scale remodeling of histones H2A and H2B

3.1.1 An assay to monitor site-specific recombination in real-time

Rad51 ChIP was recently reported as the first method that allows the direct monitoring of homology search during HR⁴⁷. Generally, the signals of Rad51 determined via ChIP following synchronized induction of a single and site-specific DSB are twofold. Very high enrichments at close distances to the break site reflect formation of the Rad51 filament. In contrast, comparably low enrichments measured over large areas of surrounding DNA were hypothesized to reflect an ongoing and random homology sampling of the Rad51 filament, only transiently probing certain loci in a sub-population of cells at a certain time. Indeed, it was shown that the observed DSB-distant accumulation of Rad51 does neither result from extended single-stranded presynaptic filaments nor from unspecific binding of Rad51 to double-stranded DNA⁴⁷. Nevertheless, the final proof that these signals indeed mirror the efficiency of homology search required their correlation with completion of HR. To verify this model, I decided to generate a site-specific recombination assay that allows monitoring DSB-induced recombination efficiency in real-time^{††}. Notably, the development of such an assay would not only allow the verification of Rad51 ChIP as a suitable method to monitor homology search, but more importantly could additionally provide the first clear evidence that the efficiency of HR correlates with spatial proximity, as predicted from the findings on the homology search⁴⁷.

An important prerequisite for a universally applicable recombination system is that recombination proceeds between homologous sequences that are otherwise not present in the genome of *S. cerevisiae*. One such sequence is the one encoding for the green fluorescent protein (GFP), often used for tagging endogenous yeast proteins for visualization via microscopy or immunoprecipitation approaches. I thus decided to use as a basis for the proposed recombination system available plasmids for PCR-based GFP-tagging^{172,173} and combine it with yeast strains harboring the HO endonuclease gene under control of the galactose promoter – the method of choice for generating site-specific DSBs in *S. cerevisiae*¹⁷⁴. Importantly, the respective strains are also deleted for the endogenous HO recognition site on chromosome III and thus entirely rely on artificially

^{††} Plenty of recombination assays are available in *S. cerevisiae*, but most systems either are limited to specific loci or the measurement of only spontaneous recombination rates.

RESULTS

integrated sequences for DSB induction. To generate the two recombination alleles, I cloned a 36 bp HO recognition site (GFP-HO_{cs}) or an incleavable variant containing two point mutations¹⁷⁵ (GFP-HO_{inc}) in the middle of the GFP encoding sequence.

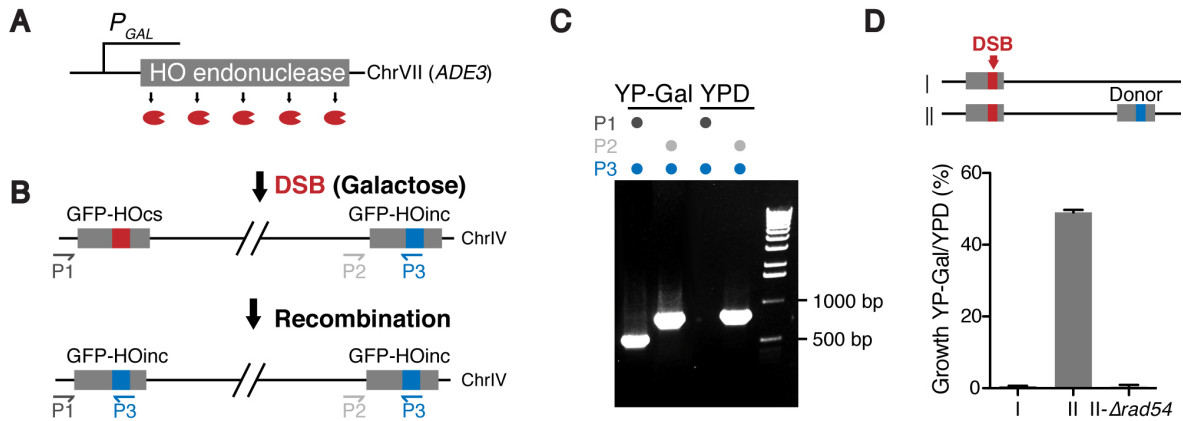


Figure 6 | A flexible assay to monitor recombination between different genomic loci

(A) Scheme of a yeast strain expressing the HO endonuclease from the *ADE3* locus on ChrVII under control of the *GAL1* promoter. (B) Scheme of a yeast strain with integrated constructs to measure site-specific recombination. Usage of galactose as a carbon source results in HO-mediated DSB induction inside the GFP-HO_{cs} sequence. Specific PCR primer (P) can be used to monitor successful recombination using the GFP-HO_{inc} sequence. (C) PCR reaction on genomic DNA isolated from strains with GFP-HO_{cs} on ChrIV 491 kb and GFP-HO_{inc} on ChrIV 625 kb grown on galactose (YP-Gal) or glucose (YPD) as a carbon source verifies specificity of the recombination reaction. Primer as in (B). (D) Recombination using the system described in (A-C) depends on both the presence of a homologous donor as well as the *bona fide* recombination factor Rad54. Cells were grown on agar plates supplemented with raffinose as a carbon source and an equal number of cells was then plated on YPD or YP-Gal. Single colonies were counted after 2-3 days and the ratio of survival calculated under HO expressing vs. non-expressing conditions. Mean plus SD of three independent experiments are shown.

In addition, a unique 23 bp sequence was integrated exclusively next to the incleavable recognition site. Once these constructs have been integrated into the site of choice of the *S. cerevisiae* genome using a previously described PCR-based strategy^{172,173}, the unique sequence will allow to specifically monitor recombination by quantitative real-time PCR (qPCR) following DSB induction (Figure 6 A and B). Indeed, in a yeast strain bearing the GFP-HO_{cs} sequence at an intergenic position at 491 kb on chromosome IV and the GFP-HO_{inc} sequence at an intergenic region at 625 kb on chromosome IV, exclusively growth on galactose as a carbon source resulted in the emergence of a recombination product amplified from genomic DNA (Figure 6 C). Furthermore, I expected the growth of this strain on galactose medium to depend on recombination, as only in this scenario the incleavable HO recognition sequence will replace its canonical counterpart. Attempts to repair the induced DSB by NHEJ will instead result in continuous repair-cleavage cycles and constant cell-cycle arrest under such conditions¹⁷⁶. Indeed, cell survival entirely depended both on the presence of a homologous donor and the essential recombination factor Rad54, proving that recombination occurred between the GFP-based homologies

(Figure 6 D). Interestingly, also in presence of the donor only 50 % of all cells are able to survive, indicating that there are limitations for the efficiency of distant recombination events¹⁷⁷ (see also section 3.1.3).

3.1.2 Recombination efficiency correlates with homology search signals and is determined by the nuclear architecture

With this assay in hand, I next aimed to correlate the strength of homology search signals measured by Rad51 ChIP with the efficiency of HR *in cis*. To do so, I generated two additional yeast strains both harboring the GFP-HO_{cs} sequence at position 491 kb on chromosome IV, but with the homologous donor (GFP-HO_{inc}) either integrated at position 795 kb or 820 kb, respectively, on the same chromosome. Importantly, homology search signals in a donor-deficient background at these sites were significantly weaker compared to those at 625 kb, correlating with an increased distance to the DSB (Figure 7 A). Recombination was subsequently monitored by qPCR at different time points following DSB induction in all three strains. As anticipated, the strain with the donor at the DSB-close position (625 kb) showed much faster accumulation of the recombination product compared to the two strains with the distant donors (Figure 7 B). Surprisingly, even when comparing the latter, the accumulation of the recombination product dropped again about 50 % in case of the 795 kb compared to the 820 kb donor. While Rad51 ChIP signals were already at the detection limit at these sites, this further strengthened the idea that recombination is largely influenced by the physical distance between the DSB and homologous donor. When I monitored Rad51 distribution itself in the three recombination-competent (donor-proficient) strains, I found that it efficiently accumulates close to the potential donor integration sites only when a donor had also been integrated there (Figure 7 C). Importantly, these Rad51 signals did not reflect latent cleavage of the mutated HO recognition site at the donor, as they were absent in strains where only the donor site had been integrated (Figure 7 D). Instead, these signals most likely reflected ongoing repair by synapsis between the presynaptic filament and the homologous donor. Taken together, the presented data verified Rad51 ChIP in a donor-deficient scenario as a measure of homology search and thus as an indicator of recombination efficiency when a specific donor is available.

RESULTS

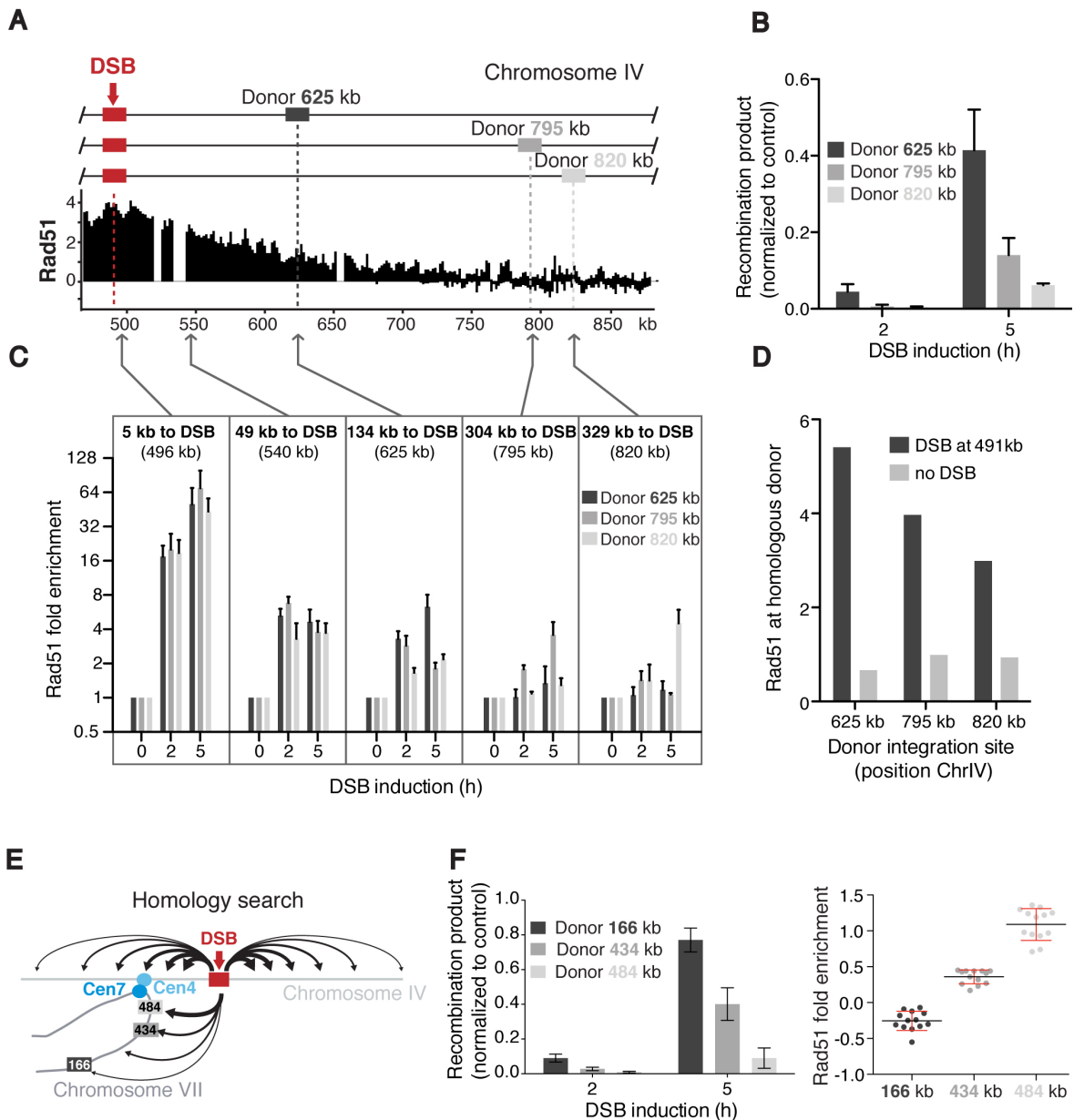


Figure 7 I Homology search signals correlate with recombination efficiency

(A) Homology search signals decrease with increasing linear distance from the DSB. Rad51 ChIP-chip profile of a part of ChrIV following DSB induction at position 491 kb. Data taken from reference 47. **(B)** Recombination efficiency decreases with increasing linear distance between DSB and donor site. qPCR determination of recombination following DSB induction at position 491 kb on ChrIV in three different yeast strains, each harboring one donor template placed at one of the indicated positions (see also A). **(C)** Rad51 accumulates over time at the homologous donor. Rad51 ChIP-qPCR at indicated locations using the three strains depicted in (B). Rad51 enrichments at positions 625 kb, 795 kb and 820 kb are donor-specific. **(D)** Rad51 accumulation at the donor site is not due to latent cleavage of the GFP-HOinc constructs. Rad51 ChIP at donor sites in strains with and without DSB induction (i.e. integrated GFP-HOCs sites) **(E)** Scheme of how centromere clustering affects the 3D genome organization. Centromere proximal loci on ChrVII have a closer spatial proximity to the DSB on ChrIV than centromere distal loci. **(F)** Recombination and homology search efficiencies anti-correlate with increasing 3D distance between DSB and donor site. Left: qPCR analysis of recombination following DSB induction at position 491 kb on ChrIV in three different yeast strains, each harboring one donor template placed at one of the indicated positions (see also E). Right: Rad51 ChIP signals collected within 1 kb windows around the donor integration sites obtained from a corresponding donor-deficient strain. Data taken from reference 47.

Data represented in (B), (C) and (F) represent mean plus SD of three independent experiments. Data in (D) represent results from one experiment. All qPCR data were normalized to a control locus on ChrX and all ChIP data also to the time before DSB induction (0 h).

Recombination between distant donors cannot only proceed *in cis* within the same chromosome, but also *in trans* between different chromosomes, albeit the first scenario is the preferred one^{178,179}. In line with this idea, homology search measured via Rad51 ChIP is generally hardly detectable on unbroken chromosomes. Intriguingly, this differs in a scenario where a DSB is induced close to a centromere. Here, Rad51 signals were subsequently detected at centromeres of all other chromosomes as well, a finding that was explained by the fact that centromeres cluster inside the yeast nucleus^{180,181}. Consequently, it was suggested that the homology search efficiency does not necessarily correlate with the linear, but the three-dimensional distance to a DSB⁴⁷. To investigate whether also recombination may be guided by the three-dimensional nuclear architecture, yeast strains bearing the GFP-HO_{cs} sequence at position 491 kb on chromosome IV (51 kb distant to CenIV_{450kb}) and donor sequences at distances of 13 kb, 63 kb or 331 kb away from the centromere on chromosome VII, were generated (Figure 7 E). Perfectly matching the previously measured strengths of homology search, these strains showed decreasing recombination efficiencies with increasing distance of the donor site from the centromere (Figure 7 F). This finding showed for the first time^{§§} that HR seems to be linked to the three-dimensional nuclear architecture and once more the remarkable possibility to estimate recombination potentials even on the basis of Rad51 signals close to the detection limit.

3.1.3 Rad54 and Rdh54 are important regulators of the homology search process

The verification of genome-wide Rad51 ChIP as a method to directly monitor homology search opened new avenues to analyze this process in more detail. Specifically, it allowed addressing the fundamental question of a potential requirement for chromatin remodeling factors during this process. An interesting candidate protein in this regard was Rad54, a multifunctional DNA translocase also known as the “Swiss Army knife” of HR¹⁸³, thereby reflecting its various functions ranging from pre- to post-synaptic steps during the pathway. Although the main function of Rad54 lies at the (post-)synaptic modulation of Rad51, it was hypothesized that it might also be involved in the earlier process of homology search by a remodeling of nucleosomes.

^{§§} Since the publication of these results⁴⁷, two other groups addressed this correlation more globally and came to similar conclusions^{177,182}.

RESULTS

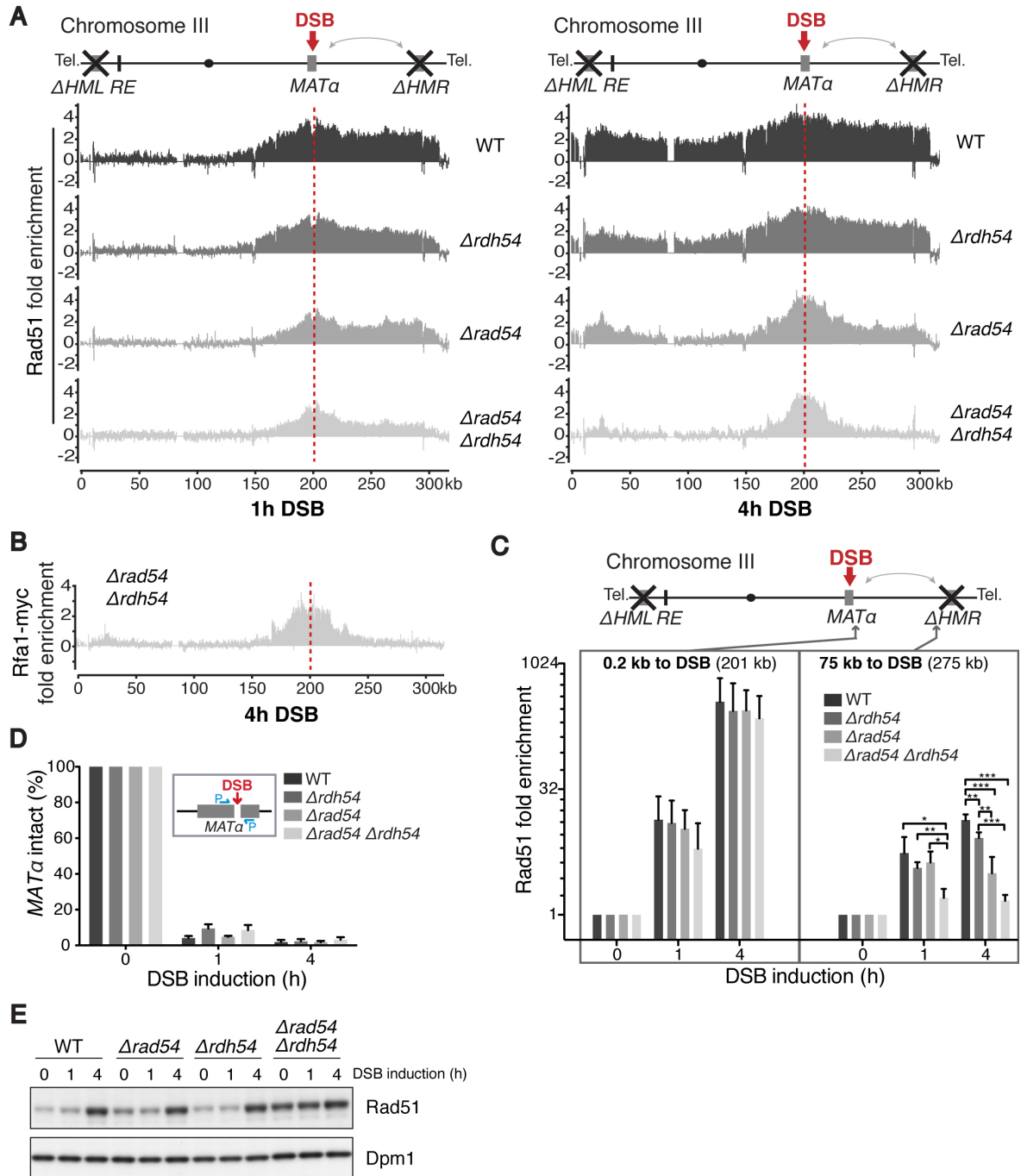


Figure 8 | The Rad54 family proteins Rad54 and Rdh54 are essential for the homology search

(A) Rad54 and Rdh54 are required for homology search, but not Rad51 filament formation. Top: scheme of ChrIII, indicating preferential homology search on the right chromosome arm in *MAT α* cells. Bottom: time-resolved Rad51 ChIP-chip experiment following DSB induction at the *MAT* locus in strains lacking Rad54, Rdh54 or both. **(B)** Rad51 and RPA accumulation are confined to the same area in absence of Rad54 and Rdh54. Rfa1-9myc ChIP-chip experiment in the $\Delta rad54 \Delta rdh54$ strain. **(C)** Rad51 ChIP-qPCR at regions close and distal to the DSB in the indicated strains. Verifies conclusion from (A) that Rad54 and Rdh54 are specifically required for homology search. **(D)** DSB induction kinetics is not changed in absence of Rad54 and Rdh54. qPCR analysis of *MAT* locus cleavage using primers spanning the HO recognition site in the indicated strains. **(E)** Defective homology search in absence of Rad54 and Rdh54 is not due to decreased Rad51 protein levels. Immunoblot analysis against Rad51 using total cell extracts prepared following DSB induction. Data in (A) and (B) represent mean of two independent experiments, including a dye-labeling swap and are depicted on a log₂ scale. Data in (C) and (D) represent mean and SD of three independent experiments. Statistical analysis was conducted using Student's t-test with asterisks indicating $p < 0.05$ (*), $p < 0.01$ (**) or $p < 0.001$ (***). All qPCR data were normalized to a control locus on ChrX and all ChIP data also to the time before DSB induction (0 h).

RESULTS

To investigate a possible function of Rad54 during homology search, I performed ChIP against Rad51 in donor-deficient strains where a DSB was induced at the *MAT* locus on chromosome III. In absence of Rad54, Rad51 signals were markedly reduced at sites corresponding to an ongoing homology search, but importantly not at sites close to the DSB that reflect formation of the Rad51 filament (Figure 8 A and C). Because homology search was not completely deficient in the absence of Rad54, I wondered whether the Rad54 homologue Rdh54 was involved in the process as well¹⁸⁴. Although removal of Rdh54 alone showed only little defects in homology search, the protein became important in the absence of Rad54, as reflected by the virtual absence of all homology search signals when both proteins were deleted (Figure 8 A and C). Hence, the only detectable Rad51 signals in the $\Delta rad54 \Delta rdh54$ background were limited to sites of Rad51 filament formation. This was further corroborated by the nearly perfect overlap of Rad51 and Rfa1 signals in this strain, with the latter indicating the generation of single-stranded DNA during DNA end resection (Figure 8 A and B). Of note, Rfa1 accumulation appeared to a similar extent as previously observed in wild type (WT) cells⁴⁷. Importantly, neither delayed DSB induction kinetics (Figure 8 D) nor decreased Rad51 protein levels (Figure 8 E) could account for the observed Rad51 accumulation defects in the ChIP experiments. Instead, Rad51 expression was even up-regulated at early time points in the double mutant (Figure 8 E), likely reflecting a compensation for an intrinsically higher damage load of this strain. Similar functionalities for the Rad54 and Rdh54 proteins could be obtained upon DSB induction on a different chromosome (data not shown), further corroborating the previous observations.

Results so far placed Rad54 and Rdh54 as central components of the homology search process, possibly traveling with the Rad51 filament and exerting their functions directly at the sites of transient homology sampling. To investigate this idea, I aimed to visualize Rad54 and Rdh54 directly at sites of homology search via ChIP. However, ChIP efficiency of both proteins and especially the more important Rad54 was repeatedly very weak, possibly due to poor protein expression levels (data not shown). I thus decided to make use of a different strategy to investigate whether Rad54 exerts its function in conjunction with Rad51. Expression of the Hed1 protein under natural conditions is restricted to meiosis, where it inhibits the protein-protein interaction between Rad51 and Rad54¹⁸⁵ (Figure 9 A). This allows meiotic recombination to proceed by the recombinase Dmc1, which is important for repair via homologs instead of sister chromatids¹⁸⁶.

RESULTS

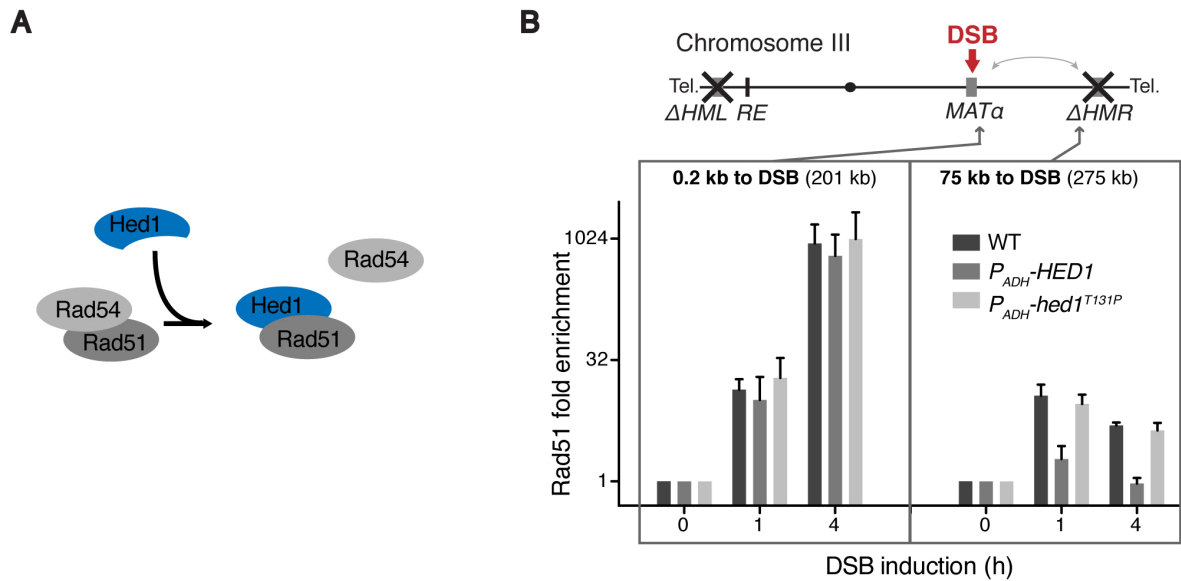


Figure 9 | Rad54 family proteins require binding to Rad51 to function in homology search

(A) Scheme of how presence of Hed1 affects the interaction of Rad51 and Rad54. **(B)** Overexpression of Hed1 abolishes homology search. Rad51 ChIP signals analyzed by qPCR at locations close and distant to the DSB in strains overexpressing either wild-type *HED1*, *hed1*^{T131P} or none of them. Data were normalized to the time before DSB induction as well as a control locus on ChrX and represent the mean plus SD of three independent experiments.

As artificial expression of Hed1 in mitotic cells was shown to inhibit the Rad51-Rad54 interaction as well¹⁸⁵, such a scenario should result in an inhibition of the Rad51-mediated homology search if it required Rad54 functionality directly linked to Rad51. When performing the corresponding Rad51 ChIP experiment, I indeed found a nearly complete abrogation of Rad51 accumulation at sites of homology search, but no effect on Rad51 recruitment at the DSB (Figure 9 B). Importantly, this effect was gone when a Hed1 mutant variant that cannot bind to Rad51 was expressed¹⁸⁷ (Figure 9 B). Interestingly, the effect of Hed1 overexpression very much resembled the phenotype of the Δ *rad54* Δ *rdh54* strain, although Hed1 was reported to have only mild effects on inhibiting the interaction between Rdh54 and Rad51¹⁸⁵.

Because Rad54 levels are very low, I wondered whether its important function in the homology search could be a limiting factor during HR. When measuring ectopic recombination between the GFP-HO_{cs} sequence at position 491 kb on chromosome IV and a donor ~300 kb downstream by qPCR, repair was significantly faster when Rad54 was overexpressed (Figure 10 A). Moreover, the accumulation of the recombination product correlated with the levels of Rad54, as estimated from the strength of the promoter under which they were expressed. On the whole cell population level, 25 % of all cells were able to survive with the donor site located 300 kb away from the DSB and this number could be almost doubled upon strong Rad54 expression (Figure 10 B).

RESULTS

Remarkably, Rad54 overexpression thereby mimicked repair efficiency in a case where the donor site is located less than half the distance away from the break.

In summary, Rad54/Rdh54 promote homology search by direct binding to Rad51. This complex seems sub-stoichiometric, and increasing the ratio of at least Rad54 to Rad51 results in enhanced recombination levels.

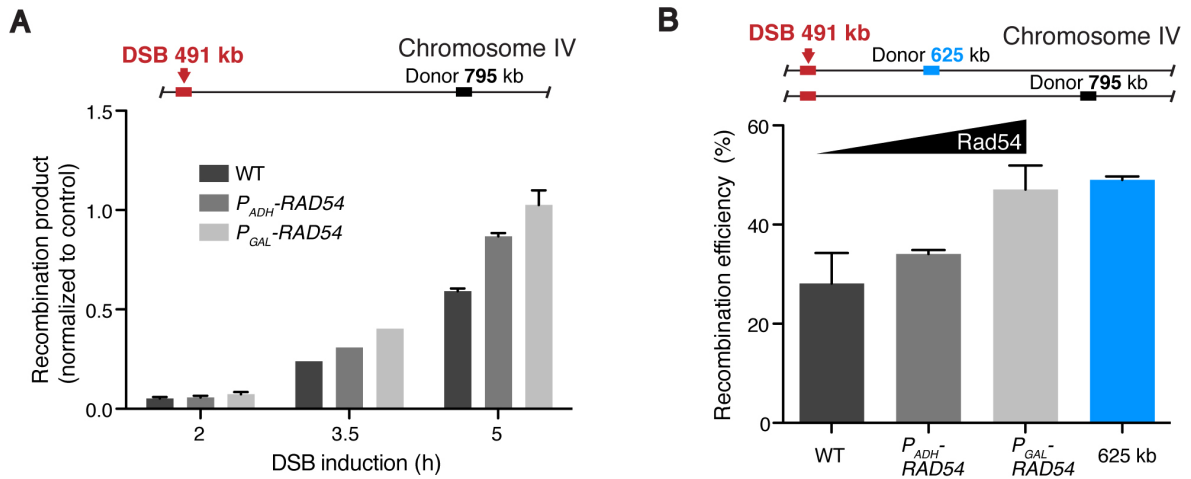


Figure 10 | **Rad54 is a limiting factor for homologous recombination**

(A) Rad54 overexpression correlates with increased recombination levels. Time-resolved qPCR analysis of intra-chromosomal recombination on ChrIV in WT strains or strains overexpressing *RAD54* from different promoters. Data were normalized to a control locus on ChrX. **(B)** *RAD54* overexpression phenocopies increased spatial proximity between DSB and donor with respect to recombination. Growth assay analysis of strains depicted in (A) compared to a WT strain with less than half the linear DSB-donor distance. All data represent mean plus SD of three independent experiments.

3.1.4 Sites of homology search display changes in chromatin structure

Rad54 and Rdh54 are members of the Snf2/Swi2 family of chromatin remodeling enzymes⁶⁸ and at least Rad54 has been linked to chromatin remodeling during the synaptic stages of HR both in vitro and in vivo^{160,188,189}. Their specific function during homology search thus raises the possibility for a remodeling of nucleosomes underlying this process as well.

To investigate a potential chromatin remodeling at sites of homology search, I conducted a genome-wide analysis of nucleosome occupancy following DSB induction by performing ChIP against histone H2B coupled to microarray analysis (ChIP-chip). By comparing yeast strains where a DSB was induced either at the *MAT* locus on chromosome III or at position 491 kb on chromosome IV with a strain harboring no HO endonuclease recognition site, a DSB-specific, wide-ranged drop of H2B levels on the broken chromosomes could be observed (Figure 11 A).

RESULTS

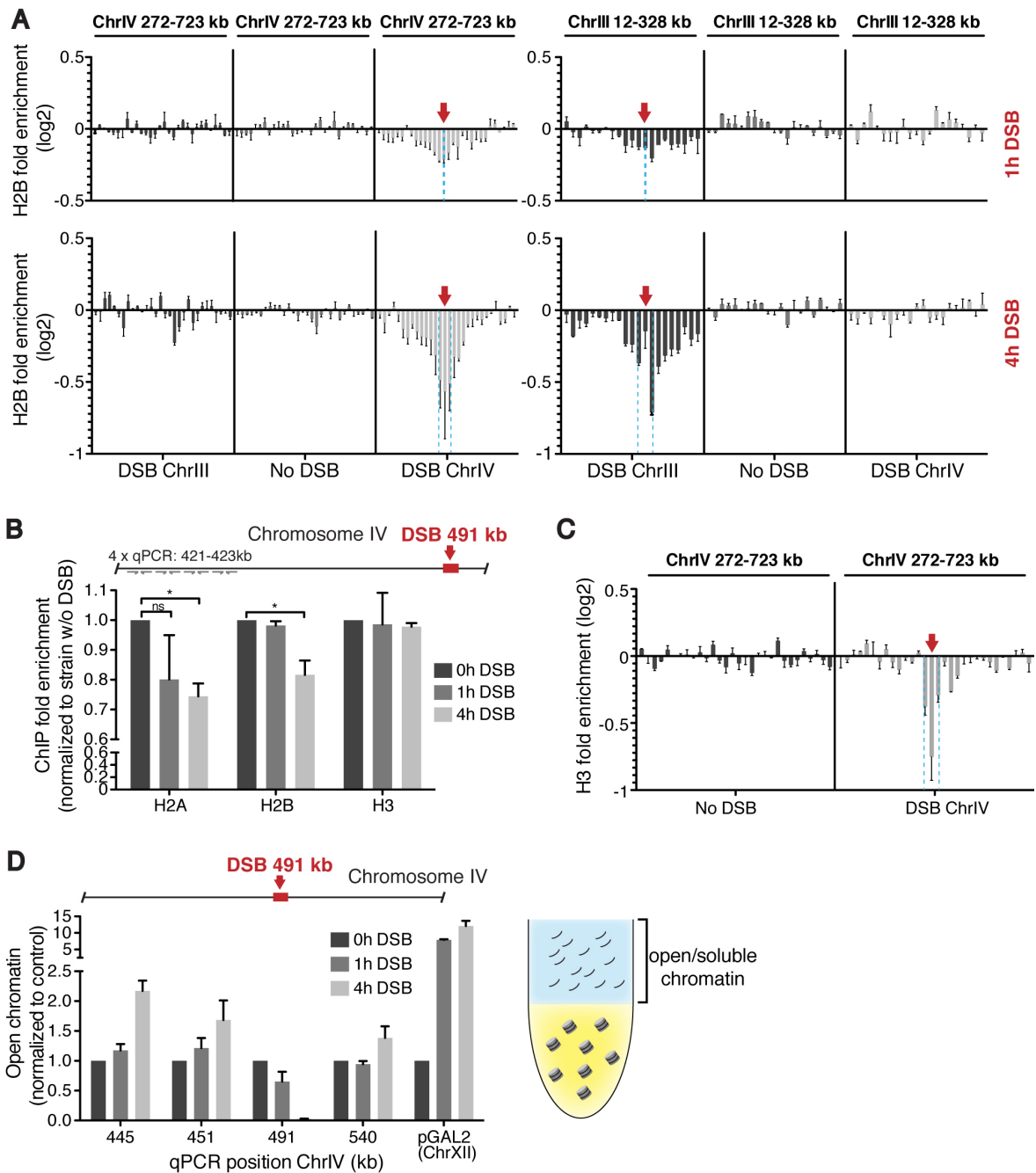


Figure 11 | Chromatin remodeling at sites of homology search

(A) Histone H2B levels are reduced at sites of homology search. Time-resolved H2B ChIP-chip analysis following HO induction in strains bearing HO recognition sites on ChrIII or ChrIV or a control. Enrichments are depicted as log₂ values with each bar representing the mean of a 15 kb window. Dashed blue lines indicate the estimated area of DNA end resection. Left: data depicted for a region of ChrIV. Right: data depicted for a region of ChrIII. **(B)** Different histones show differential behavior during homology search. Time-resolved ChIP against histones H2A, H2B and H3 following induction of a DSB on ChrIV. Enrichments are shown for the 421-423 kb region, as determined by the mean of four qPCR primer pairs normalized to the mean of four random control pairs on different chromosomes. Additionally, data were normalized to a strain in which HO is expressed, but no DSB is generated. **(C)** Histone H3 levels remain unchanged at sites of homology search. H3 ChIP-chip analysis following DSB induction on ChrIV compared to a control strain. Data are depicted as described in (A). **(D)** Detection of open chromatin at sites of homology search. The chromatin fraction was isolated and DNA purified by Phenol-Chloroform extraction then analyzed by qPCR at the indicated positions. Data in (A) and (C) represent mean plus SEM of two independent experiments including a dye-labeling swap. Data in (B) and (D) represent mean plus SD of two independent experiments. Statistical analysis was conducted using Student's t-test with asterisks indicating $p < 0.05$. ns: not significant. All qPCR data were normalized to a control locus on ChrX and to the time before DSB induction (0 h).

RESULTS

The effect was generally strongest in the area of DNA end resection (indicated by dashed blue lines, Figure 11 A), but clearly emanated up to several hundred kb beyond these sites. Moreover, the intensity of H2B removal increased over time and decreased with increasing distance to the DSB. As ChIP-chip only allows semi-quantitative analysis due to DNA amplification and microarray hybridization, H2B effects were additionally quantified via qPCR. Because such small changes were repeatedly observed to lie within the range of natural qPCR fluctuation for single sites (data not shown), I developed a special protocol to visualize them more robustly. To this end, the average of four qPCR primer pairs together spanning a region of 2 kb in an area of efficient homology search are normalized to the average of four different control primers randomly distributed on different chromosomes. Using this method, H2B levels were found to significantly decrease about 20 % at an area ~70 kb away from the DSB 4 h following break induction, although the weaker changes at the 1 h time point observed in the genome-wide analysis could not be recapitulated (Figure 11 B). Interestingly, ChIP against other histone proteins revealed a differentiated picture. A similar drop was detected for H2A, however with a tendency for this histone to be removed more robustly already 1 h following DSB induction. In contrast, H3 levels remained constant (Figure 11 B), and preliminary results indicated similar observations for H4 (data not shown). This finding was further corroborated by genome-wide analysis, where the decrease in H3 occupancy was limited to the area of DNA end resection (Figure 11 C). Thus not the nucleosome per se, but only the more unstable H2A-H2B dimers seemed to be affected at sites of homology search.

I next asked whether the observed drop in H2A and H2B levels resulted in a generally more open chromatin status at sites of homology search. Formaldehyde-assisted isolation of responsive elements (FAIRE) is a method initially developed to identify regulatory DNA elements that are characterized by poor nucleosome occupancy¹⁹⁰. This “naked” DNA is enriched throughout the protocol and its presence can subsequently be quantified by qPCR. Intriguingly, DNA at sites of ongoing homology search could be enriched up to two-fold following DSB induction, indicating that homology search possibly correlates with an opening of the chromatin at these sites (Figure 11 D). In contrast, DNA directly next to the HO recognition site was lost following DSB induction, possibly due to both DNA end resection and tight binding of Rad51 to ssDNA.

These findings indicated the induction of chromatin remodeling linked to homology search. Nevertheless, the possibility remained that the observed effects either emerged from a few cells generating particularly long stretches of ssDNA several hours after DSB induction or unspecific, “linear” chromatin remodeling along the affected chromosome.

RESULTS

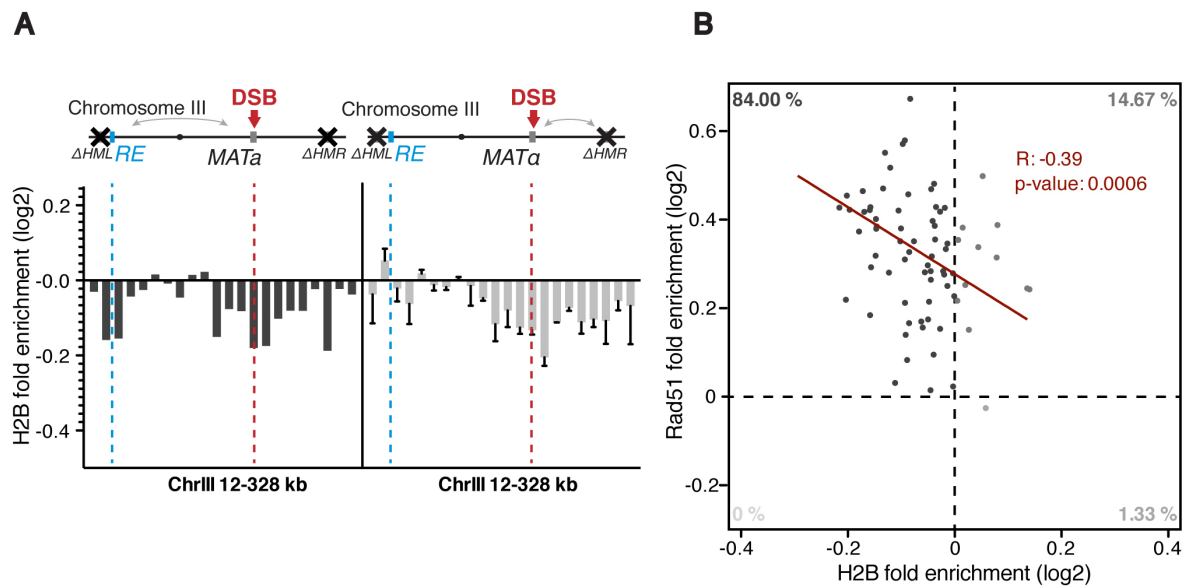


Figure 12 | The reduction in histone occupancy correlates with the 3D homology search efficiency

(A) H2B levels drop in relation to the homology search preference in the yeast mating-type system. Top: scheme representing preferential homology search to either the left or the right side in *MATa* or *MATa* cells, respectively, dependent on the activity of the recombination enhancer (*RE*) element. Bottom: H2B ChIP-chip data 1 h following DSB induction on ChrIII either in *MATa* or *MATa* cells. Each bar represents the average of a 15 kb window. Data for *MATa* represent mean and SEM of two independent experiments including a dye-labeling swap (same data as in Figure 11 A). Data for *MATa* are from a single experiment. **(B)** H2B levels anti-correlate with Rad51 levels around centromeres following induction of a centromere-proximal DSB at position 491 kb on ChrIV. ChIP-seq experiments against Rad51 and H2B 4 h following DSB induction. An area of 25 kb around each centromere (except CenIV) was analyzed in 5 kb windows and the Rad51 and H2B values plotted and correlated by a linear regression. Dashed lines separate different quadrants with either increased or reduced presence of Rad51 and H2B compared to 0 h time point and the corresponding numbers are given as percentage values. Data represent the mean of three independent experiments and were normalized to the time before DSB induction.

All data are depicted on a log2 scale.

The strongest evidence to exclude such possibilities would be the identification of chromatin changes at sites of homology search that are not linearly linked to the DSB. In yeast cells of the “a” mating type (*MATa*), the left arm of chromosome III forms a loop and thereby gains close proximity to the *MAT* locus, mediated by an element called the recombination enhancer (*RE*)^{47,191}. This results in efficient homology search around the *RE*, but not at sites in between this element and the DSB. In contrast, in yeast cells of the “ α ” mating type (*MATa*), the *RE* is inactive and homology search cannot efficiently sample this area. When comparing H2B occupancy following DSB induction at the *MAT* locus on chromosome III in *MATa* and *MATa* cells, a *MATa*-specific drop could be observed 30 kb around the *RE*, indicating that this remodeling indeed also happens *in trans* (Figure 12 A). Along this line, DSB-induction on chromosome IV at position 491 kb resulted in a specific drop of H2B levels *in trans* around the centromeres of all other chromosomes and more importantly, this drop anti-correlated weakly, but significantly with the strength of homology search as measured by Rad51 accumulation (Figure 12 B).

Taken together, these data support the idea that sites of homology search are reflected by a decrease in the occupancy of histones H2A and H2B, which results in an at least partially opened chromatin structure.

3.1.5 Rad54 and Rdh54 indirectly influence the remodeling of histones H2A and H2B at sites of homology search

Having identified for the first time chromatin remodeling at sites of homology search during HR in vivo, the question remained whether these changes might be linked to the function of Rad54 and Rdh54. To this end, I performed ChIP against H2A and H2B following DSB induction in WT and $\Delta rad54 \Delta rdh54$ deletion strains. Both in case of H2A and H2B, the only significant drops in histone occupancy were observed 4 h after DSB induction and this was dependent on the presence of Rad54 and Rdh54 (Figure 13 A). Particularly the loss of H2B was strongly influenced by both translocases and this was confirmed by analyzing H2B occupancy on a larger area along the broken chromosome via ChIP-chip (Figure 13 B). Of note, H2B levels here were not only affected at the sites of homology search, but also strongly within the area of DNA end resection, i.e. at the Rad51 filament (indicated by dashed blue lines, Figure 13 B). This was surprising, as neither defective Rfa1 accumulation, nor defective Rad51 filament formation were observed in absence of Rad54 and Rdh54 before (Figure 8 A and B).

While the remodeling of histones H2A and H2B during homology search seems thus to be linked to Rad54/Rdh54, it remained puzzling that H2A showed a tendency to be remodeled earlier than H2B. This would in principle be inconsistent with the idea that the observed effects result from the same remodeling event. Intriguingly, a recent report demonstrated a comparable, timely separated alteration of H2A and H2B following DSB induction¹⁹². Specifically, a novel C-terminal damage-induced phosphorylation on H2B was identified, at an equivalent site to the serine in H2A that is modified during the formation of the famous γ H2AX (in the following referred to as γ H2A). Although established by the same kinases, γ H2A peaked already 30-60 min following DSB induction, while the newly identified H2B phosphorylation (γ H2B) only did so after 2 h. Consequently, I asked whether the previously observed drop in the occupancies of H2A and H2B was linked to their DSB-induced phosphorylation. To this end, I generated yeast strains in which the phospho-acceptor serines or threonines in both alleles of either H2A or H2B, respectively, were replaced by non-phosphorylatable alanine residues and subjected these strains to H2A and H2B ChIP.

RESULTS

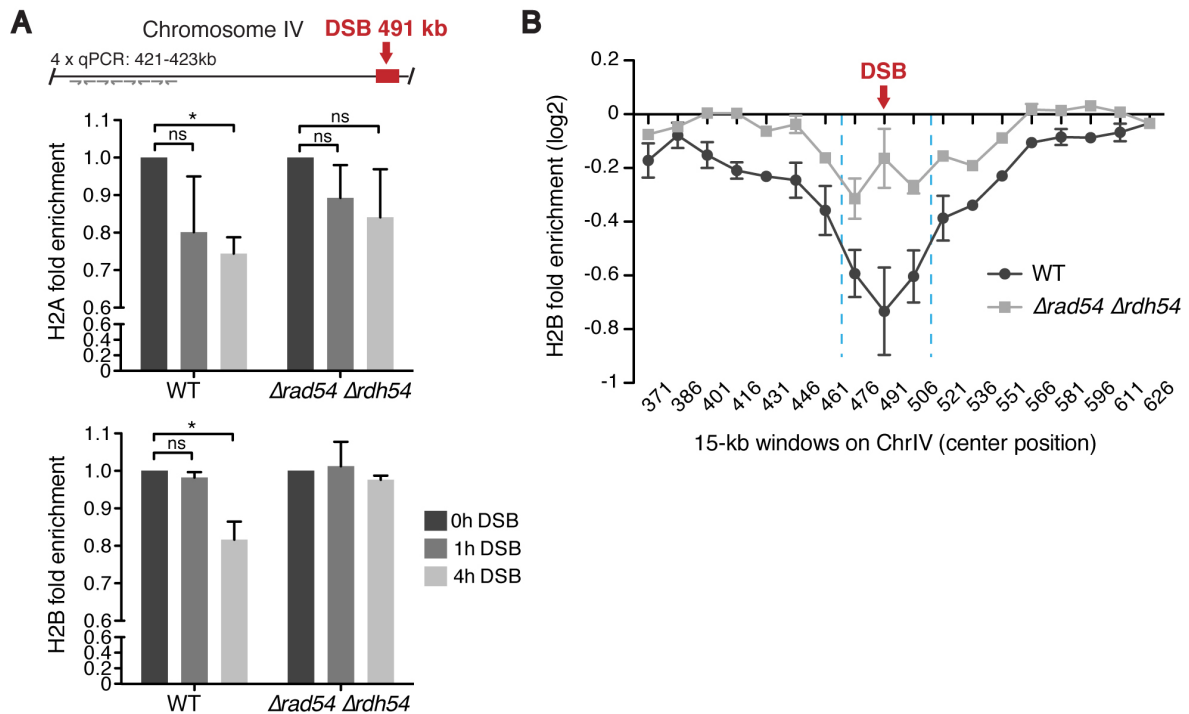


Figure 13 | Reduction in histone occupancy at sites of homology search requires Rad54 and Rdh54

(A) Time-resolved H2B ChIP following DSB induction on ChrIV at 491 kb in WT and $\Delta rad54 \Delta rdh54$ strains. Enrichments are shown for the 421-423 kb region on ChrIV, as determined by the mean of four qPCR primer pairs normalized to the mean of four random control pairs on different chromosomes. Additionally, data were normalized to a strain in which HO is expressed, but no DSB is generated. Note that data for WT strain are similar to Figure 11 B. **(B)** H2B ChIP-chip analysis 4 h following DSB induction in a similar scenario as indicated in (A). Dashed blue lines indicate the estimated area of DNA end resection.

Data represent mean plus SD (A) or SEM (B) of two independent experiments. Statistical analysis was conducted using Student's t-test with asterisks indicating $p < 0.05$. ns: not significant. All data were normalized to the time before DSB induction and qPCR data in (A) additionally to a control locus on ChrX.

In the strain expressing mutated H2A, the drop in the occupancy of this histone could not be observed anymore, while H2B still dropped like in WT cells (Figure 14 A). In contrast, the strain expressing mutated H2B showed the corresponding specific effect for H2B. Here, H2A levels remained unchanged compared to WT cells, while the drop in H2B occupancy completely disappeared (Figure 14 B). This data demonstrated that the observed drop in the occupancies of histone H2A and H2B during homology search strongly depends on their C-terminal phosphorylation. Of note, antibodies used to immunoprecipitate H2A and H2B were of a polyclonal nature. Thus, their functionality should not depend on the recognition of a single epitope at the C-terminus that would possibly be masked by phosphorylation. In line with that, a drop in H2A and H2B occupancy could still be observed when HA-tagged H2A or H2B were immunoprecipitated with an HA antibody, albeit to a somewhat weaker extent (data not shown).

RESULTS

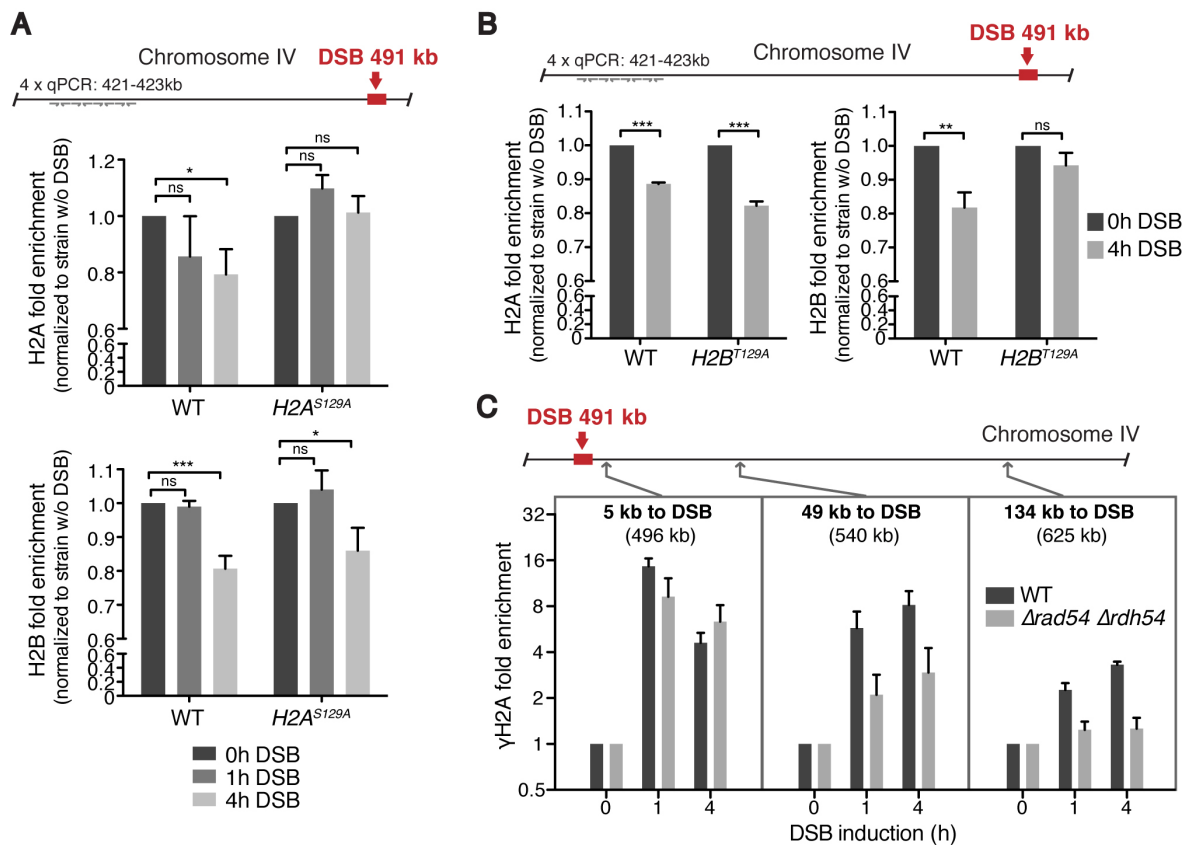


Figure 14 | Reduction in histone occupancy at sites of homology depends on the C-terminal phosphorylation of H2A and H2B

(A) Levels of a non-phosphorylatable H2A variant do not change during homology search. ChIP-qPCR analysis against H2A and H2B in WT and H2A mutant backgrounds. Enrichments are shown for the 421-423 kb region on ChrIV, as determined by the mean of four qPCR primer pairs normalized to the mean of four random control pairs on different chromosomes. Additionally, data were normalized to a strain in which HO is expressed, but no DSB is generated. **(B)** Levels of a non-phosphorylatable H2B variant do not change during homology search. ChIP-qPCR analysis against H2A and H2B in WT and H2B mutant backgrounds. Data were analyzed as indicated in (A). **(C)** DSB-distant H2A phosphorylation depends on the presence of Rad54 and Rdh54. Time-resolved γ H2A ChIP following DSB induction on ChrIV analyzed by qPCR at the indicated regions.

Data represent mean plus SD of two independent experiments. Statistical analysis was conducted using Student's t-test with asterisks indicating $p < 0.05$ (*), $p < 0.01$ (**) or $p < 0.001$ (***). ns: not significant. All qPCR data were normalized to a control locus on ChrX and to the time before DSB induction (0 h).

As a consequence of these results, I tested the possibility that Rad54/Rdh54 only indirectly influence the status of H2A and H2B levels on chromatin by promoting their phosphorylation. Evidence for this model came from earlier results that showed the formation of at least γ H2A to depend on a functional homology search, possibly via kinases bound to the Rad51 filament¹³⁶. When the induction of γ H2A was directly compared between WT and $\Delta rad54 \Delta rdh54$ cells, its accumulation was strongly reduced at sites of homology search, but not close to the DSB in the mutant compared to the WT cells (Figure 14 C). Although similar experiments could not be conducted for γ H2B due to lack of a commercially available antibody, I conclude from the results that phosphorylation

RESULTS

of H2A and H2B is likely the primary trigger for their observed remodeling at sites of homology search.

3.1.6 Homology search does not require phosphorylation-induced remodeling of histones H2A and H2B

A functional homology search process itself is responsible for the formation of both γ H2A and γ H2B, and thus for the associated decreased occupancy of these modified histones on chromatin. Following the initial hypothesis, I asked whether the same accounts *vice versa*, i.e. whether the observed chromatin remodeling is also a prerequisite for the homology search. Earlier results showed that homology search is not influenced when H2A phosphorylation (and thus drop from chromatin) is prevented⁴⁷. Yet, I hypothesized that a detectable effect might require the forced stability of both H2A and H2B. However, Rad51 ChIP experiments with yeast strains expressing non-phosphorylatable H2B or both H2A and H2B phospho-mutant variants revealed no significant changes in the homology search intensity (Figure 15 A and B). I concluded from these results that the observed large-scale chromatin remodeling accompanies the homology search, but is not a requirement for this process.

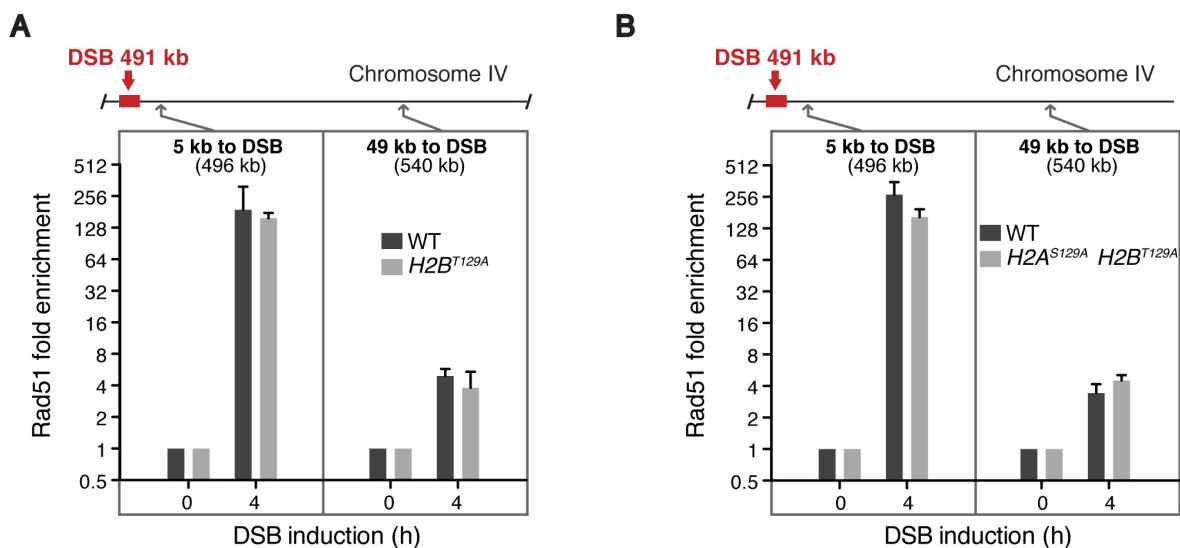


Figure 15 | **Homology search does not depend on the formation of γ H2A and γ H2B**

(A) Rad51 ChIP following DSB induction on ChrIV analyzed by qPCR at the indicated regions in WT or H2B mutant strains. (B) Rad51 ChIP following DSB induction on ChrIV analyzed by qPCR at the indicated regions in WT or H2A and H2B mutant strains.

Data represent the mean plus SD of two independent experiments and were normalized to a control locus on ChrX as well as the time before DSB induction (0 h).

RESULTS

Taken together, in the first part of this study, I established a flexible recombination assay that allows measuring recombination between any two loci in a genome either in real-time or on the absolute efficiency level. Using this assay, I proved the suitability of Rad51 ChIP as a method to measure the intensity of homology search across a genome and verified that not only the search, but also recombination is largely guided by the nuclear architecture^{47,71}. With Rad51 ChIP as a method to monitor the homology search in hand, I identified a specific involvement of the Rad54/Rdh54 proteins to promote homology search by a still unknown mechanism^{47,71}. Rad54/Rdh54-driven homology search subsequently triggers the C-terminal phosphorylation of histones H2A and likely also H2B, which results in a detectable drop of these histones from chromatin. Possible mechanisms for the Rad54/Rdh54 function, nature of and reasons for the remodeling of histones H2A and H2B are discussed in sections 4.2 and 4.3.

3.2 INO80 promotes Rad51 filament formation and recombination by removal of the histone variant H2A.Z

3.2.1 The INO80 chromatin remodeler is required for Rad51 filament formation

The determination of histone occupancy during homology search could not reveal a specific requirement of nucleosome remodeling for the homology search process. Similarly, although Rad54 and Rdh54 are novel factors specifically implicated in the search, their activity in nucleosome remodeling is rather poor and they are known to have various other activities⁶⁸. In contrast, testing an involvement of the classical, multi-subunit nucleosome remodeling complexes during homology search seemed a promising alternative to uncover a potential requirement for chromatin remodeling in this process.

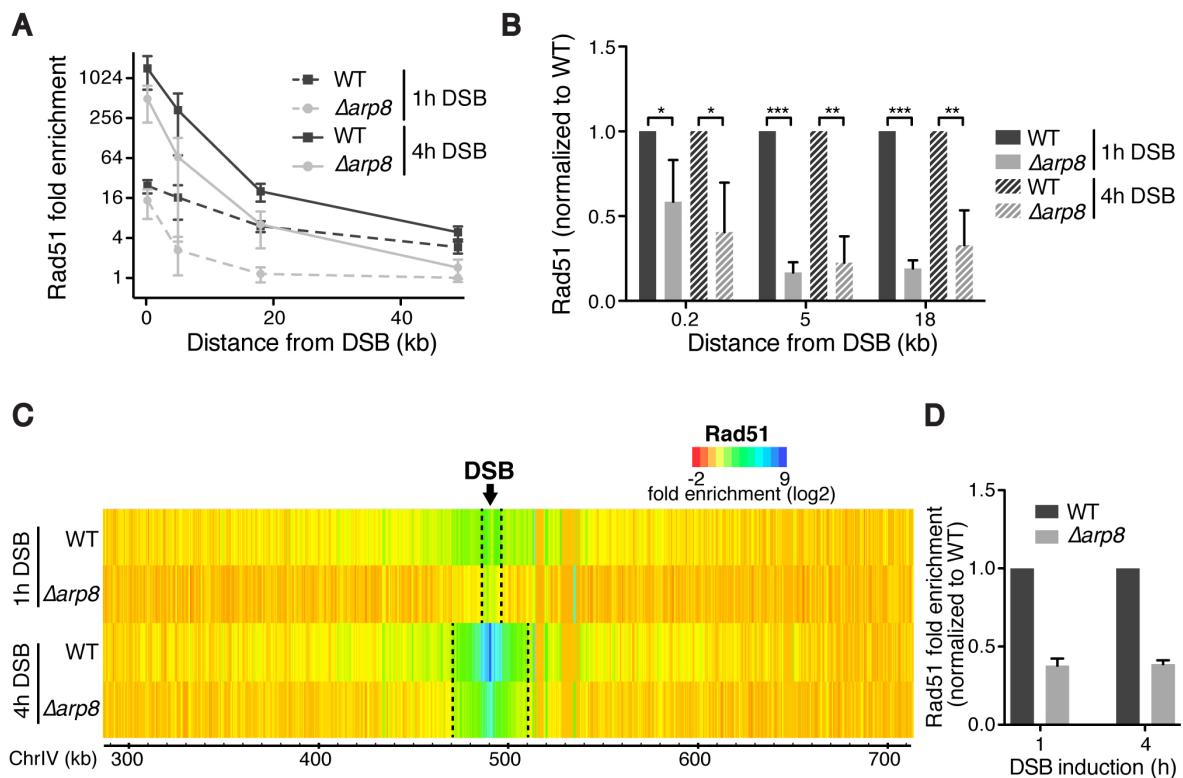


Figure 16 | **INO80 is required for Rad51 filament formation**

(A) Rad51 signals at sites of ssDNA and homology search are reduced in absence of INO80 activity. Rad51 ChIP-qPCR analysis following DSB induction on ChrIV at the indicated distances from the DSB in WT and $\Delta arp8$ strains. **(B)** Rad51 ChIP signal reduction in $\Delta arp8$ cells is statistically significant. Data from (A) were additionally normalized to the WT strain at the indicated positions and analyzed by Student's t-test. Asterisks indicate $p < 0.05$ (*), $p < 0.01$ (**) or $p < 0.001$ (***). **(C)** Time-resolved Rad51 ChIP-seq analysis following DSB induction at position 491 kb on ChrIV depicted for the 300-700 kb region. Data are depicted on a log₂ scale and dashed lines indicate the estimated area of DNA end resection. **(D)** Quantification of Rad51 enrichments in the estimated area of DNA end resection as indicated in (C).

Data in (A) and (B) represent the mean plus SD of three independent experiments. Data depicted in (C) and (D) represent mean plus SEM (only D) of two independent experiments. All data were normalized to the time point before DSB induction and qPCR data additionally normalized to a control region on ChrX.

RESULTS

To test this possibility, I generated yeast strains defective in the activities of RSC, SWR1, SWI/SNF and INO80 chromatin remodelers and analyzed time-resolved Rad51 accumulation following induction of a single DSB by qPCR. Neither absence of RSC, SWR1, nor SWI/SNF activities led to more than a delayed accumulation of Rad51 signals (data not shown). Instead, deficiency in INO80, generated by knockout of the *ARP8* gene¹⁹³, resulted in a nearly complete absence of Rad51 signals at a site of ongoing homology search ~50 kb distant to the DSB (Figure 16 A). Surprisingly however, qPCR analysis of Rad51 accumulation at further loci that mirror formation of the Rad51 filament showed that Rad51 signals were also largely diminished at these regions. Although the reduction of around 60-70 % initially seemed to be statistically not significant, signal normalization to the WT strain within each experiment demonstrated statistical robustness (compare Figure 16 A and B). The reason for this observation was the strong variation of extremely high enrichments at sites of Rad51 filament formation between different experiments (up to 2000-fold), resulting from the normalization to very low background Rad51 signals prior to the induction of the DSB. Nevertheless, I aimed to confirm these observations by monitoring Rad51 accumulation genome-wide and thus analyzed immunoprecipitated DNA by next-generation sequencing (ChIP-seq). To determine formation of the Rad51 filament, areas of single stranded DNA were estimated using previously published resection rates of 4-5 kb/h⁴², which in fact correlated well with the main Rad51 peaks at different time points following DSB induction (Figure 16 C). As determined by qPCR analysis, Rad51 levels in these areas were reduced around 60 % in mutant compared to WT cells (indicated by dashed black lines in Figure 16 C and quantified in D), and those beyond these areas, reflecting the homology search, appeared nearly entirely absent. I conclude from these data that *Δarp8* cells are defective in Rad51 filament formation and as a consequence also display a defective homology search.

I next asked whether the observed defects in Rad51 filament formation and homology search would also translate into a recombination defect of INO80-deficient cells. Using the previously established recombination assay, I determined the repair efficiency between a DSB on chromosome IV and a donor ~300 kb downstream on the same chromosome. Both the analysis of a recombination product by qPCR as well as the overall cell survival on galactose medium indicated a significant deficiency of *Δarp8* cells in completing recombination^{§§} (Figure 17 A and B).

^{§§} While this thesis was carried out, two other labs published similar (side) observations on reduced ectopic recombination in *Δarp8* cells^{130,182}.

RESULTS

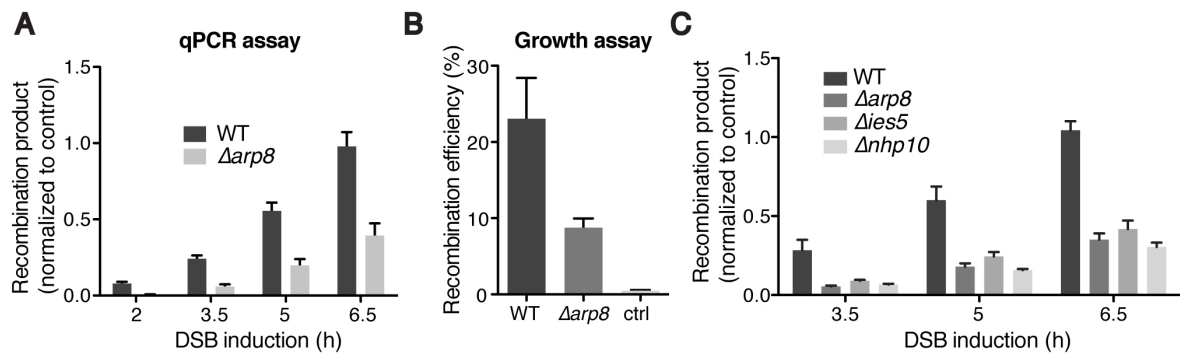


Figure 17 | **INO80 is required for efficient homologous recombination**

(A) qPCR analysis of recombination following DSB induction at position 491 kb on ChrIV using a donor at position 795 kb in WT and $\Delta arp8$ strains. (B) Recombination between the same loci as indicated in (A) measured via cell survival and including a control (ctrl) strain lacking the donor. (C) qPCR recombination analysis as in (A) including two additional INO80-deficient strains ($\Delta ies5$ and $\Delta nhp10$). All data are depicted as the mean plus SD of three independent experiments. qPCR data have been normalized to a control region on ChrX.

The strength of the defect that was measured thereby markedly correlated with the previously measured strength of defective Rad51 filament formation, indicating that these effects might be directly linked to each other. To corroborate the specific involvement of INO80 activity in the observed phenotype, I generated knockout yeast strains of two further unique INO80 subunits, *ies5* and *Nhp10*, which both showed similar defects compared to the $\Delta arp8$ strain (Figure 17 C). Removal of the catalytic subunit Ino80 appeared lethal in the genetic background used and thus an involvement of the INO80 ATPase activity in this phenotype could not be tested directly.

3.2.2 Defective Rad51 recruitment in INO80-deficient cells is independent of DNA end resection or recombination mediators

Although the observed homology search defect in absence of INO80 seemed to arise only indirectly, I decided to follow up on this finding, as it suggested a potential requirement for a chromatin remodeler at an entirely unexpected step during HR – Rad51 filament formation. To investigate whether INO80 does promote Rad51 loading directly and not indirectly via DNA end resection, I performed a similar CHIP-seq experiment as before, but as a measure of DNA end resection analyzed the distribution of RPA (RFA) along the chromatin.

As in case for Rad51, the area of the main RPA peak correlated again well with the region of ssDNA expected from general resection kinetics (compare Figure 18 A and Figure 16 C). More importantly however, RPA accumulation in $\Delta arp8$ cells showed no defect compared to WT cells and quantification even indicated slightly elevated RPA

RESULTS

levels in the mutant cells (Figure 18 A and B). This was verified by additional qPCR analysis, which indicated significantly enriched RPA accumulation in $\Delta arp8$ cells compared to WT cells directly next to the DSB (Figure 18 C). Instead of measuring DNA end resection indirectly via the accumulation of RPA, it can also be detected in a direct but non-quantitative manner via loss of DNA next to the DSB.

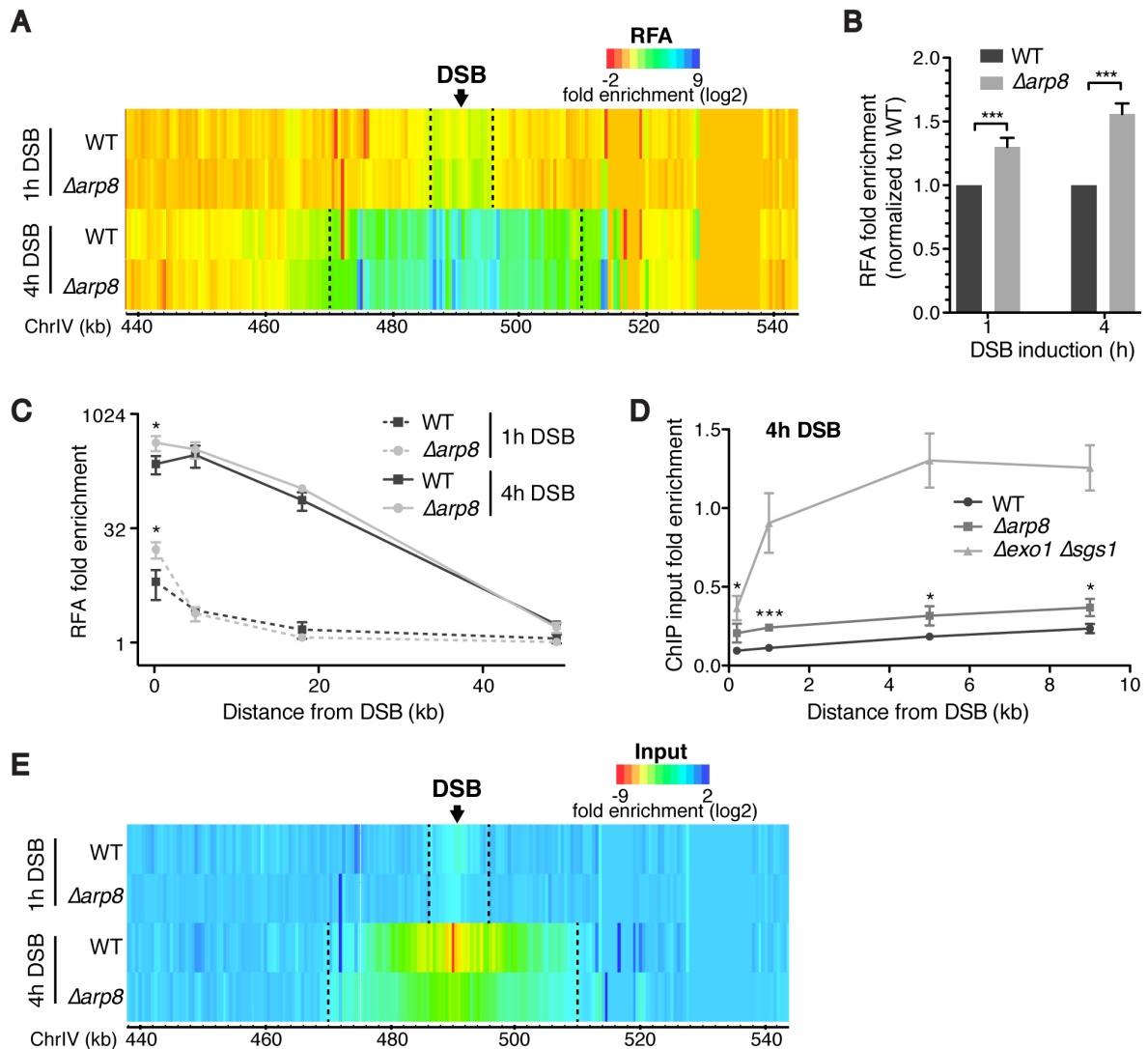


Figure 18 I Uncoupling of resection and RPA enrichment in absence of INO80 activity

(A) Slightly enriched RPA (RFA) accumulation in $\Delta arp8$ compared to WT cells. Time-resolved RFA ChIP-seq analysis following DSB induction at position 491 kb on ChrIV depicted for the 440-540 kb region. Data are depicted on a log₂ scale and dashed lines indicate the estimated area of DNA end resection. **(B)** Quantification of RFA signals in the estimated area of DNA end resection as indicated in (A). **(C)** Time-resolved RFA ChIP-qPCR analysis following DSB induction at 491 kb on ChrIV at the indicated distances from the break in WT and $\Delta arp8$ strains. **(D)** $\Delta arp8$ cells exhibit a mild DNA end resection defect. qPCR quantification of ChIP input DNA 4 h following DSB induction at the indicated distances from the break. Asterisks denote statistical difference between WT and $\Delta arp8$ strains. **(E)** Deep sequencing analysis of ChIP input DNA following DSB induction as depicted for the 440-540 kb region on ChrIV. Input from the same experiment and as depicted in (A).

Data in (A), (B) and (E) represent mean plus SEM (only B) from two independent experiments. Data in (C) and (D) represent mean plus SD of three independent experiments. Statistical analysis was conducted using Student's t-test with asterisks indicating $p < 0.05$ (*), $p < 0.01$ (**) or $p < 0.001$ (***). All data were normalized to the time point before DSB induction and qPCR data additionally to a control region on ChrX.

RESULTS

Importantly, this loss can be observed from the same RPA ChIP experiment, by solely analyzing the input DNA which is used to normalize IP enrichments¹⁶⁶. Additional comparison with cells deleted for the long-range resection factors Exo1 and Sgs1, revealed a minor, but significantly reduced drop in the ChIP input levels of $\Delta arp8$ cells compared to WT cells (Figure 18 D and E). While this minor function of INO80 in DNA end processing was reported before^{154,194}, it surprisingly did not correlate with the enrichment of RPA. The combination of these data with the reduced Rad51 accumulation observed before thus led to the conclusion that in absence of INO80 activity RPA is not properly replaced for Rad51 on ssDNA. Of note, it was recently shown that absence of Fun30 and therefore reduced end resection is beneficial for ectopic recombination events due to the prevention of RPA exhaustion¹⁷⁷, indicating that the recombination defect observed in INO80-deficient cells (Figure 17) likely comes directly through defective Rad51 loading.

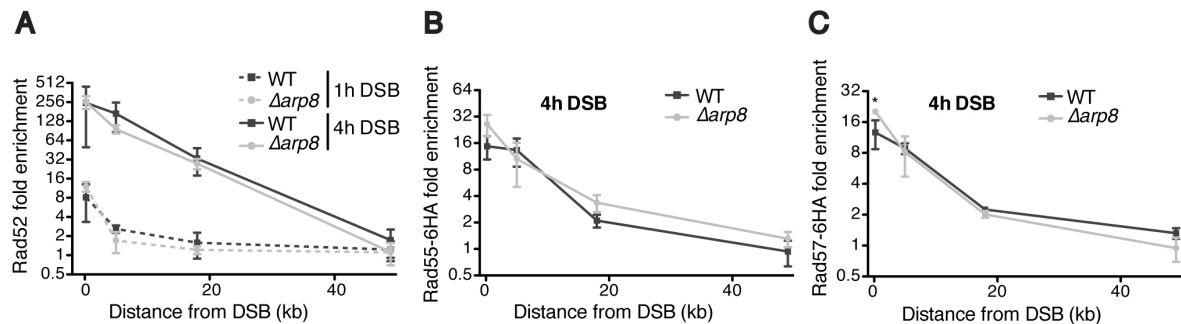


Figure 19 | Absence of INO80 activity does not influence the recruitment of recombination mediator proteins

(A) Time-resolved Rad52 ChIP-qPCR experiment following DSB induction on ChrIV at the indicated distances from the break in WT and $\Delta arp8$ strains. **(B)** HA ChIP against HA-tagged Rad55 4 h following DSB induction as in (A). **(C)** HA ChIP against HA-tagged Rad57 4 h following DSB induction as in (A).

All data are depicted as the mean plus SD of three independent experiments and qPCR values were normalized to the 0 h time point and to a control region on ChrX.

Rad51 loading at resected DNA requires a number of recombination mediator proteins and I next tested, whether the central factors Rad52, Rad55 and Rad57, were influenced by absence of INO80 activity. However, when performing ChIP experiments against Rad52 or HA-tagged Rad55 and Rad57, none of these proteins showed a defective recruitment in $\Delta arp8$ compared to WT cells (Figure 19 A-C). Instead, the filament stabilizing Rad55 and Rad57 proteins even appeared slightly enriched especially close to the DSB in $\Delta arp8$ cells.

Collectively, since the recruitment of neither RPA nor recombination mediator proteins is negatively affected in an absence of INO80, I conclude that the chromatin remodeling activity of this complex is required to promote the loading of Rad51 at DSBs by a potentially novel mechanism.

RESULTS

3.2.3 INO80 regulates H2A.Z at a DSB

I next wondered which molecular activities of the INO80 chromatin remodeler could promote Rad51 loading. Very interesting in this regard is the emerging importance of its capacity to remove the histone H2A variant H2A.Z from chromatin, which amongst other activities confers cellular resistance to replication stress¹⁶⁴.

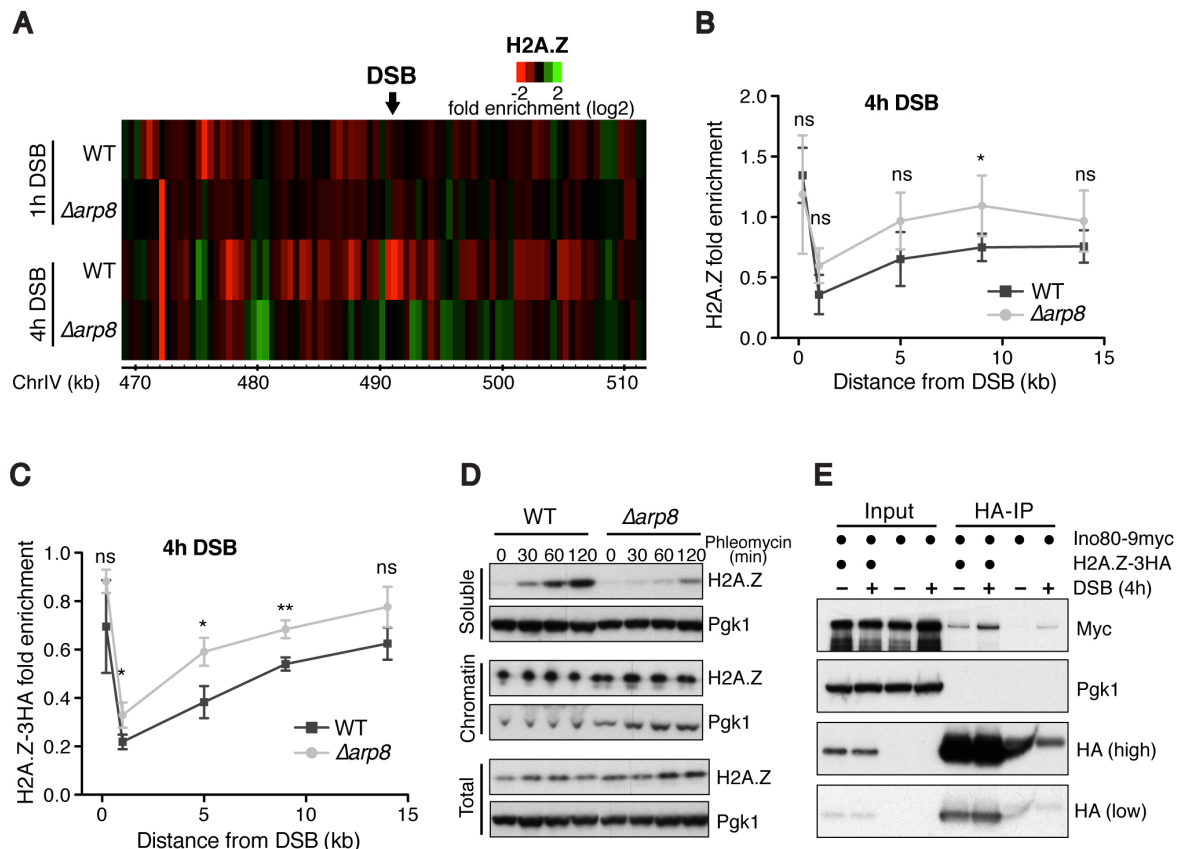


Figure 20 | INO80 removes H2A.Z from the vicinity of DSBs

(A) Time-resolved H2A.Z ChIP-seq analysis following DSB induction at position 491 kb on ChrIV in WT and $\Delta arp8$ strains depicted for the 470-510 kb region. Data are presented on a log₂ scale. **(B)** H2A.Z ChIP-qPCR analysis following DSB induction on ChrIV in WT and $\Delta arp8$ strains at the indicated distances from the break. **(C)** HA ChIP-qPCR against HA-tagged H2A.Z as indicated in (B). **(D)** H2A.Z enriches in the soluble protein fraction following DNA damage induced by phleomycin. Separation of chromatin-bound and soluble protein fractions by a sucrose-gradient and subsequent immunoblotting against H2A.Z. **(E)** H2A.Z and INO80 interact preferentially following DSB induction. Immunoprecipitation of HA-tagged H2A.Z and subsequent immunoblot analysis for the co-immunoprecipitation of myc-tagged Ino80 protein 4 h following DSB induction on ChrIV or in control cells.

ChIP-seq in (A) represents the mean of two independent experiments, ChIP-qPCR in (B) and (C) the mean plus SD of three independent experiments. All qPCR data were normalized to the 0 h time point and to a control region on ChrX.

To investigate if INO80 controls H2A.Z levels also directly at DSBs, I performed time-resolved H2A.Z ChIP-seq following the induction of a DSB on chromosome IV as done earlier for other proteins. In WT cells, H2A.Z was removed from sites next to the DSB with increasing efficiency over time (Figure 20 A). Strikingly, in the absence of INO80

RESULTS

activity, H2A.Z removal is not only dramatically diminished, but the histone variant even accumulated at certain sites along the chromosome compared to its abundance prior to DSB induction (Figure 20 A). I hypothesized that this at least partially stems from active incorporation of H2A.Z following DSB induction to promote DNA end resection and nuclear anchoring of non-repairable DSBs¹²⁵. Although loss of H2A.Z was weak compared to histone loss at promoters¹⁹⁵, I repeatedly observed similar effects via qPCR analysis, also when a HA-tagged variant of H2A.Z was immunoprecipitated using an antibody directed against the tag (Figure 20 B and C). Of note, total IP to input ratios were orders of magnitude lower when the target protein was not expressed (data not shown).

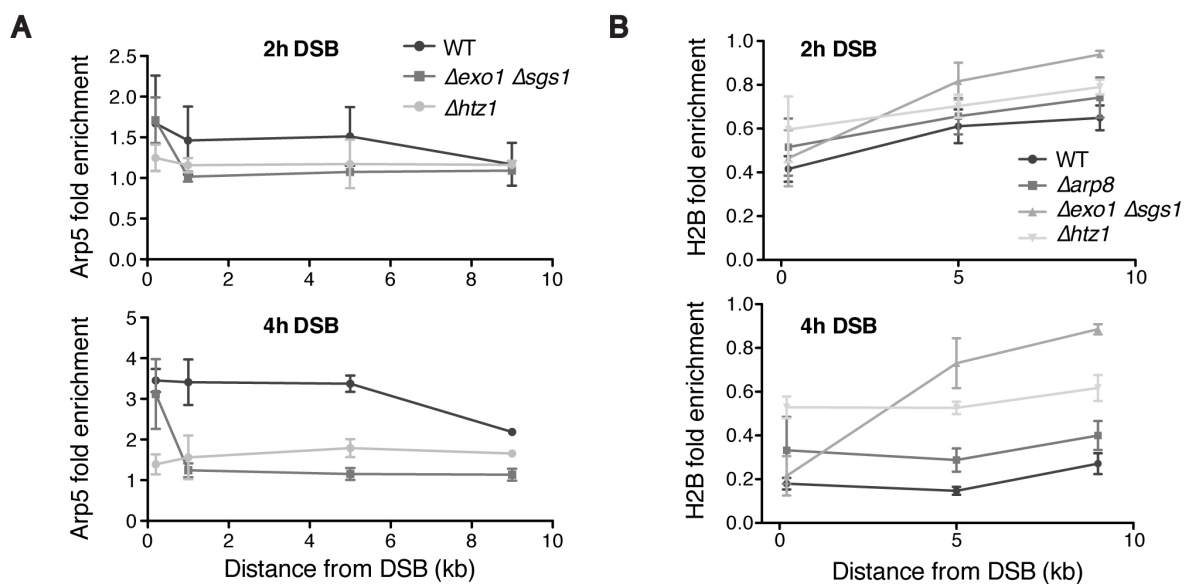


Figure 21 | H2A.Z recruits INO80 to DSBs

(A) Arp5 ChIP-qPCR analysis 2 h (upper panel) and 4 h (lower panel) following DSB induction on ChrIV at the indicated distances from the break in WT, $\Delta htz1$ and $\Delta exo1 \Delta sgs1$ strains. **(B)** H2A.Z and INO80 support the removal of histone H2B from the vicinity of a DSB. H2B ChIP q-PCR analysis as indicated in (A).

Data represent the mean plus SD of three independent experiments. All data were normalized to the time point before DSB induction (0 h) as well as to a control region on ChrX.

To test loss of H2A.Z using an independent assay, I subjected cells to DNA breaks by phleomycin treatment and observed H2A.Z removal from chromatin by cell fractionation and subsequent immunoblotting. While in WT cells H2A.Z quickly enriched in the soluble protein fraction following damage induction, $\Delta arp8$ cells showed only little soluble H2A.Z, indicative of an impaired removal of the histone variant from chromatin (Figure 20 D). However, no corresponding drop of H2A.Z was observed in the chromatin fraction, likely because the amount of H2A.Z that was shifted to the soluble pool was too low in this regard.

If INO80 catalyzes the removal of H2A.Z from DSBs, both factors should interact following DSB induction. Indeed, immunoprecipitation of H2A.Z from native protein

extracts reproducibly pulled down the INO80 catalytic subunit Ino80, with an increased interaction following DSB induction (Figure 20 E).

Because INO80 was previously reported to be involved in the removal of canonical nucleosomes from the DSB^{127,196}, I was interested in testing the primary role of INO80 activity at damage sites. To this end, I assayed for the recruitment of INO80 to a DSB by time-resolved ChIP using antibodies against the INO80 subunit Arp5. As previously reported¹⁴⁴, INO80 could be enriched at sites close to the DSB and this was dependent on the STR and Exo1 pathways of DNA end-resection (Figure 21 A). Only directly next to the DSB, where Mre11 drives end processing together with Sae2, $\Delta sgs1\Delta exo1$ cells displayed strong Arp5 recruitment. Most importantly however, INO80 recruitment to the DSB was strongly diminished in absence of H2A.Z at all analyzed genomic locations (compare WT and $\Delta htz1$ ^{***}, Figure 21 A). This indicates that H2A.Z seems to be the primary substrate of INO80 at the break and suggests that canonical nucleosomes are removed alongside with the variant. In line with this idea, cells deficient for H2A.Z expression showed a markedly reduced removal of the canonical histone H2B upon DSB induction, even exceeding the reduction observed in $\Delta arp8$ cells (Figure 21 B).

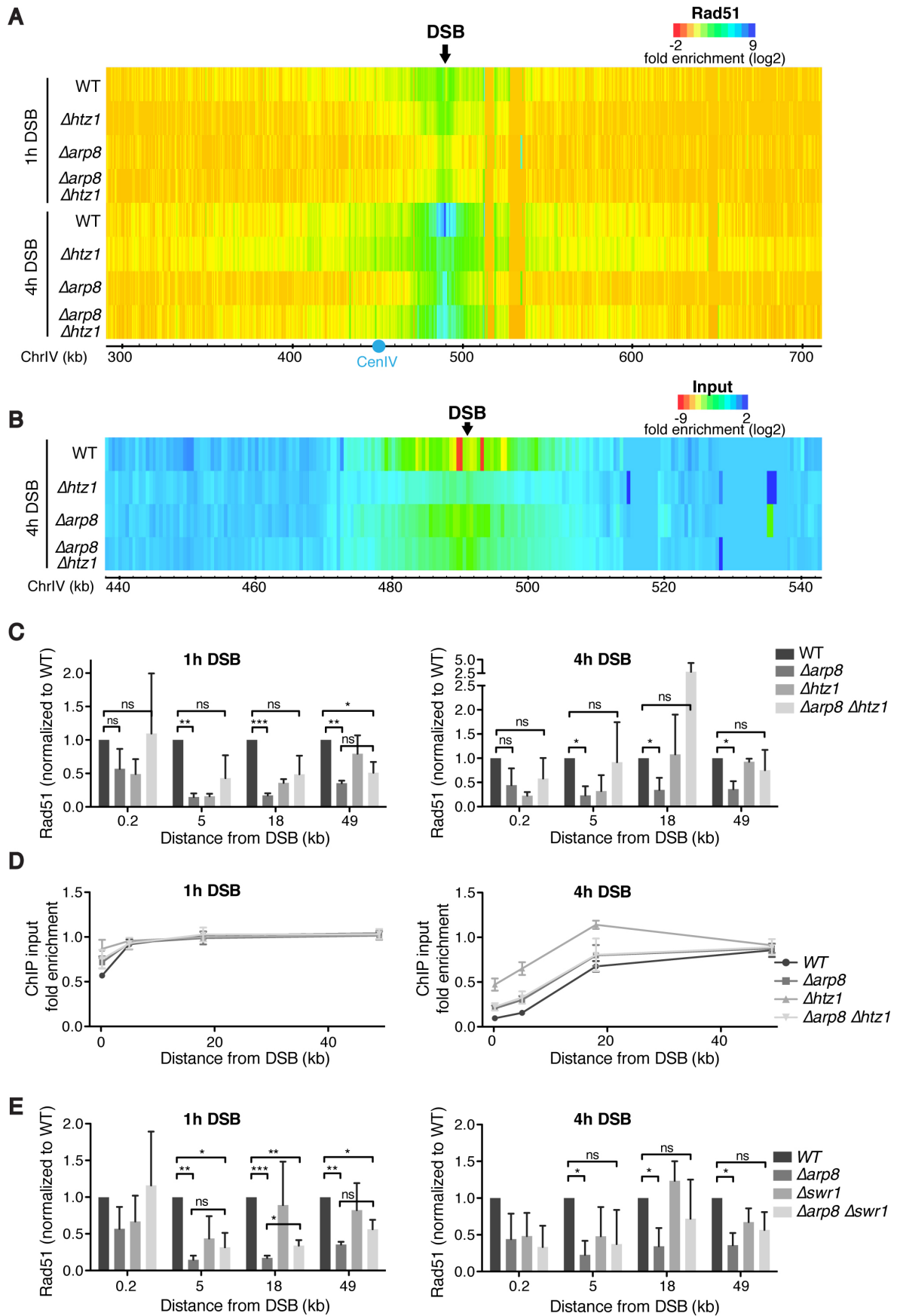
In summary, H2A.Z recruits INO80 to DSBs, which later catalyzes the removal of this histone variant from chromatin, likely together with other histones as well.

3.2.4 Removal of H2A.Z rescues Rad51 filament formation and recombination in the absence of a functional INO80 complex

Motivated by the finding that H2A.Z seems to be a major substrate of INO80 at DSBs, I wondered whether the unscheduled presence of this histone variant explains the diminished Rad51 accumulation in absence of a functional INO80 complex. To test this model, I performed time-resolved ChIP-seq experiments against Rad51 in strains lacking Arp8, H2A.Z or both proteins. Intriguingly, simultaneous deletion of *HTZ1* and *ARP8* largely rescued the defective accumulation of Rad51 signals seen in $\Delta arp8$ cells, both at sites of Rad51 filament formation and ongoing homology search (Figure 22). Analysis of input DNA levels showed that $\Delta arp8 \Delta htz1$ cells displayed a resection defect comparable to *ARP8* single knockout cells (Figure 22 B), again confirming that resection and Rad51 loading are separable events with regards to INO80 activity. While defects in Rad51 accumulation at the late 4 h time point were rescued to near-WT level, rescue at the 1 h time point was less strong, especially with respect to homology search (Figure 22 A).

*** The gene encoding for H2A.Z in *S. cerevisiae* is *HTZ1*.

RESULTS



RESULTS

Figure 22 | H2A.Z inhibits Rad51 filament formation in absence of INO80 activity

(A) Defective Rad51 filament formation and homology search in the absence of INO80 activity are rescued by additional removal of H2A.Z ($\Delta htz1$). Time-resolved Rad51 ChIP-seq analysis following DSB induction at position 491 kb on ChrIV in strains lacking Arp8, H2A.Z, or both, depicted for the 300-700 kb region on ChrIV. **(B)** Deletion of *HTZ1* in the $\Delta arp8$ background does not rescue the DNA end resection defect of $\Delta arp8$ cells. Deep sequencing analysis of ChIP input DNA otherwise as in (A). **(C)** ChIP-qPCR analysis 1 h (left panel) or 4 h (right panel) following DSB induction on ChrIV at the indicated distances from the DSB in strains lacking Arp8, H2A.Z, or both. Data were normalized to the WT strain. **(D)** qPCR analysis of ChIP input DNA from (C). **(E)** ChIP-qPCR as in (C), but in strains lacking Arp8, Swr1, or both. Data depicted in (A) and (B) represent mean of two independent experiments and are depicted on a log₂ scale. Data depicted in (D-E) represent mean plus SD of three independent experiments. Statistical analysis was conducted using Student's t-test with asterisks indicating $p < 0.05$ (*), $p < 0.01$ (**) or $p < 0.001$ (***). ns: not significant. All data were normalized to the time before DSB induction and qPCR values were additionally normalized to a control locus on ChrX.

I reasoned that this might have been due to the diminished Rad51 accumulation in the $\Delta htz1$ strain itself, probably as a direct consequence of the altered resection kinetics in this strain¹²⁵ (Figure 22 B). To corroborate the above observations, I additionally analyzed Rad51 ChIP signals at specific loci by qPCR (Figure 22 C). While Rad51 accumulation measured at sites both close and distant to the DSB was generally significantly defective in $\Delta arp8$ cells, I could not observe any significant changes in $\Delta arp8 \Delta htz1$ compared to WT cells. Surprisingly, Rad51 accumulation close to the DSB in the double mutant appeared almost normal despite clear defects in both single mutant strains (Figure 22 A and also C). While this seemed initially puzzling, analysis of ChIP input levels showed that the resection defect of the $\Delta htz1$ strain was substantially larger than the one of the $\Delta arp8$ strain, as well as the one of the double mutant (Figure 22 B and D). Although the reason for this finding was unclear, it suggests that the initial problems of Rad51 accumulation in both the $\Delta arp8$ and $\Delta htz1$ strains, which are presence of H2A.Z and delayed end resection, respectively, are overcome in the double mutant.

To further corroborate the model that unscheduled presence of H2A.Z at DSBs inhibits Rad51 loading, I assayed for Rad51 ChIP signals via qPCR in strains lacking Arp8, the catalytic subunit of the SWR1 chromatin remodeler, or both proteins. Defective Rad51 accumulation in $\Delta arp8$ cells was rescued by additional knockout of the *SWR1* gene (Figure 22 E), as in case of additional *HTZ1* deletion. Thus, not solely H2A.Z expression, but its incorporation into chromatin by the SWR1 complex represses Rad51 accumulation in the absence of a functional INO80 complex. An important observation however were the generally weaker phenotypes observed upon *SWR1* deletion than upon *HTZ1* deletion, both for Rad51 accumulation in the single mutant and combination with $\Delta arp8$ (compare Figure 22 C and E). Such a tendency was observed previously in response to various genotoxic agents¹¹⁷, and might indicate some SWR1-independent H2A.Z incorporation into chromatin.

RESULTS

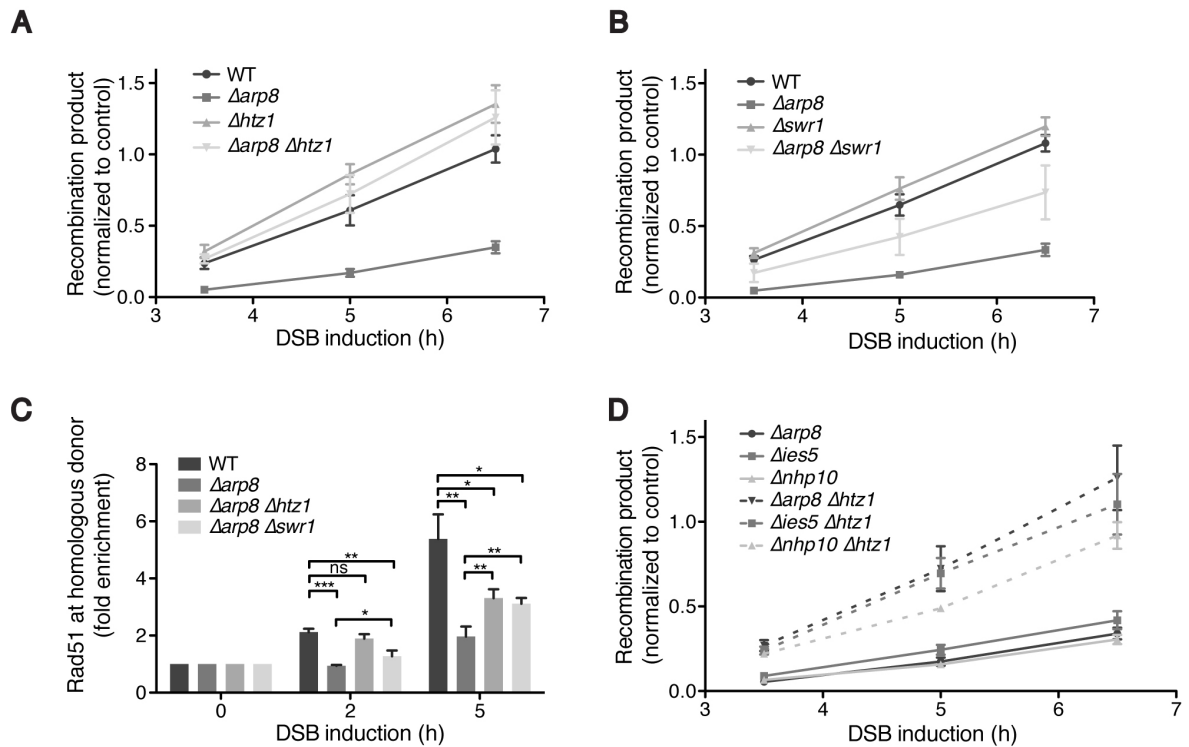


Figure 23 | H2A.Z inhibits homologous recombination in absence of INO80 activity

(A) Deletion of H2A.Z ($\Delta htz1$) rescues the recombination defect of $\Delta arp8$ cells. qPCR analysis of recombination between a DSB at position 491 kb on ChrIV and a donor sequence at position 795 kb on the same chromosome in WT strains or strains lacking Arp8, H2A.Z, or both proteins. **(B)** Deletion of *SWR1* partially rescues the recombination defect of $\Delta arp8$ cells. Analysis as in (A), but using strains lacking Arp8, Swr1, or both. **(C)** Absence of H2A.Z from chromatin partially rescues defective Rad51 accumulation at the donor in $\Delta arp8$ cells. Time-resolved Rad51 ChIP-qPCR analysis at position 795 kb on ChrIV next to the integrated donor site following induction of a DSB at 491 kb. **(D)** Deletion of *HTZ1* rescues recombination defects of various INO80 mutant strains. qPCR analysis of recombination as indicated in (A) using $\Delta arp8$, $\Delta ies5$ and $\Delta nhp10$ with or without additional *HTZ1* deletion.

All data represent the mean plus SD of three independent experiments. Statistical analysis was conducted using Student's t-test with asterisks indicating $p < 0.05$ (*), $p < 0.01$ (**) or $p < 0.001$ (***). ns: not significant. All data have been normalized to a control region on ChrX and data depicted in (C) additionally to the time before DSB induction (0 h).

I next asked whether the rescue of Rad51 accumulation in cells with H2A.Z-devoid chromatin was also sufficient to restore recombination in $\Delta arp8$ cells. To this end, I switched again to a donor-proficient test system, in which cells are able to repair an induced DSB using a donor sequence elsewhere in the genome. Strikingly, when I investigated recombination events using the qPCR-based assay described previously, the strong recombination defect of $\Delta arp8$ cells was entirely rescued in the $\Delta arp8 \Delta htz1$ double mutant cells (Figure 23 A). The same tendency could be observed in $\Delta arp8 \Delta swr1$ cells, albeit to an again significantly weaker extent, quantified to around 50 % (Figure 23 B). Interestingly, both $\Delta swr1$ and $\Delta htz1$ strains themselves showed slightly enhanced recombination levels compared to WT, reminiscent of the increased homology search signals of the H2A.Z single mutant (compare Figure 22 A). Due to the vast growth defects of the $\Delta arp8 \Delta htz1$ and $\Delta arp8 \Delta swr1$ strains, likely reflecting overlapping functions of

RESULTS

H2A.Z and the INO80 complex in other essential cellular processes¹⁶⁴, recombination could not be determined by total cell survival on galactose media. To underpin the results obtained using the PCR-based recombination assay, I additionally monitored Rad51 accumulation at the homologous donor, which is indicative of ongoing repair (compare Figure 7). Here, both the additional deletion of *SWR1* and *HTZ1* in $\Delta arp8$ cells led to a partial restoration of Rad51 signals at the donor site, with *HTZ1* deletion again having a slightly larger impact than *SWR1* (Figure 23 C). Finally, combination of *HTZ1* deletion with other INO80 complex subunit deletions as well showed robust rescues of their corresponding recombination defects (Figure 23 D), thereby underscoring the specificity of H2A.Z in inhibiting recombination in the absence of INO80.

3.2.5 H2A.Z is required for centromere-linked recombination

I wondered whether inter-chromosomal homology search would be affected similarly than intra-chromosomal homology search in the absence of Arp8, H2A.Z, or both proteins.

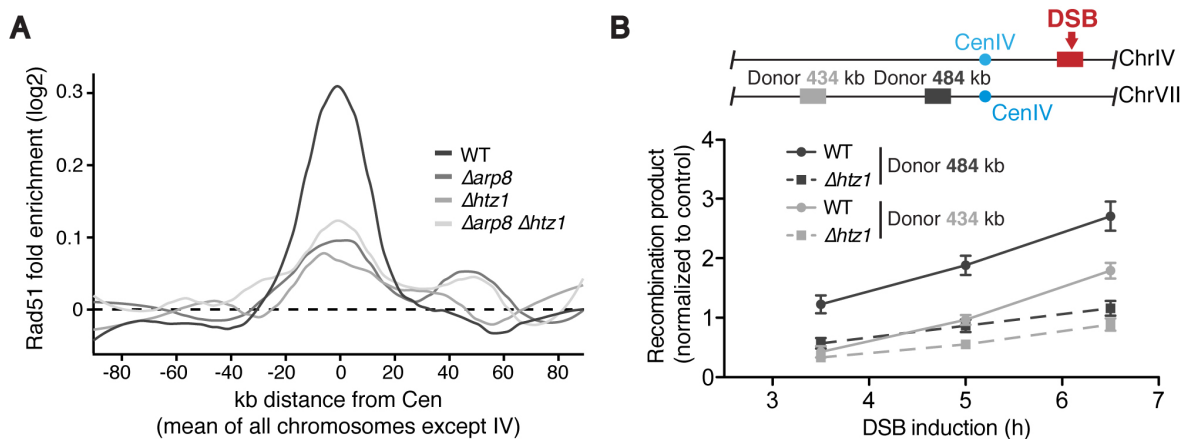


Figure 24 | **H2A.Z is required for centromere-linked recombination**

(A) Deletion of H2A.Z ($\Delta htz1$) does not rescue centromere-linked Rad51 signals in $\Delta arp8$ cells. Rad51 ChIP-seq data as depicted in Figure 22. Normalized Rad51 signals 4 h following DSB induction were calculated in the areas of 90 kb surrounding each centromere (except CenIV). Signals with similar centromere distance were averaged and the fitted curves plotted. **(B)** H2A.Z is required for recombination between centromere-linked alleles. qPCR analysis of recombination between the centromere proximal DSB at position 491 on ChrIV and two donor sites with different distances from the centromere on ChrVII.

All data represent mean of two independent experiments plus SD (only B).

Using the Rad51 ChIP-seq data generated before (Figure 22 A), I analyzed the mean efficiency of the inter-chromosomal homology search around all centromeres, excluding the one on the broken chromosome IV. As expected, the inter-chromosomal Rad51 signals in the $\Delta arp8$ strain were largely defective, similar to the case on the DSB-affected chromosome IV (Figure 24 A and Figure 22 A). Surprisingly, a comparable defect was

RESULTS

also present in the *Δhtz1* and the *Δarp8 Δhtz1* strains, despite the fact that both of these strains showed robust Rad51 accumulation on the broken chromosome and importantly around the centromere on chromosome IV. I aimed to confirm these results on the level of recombination, allowing the cells to repair the DSB induced on chromosome IV using a centromere-linked donor site on chromosome VII (compare Figure 7 E and F). Strikingly, deletion of *HTZ1* resulted in reduced recombination levels, with the strongest defect present in the strain with the donor site closest to centromere VII (Figure 24 B). Together, these results indicated the possibility that H2A.Z might be generally required for centromere-linked or inter-chromosomal recombination, although further work involving differently located homology pairs will be required to verify this hypothesis.

Collectively, in the second part of this study I identified INO80 as the first chromatin remodeler specifically involved in the formation of Rad51 filaments during HR. Absence of INO80 chromatin remodeling activity results in the unscheduled accumulation of the histone variant H2A.Z next to DSBs. H2A.Z interferes with the loading of Rad51 onto RPA-coated ssDNA, despite normal presence of canonical recombination mediators. Finally, removal of H2A.Z largely eradicates both the Rad51 filament formation as well as total recombination defects of INO80-deficient cells.

4 DISCUSSION

4.1 Homologous recombination in a three-dimensional and chromatinized environment

Since the proposal of the famous DSB repair model for recombination in 1983¹⁹⁷, the biochemistry behind the HR pathway as well as important variations from it have been well established. A multitude of key enzymes in core recombination steps such DNA end resection, presynaptic filament formation, synapsis and strand exchange as well as Holliday junction dissolution/resolution have been characterized in much detail^{49,54,64,198}. However, our detailed knowledge on recombination between two genomic sequences in vivo and especially in context of the nuclear environment has lagged behind⁷¹. Coping with the dense packaging of DNA inside chromatin, recombining within a well-defined nuclear architecture as well as balancing the activity of the pathway are key challenges for the cell in this context.

While HR predominantly takes place between sister-chromatids, also non-allelic (ectopic) recombination occurs naturally between repetitive sequences and contributes to genome evolution^{93,94}. Only recently, our laboratory identified an intriguing guidance of genome-wide homology search signals by the three-dimensional nuclear architecture⁴⁷, but it remained unclear whether this transmits to a link between recombination efficiency and genomic distance as well. Using a newly developed recombination assay to monitor HR between different genomic locations in real-time, I could indeed for the first time determine a connection between nuclear architectural elements and the efficiency of recombination. The latter is generally low between chromosomes, but I could show that it markedly increases between sites that are physically linked by centromere clustering compared to unlinked loci^{††}. Importantly, since then two other laboratories corroborated this data and extended the analysis to global correlations between contact probabilities and recombination outcome^{177,182}. Overall, in the recent years nuclear architecture has emerged as a major determinant with regards to DSB repair, thereby regulating important processes such as disease-related chromosome translocations and V(D)J recombination in lymphocytes¹⁹⁹⁻²⁰¹.

In the case of chromatin, histone modifications and variants as well as ATP-dependent chromatin remodeling complexes all play important roles in DSB repair^{202,203}. Most studies placed these factors at the beginning of the repair process where they also determine the pathway choice between NHEJ and HR, often by promoting DNA end

^{††} This data has been published in the same study as the initial homology search findings⁴⁷.

resection^{124,125,127,153-155,204}. Others reported a need for nucleosome removal at the site of the homologous donor and subsequent chromatin restoration once repair is completed^{158,160,166,167}.

Employing a combination of ChIP of DNA repair and chromatin factors in a highly controllable model system of inducible DSBs in *S. cerevisiae*, I could reveal novel functions of well-known Snf2/Swi2 family chromatin remodeling enzymes in processes of HR that were previously not directly connected to chromatin remodeling. First, I demonstrated the Rad54/Rdh54 proteins to be essential factors for the in vivo homology search process (Figure 25). Although their function could not be linked to a necessary change in the chromatin structure, I unexpectedly found that such a change is instead a consequence of the homology search. Second, I identified an intriguing function of the INO80 complex in promoting the formation of the central entity of the HR pathway – the Rad51-coated ssDNA filament (Figure 26). Surprisingly, this was independent of previously known requirements for this process, such as DNA end resection and recombination mediator proteins. Instead, INO80 removes the histone variant H2A.Z – possibly from single-stranded DNA – next to a DSB, and in cells with H2A.Z-devoid chromatin Rad51 filament formation as well as recombination do not depend on the remodeler anymore.

These data raise important questions: what is the mechanistic basis for Rad54/Rdh54 function in the homology search? What are the nature and the benefit of the remodeling of histones H2A and H2B that follow this process? How can a histone variant inhibit Rad51 filament formation downstream of DNA end resection? What is the rationale behind the role of INO80-H2A.Z in regulating Rad51 accumulation?

In the following paragraphs, I will try to address these questions by discussing them in the context of the current literature and by presenting possible mechanistic models.

4.2 Rad54 and Rdh54 function during homology search

Homology search has long remained enigmatic, mainly due to the lack of adequate methodologies that monitor this process directly. The observation that minor accumulations of Rad51 outside the area of DNA end resection correspond to snapshots of transient homology sampling then enabled for the first time the investigation of the molecular components underlying the search⁴⁷. In vitro, homology probing between isolated DNA molecules is an intrinsic capability of DNA recombinases such as Rad51 or bacterial RecA, mediated by their two different DNA binding sites^{72,73,75,205}. Instead, long-ranged cellular homology search in vivo in the context of chromatin and entire chromosomes is much more complicated and expected to have higher molecular demands⁷¹. Verifying this hypothesis, I showed that the two DNA translocases Rad54 and Rdh54 are essential components for cellular homology search. Importantly, Rad51 filament formation is normal in the absence of the two translocases, arguing for a direct contribution to the homology search process. While the activities of both proteins seem to be at least partially redundant in this regard, the underlying mechanism is still unclear and several models can be envisioned (Figure 25). A possible explanation for the involvement of Rad54 and Rdh54 in the homology search is that both proteins use their intrinsic nucleosome remodeling activities to make homology probing more efficient^{188,206,207} (Figure 25 C, 1). Although this model cannot be entirely excluded, I could not link any specific chromatin remodeling event at sites of homology search to Rad54/Rdh54 so far. Alternatively, the high translocation processivity of both enzymes on dsDNA^{208,209} might not be used to remodel nucleosomes, but to increase the transient strand opening of DNA via supercoiling²¹⁰, thereby facilitating access of the Rad51 secondary DNA binding site to the target DNA (Figure 25 C, 2). In fact, a requirement for negative supercoiling of the target DNA has been observed during in vitro recombination experiments with the bacterial RecA protein^{75,211,212} and along that line the capacity of target DNA breathing seems to be beneficial when it comes to homology recognition⁷⁶. A third, more provocative possibility is the idea that Rad54 and Rdh54 could function as motor proteins, increasing the processivity and directionality of presynaptic filament sliding along the target DNA (Figure 25 C, 3)⁷⁷. This could be mediated by the direct interaction of both translocases with Rad51^{213,214}.

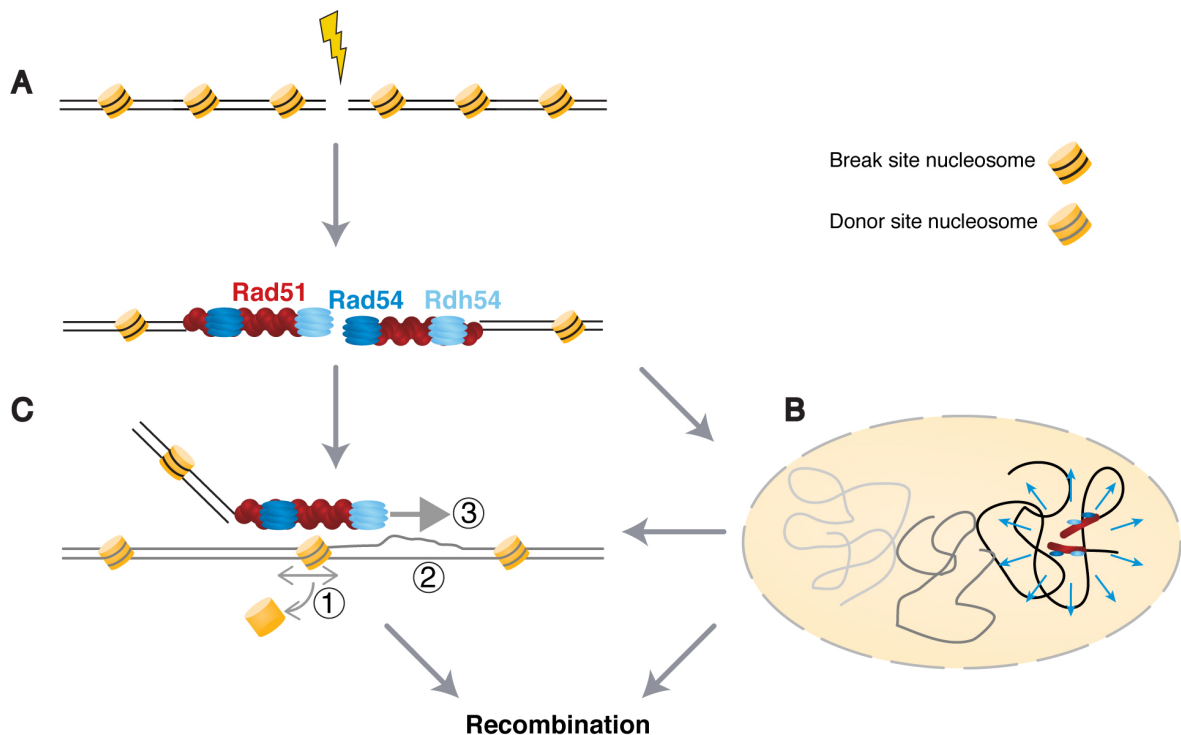


Figure 25 | **Potential mechanisms for the function of the Rad54 family proteins during homology search**

(A) DSB induction results in the formation of Rad51 filaments with sub-stoichiometric amounts of Rad54 and Rdh54 bound to it. Rad54 and Rdh54 presumably form hexameric ring-shaped structures, which enable their efficient translocation on dsDNA^{209,215}. (B) At an initial level, at least Rad54 is required for a DSB-induced chromatin mobility, which might play a role in mediating proximity between Rad51 filament and target DNA. (C) Once target DNA is nearby, Rad54 and Rdh54 could act by several means to enhance the efficiency of homology probing. First, although not observable during this study, both proteins could use their chromatin remodeling activity to enhance homology probing (1). Second, translocation-induced DNA supercoiling could generate ssDNA bubbles, acting as entry points for the Rad51 secondary binding site to sample target DNA (2). Third, robust translocation could act as a pulling force for the entire Rad51 filament and enhance its interaction with the target DNA, thus maximizing search efficiency (3).

All three proposed models place the role of both translocases directly at the site of the search, consistent with my finding that they exert their function while interacting with Rad51. Consequently, their absence would not affect the long-range homology search itself, but only the direct homology probing of the *in vivo* substrate. However, I observed that absence of Rad54 and Rdh54 also reduces the phosphorylation of histones H2A and likely also H2B, which follow the homology search. Assuming that these phosphorylation events would only require local proximity between the presynaptic filament and target histones (for further information see section 4.3), an additional or even completely different function for both proteins in enabling the presynaptic filament not only to locally probe, but also initially reach the target DNA sites would be required. Notably, such a role could be linked to the requirement of Rad54 in induced chromatin mobility at DSBs⁹⁶ (Figure 25 B). Although the majority of this mobility seems to be attributable to a DSB-

DISCUSSION

induced relief of centromeric constraints that is not necessary for the homology search¹⁰², Rad54 could still perform an independent function in this regard.

Interestingly, I also found that recombination can be enhanced by increasing the expression of Rad54; but paradoxically, increased Rad54 levels are not beneficial for cell survival *per se*²¹⁶. Thus, protein functionalities have to be specifically fine-tuned to allow the best possible outcome on the cellular level, although this might include a reduced capacity to essentially repair DNA damage on the molecular level.

4.3 Chromatin remodeling at sites of homology search

Active homology search induces the DSB-distant generation of γ H2A and likely also γ H2B^{47,192}. While it was a long-standing belief that chromatin modifications catalyzed by DDR kinases spread in a linear fashion on the broken chromosome, this picture now turns into a model in which these modifications are set onto large parts of DSB-surrounding chromatin in the three-dimensional space^{136,217,218}. In this study, I could show that the large-scale induction of γ H2A and γ H2B upon induction of a single DSB results in a reduced interaction of these histone molecules with DNA and that this event might contribute to an opening of the chromatin structure at the respective sites. There are important questions arising from these findings: how is this change in the chromatin structure achieved? What is its specific nature? What is it good for?

The presynaptic filament required for the homology search and subsequent strand invasion is not a sole entity between ssDNA and recombinase proteins. Instead, many repair proteins, once recruited to a DSB, remain there for hours, still binding after the Rad51 filament has been assembled^{47,55}. Among these molecules are the upstream DNA damage-response kinases Mec1 and Tel1 (mammalian ATR and ATM, respectively), which catalyze γ H2A and γ H2B formation. Thus, traveling of these kinases together with the filament brings potential substrates into their close physical proximity^{136,217}, which might be already sufficient for the modification of nearby histones. However, my finding that also Rad54/Rdh54 are required for the phosphorylation of at least H2A, could imply an additional need for transient homology sampling to further increase proximity or prolong interaction time with the substrate. Either way, phosphorylation results in a ChIP-detectable reduction in the occupancy of these histones with DNA. What does this tell us for the whole nucleosome? (H3-H4)₂ tetramers are considerably more stable on chromatin than H2A-H2B dimers²¹⁹⁻²²². However, the fact that H2A or H2B loss can be detected independently of each other in the respective phosphorylation mutants excludes a model in which H2A-H2B dimers are selectively lost from these sites. Also, H2A and H2B are always disassembled from or deposited onto DNA as obligate heterodimers^{109,223} and to my knowledge there has been no report in the literature on conditions where solely H2A or H2B molecules are lost from nucleosomes. Thus, the ChIP results most likely account for conditions in which DNA-histone interactions are weakened and as a consequence nucleosomes are more flexible and unstable. In line with this model, γ H2A formation has been previously associated with an intrinsic destabilization of nucleosomes both in yeast and mammals (here γ H2AX)^{140,168,224}. Local chromatin flexibility might be further enhanced by additional phosphorylation of cohesin, whose mobility on DNA is increased by this

DISCUSSION

event²²⁵. Mine as well as earlier results⁴⁷ demonstrated that this increased chromatin flexibility does not promote the homology search itself, however. Accordingly, yeast strains expressing both non-phosphorylatable H2A and H2B are generally not sensitive towards genotoxic agents¹⁹². It remains to be shown whether the same applies for survival upon ectopic recombination, which could not be tested in this study due to repeating problems in generating the respective yeast strains. Instead of promoting recombination directly, γ H2A and γ H2B may trigger an enhanced DNA damage checkpoint response, both through protein-protein interactions²²⁶ and the observed increasing chromatin flexibility¹⁰².

4.4 The histone variant H2A.Z inhibits Rad51 filament formation

The presented work places INO80 as the first chromatin remodeling complex that is directly involved in the loading of Rad51 at resected DNA (Figure 26). While this finding was surprising, there is supporting evidence from other groups. First, the remarkable initial discovery that histones are removed alongside a DSB dependent on the INO80 complex included a finding that showed also Rad51, but not RPA recruitment to a DSB to require this remodeler¹⁹⁶. The speculative conclusion that this might be due to a defective recruitment of Rad52 could however be disproved in the present study, as well as the idea that Rad51 recruitment is linked to the observed removal of canonical nucleosomes per se. Second, a recent study in mammalian cells reported a reduced number of Rad51, but not RPA foci, upon DNA damage in absence of INO80 function. Under similar conditions, also sister-chromatid recombination was defective and in both cases, this depended on the presence of H2A.Z^{227, †††}. Although the microscopic analyses carried out in that study give limited information about the detailed chromatin binding status of repair proteins, the combination with the presented data in this thesis allows important conclusions. First, the INO80-H2A.Z axis regulating recombination on the level of Rad51 is evolutionary conserved. Second, INO80-H2A.Z regulation seems important for repair of drug-induced and endonuclease-induced DSBs. Third, absence of INO80 activity likely completely blocks Rad51 filament formation in a subset of cells. The reduced ChIP signals over the average of a cell population presented in this study could similarly reflect a scenario in which all cells only assemble a shorter or patchy filament. However, both the total reduction in number of Rad51 foci in the mammalian system, as well as the strikingly similar strength of defective Rad51 signal accumulation and recombination, support the former model. Consequently, the intriguing question arises how a specific histone variant can inhibit the loading of Rad51 onto single-stranded DNA, and in principle, two scenarios can be envisioned in this regard.

In the first scenario, H2A.Z directly interferes with Rad51 loading by modulation of DSB binding proteins. On the one hand, this could involve an inhibition of pro-recombinogenic proteins, such as Rad51 itself or recombination mediators⁵⁴. On the other hand, it might favor the recruitment of proteins with anti-recombination activity²²⁸. A direct interference of H2A.Z and Rad51 appears hard to imagine, as this could only happen directly adjacent to a nucleosome and Rad51 should still be loaded properly in between those. In fact, it was recently hypothesized that presynaptic filaments might remain

††† This publication appeared after the key findings on INO80 and H2A.Z presented in this study had already been made.

DISCUSSION

nucleosome-covered, taking into account the discrepancy between actual experimental results and current models depicting nucleosome-free resected DNA²⁰³. Consistent with data presented in this study, nucleosome loss next to a DSB has previously been shown to be poor compared to inducible promoters¹⁹⁵. This is especially true for sites exceeding a distance of one or two nucleosomes away from the break^{127,153,196}. With regards to recombination mediators, increased H2A.Z levels alter neither Rad52, nor Rad55 or Rad57 binding to the DSB. Nevertheless, recently identified additional mediators such as members of the Shu complex⁶⁰ might play a role in this regard and it will be interesting to test their recruitment in INO80 mutants. Interestingly, my preliminary experiments point to a rescue of Rad51 accumulation in INO80-deficient strains upon deletion of the yeast anti-recombinase *SRS2*^{65,66} (data not shown). However, these experiments are difficult to interpret, as already *SRS2* single deletion strains appear to have strongly increased Rad51 levels at both sites of filament formation and homology search. Conversely, these strains are defective in ectopic recombination, likely due to problematic resolving of Rad51 joint molecules or Rad51 filaments stuck at non-productive microhomologies^{79,229}. Also, no specific interaction between H2A.Z and Srs2 was reported so far^{§§§}. Overall, the mass spectrometry approach I conceived to detect differential protein binding to ssDNA at a DSB could not identify significant differences in the interaction profiles of WT and $\Delta arp8$ cells (data not shown), thus demanding alternative explanations.

An alternative model is that pronounced presence of H2A.Z indirectly suppresses Rad51-mediated HR, resulting in delayed recombination or the usage of a completely alternative repair pathway. I hypothesize that such an indirect suppression could act via a H2A.Z-dependent translocation of the DSB to a more recombination-repressive compartment (Figure 27). Indeed, the histone variant contributes to the anchoring of DSBs to the nuclear pore, where classical recombination is suppressed^{125,129,130,230}. This suppression seems to involve a mechanism dependent on the SUMO-targeted ubiquitin ligases Slx5/Slx8, and my preliminary data indicate that the recombination defect of $\Delta arp8$ cells can be partially rescued by absence of either the Slx8 protein or the SUMO ligases Siz1 or Siz2. This scenario could also take into account why Rad51 loading at probably only some, but not all DSBs is affected in the absence of INO80 activity, which is hard to envision for the direct modulation of protein-protein interactions at the DSB. Instead, a timely competition between the arrival of the DSB in the recombination suppressive compartment and Rad51 loading could arise, shifting the balance to the one or the other side (see also section 4.5).

^{§§§} As annotated in the *Saccharomyces* Genome Database (<http://www.yeastgenome.org>)

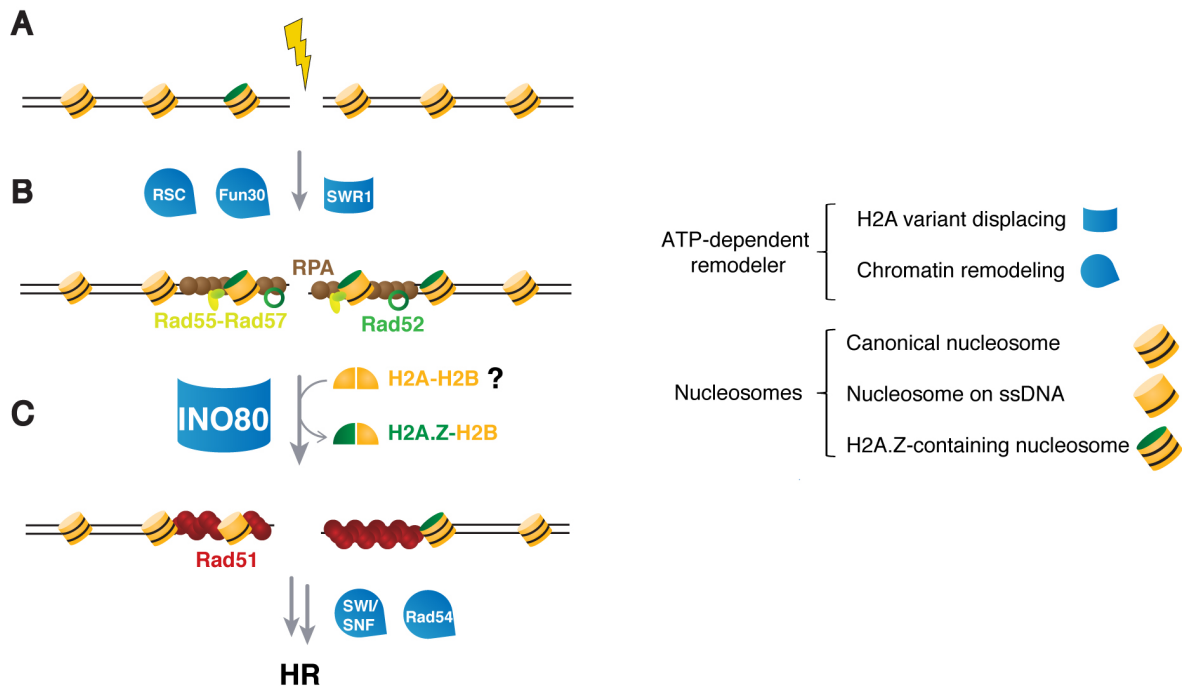


Figure 26 | **INO80 promotes Rad51 filament formation by removal of H2A.Z.**

(A) A DSB is generated by exogenous or endogenous sources. (B) A number of chromatin remodeling enzymes help to promote DNA end resection, yet some nucleosomes may remain bound to ssDNA. Resected DNA is covered by RPA, which recruits recombination mediator proteins. Mediators are not sufficient for Rad51 loading in presence of the variant histone H2A.Z. (C) INO80 removes H2A.Z, which promotes Rad51 filament formation and allows HR to be completed. It is unclear whether H2A.Z-containing nucleosomes are entirely removed or exchanged for canonical H2A-H2B dimers.

Whatever the mechanism is, the problem boils down to one question: what differentiates H2A.Z from canonical H2A? Although H2A.Z fulfills a plethora of specialized functions inside a cell and is an essential protein in higher eukaryotes¹¹⁸, there is no simple answer to this question in general and in particular regarding recombination. Studies with the *Drosophila melanogaster* H2A.Z protein have shown that only mutation of the C-terminal so called M6 region does not rescue the embryonic lethality of the null mutant²³¹. In fact, this region is required for incorporation into chromatin¹¹⁹ and thus, once part of the chromatin, it remains largely unclear which regions make H2A.Z that specific. Although due to subtle changes in the crystal structure H2A.Z-containing nucleosomes are believed to be rather unstable, it remains unclear which amino acids exactly mediate this difference. Furthermore, biochemical and biophysical experiments gave contradictory outcomes regarding the stability of variant-containing nucleosomes²³²⁻²³⁶ and it is likely the general chromatin context that determines the physical outcome of H2A.Z incorporation¹¹⁸. Along that line, the comprehensive region-swap analysis that I performed to generate multiple partially H2A-like H2A.Z variants, revealed only the M6 region as clearly important in inhibiting recombination, with some inconsistent tendencies for the N-terminal part as well (data not shown). Since the M6 mutation functionally mimics the

DISCUSSION

deletion of *SWR1*, which does not allow H2A.Z incorporation into chromatin, these data do not allow any conclusion on the function of H2A.Z once it resides inside the chromatin. Further work will be required in this regard, emphasizing the fact that the identification of a non-recombination suppressive H2A.Z variant would surely be beneficial for understanding the mechanism behind the inhibition as well.

4.5 An INO80-H2A.Z axis regulating recombination activity

The complexity of the INO80-dependent regulation of H2A.Z at DSBs is unclear. On the one hand, the anti-recombination function of H2A.Z could be a simple, accidental cost for the desired functions of this histone variant in other cellular pathways, such as gene transcription¹¹⁸. This “passive activation model” (Figure 27 A) would go along with a standardized requirement for INO80 and the concomitant removal of H2A.Z during any recombination event at a DSB. On the other hand, H2A.Z could be used as an intended tool to adapt the activity of HR to specific repair situations. This “active regulation model” (Figure 27 B) would assume a possibility to adapt at least either H2A.Z levels or the activity of INO80 at the DSB, better still both.

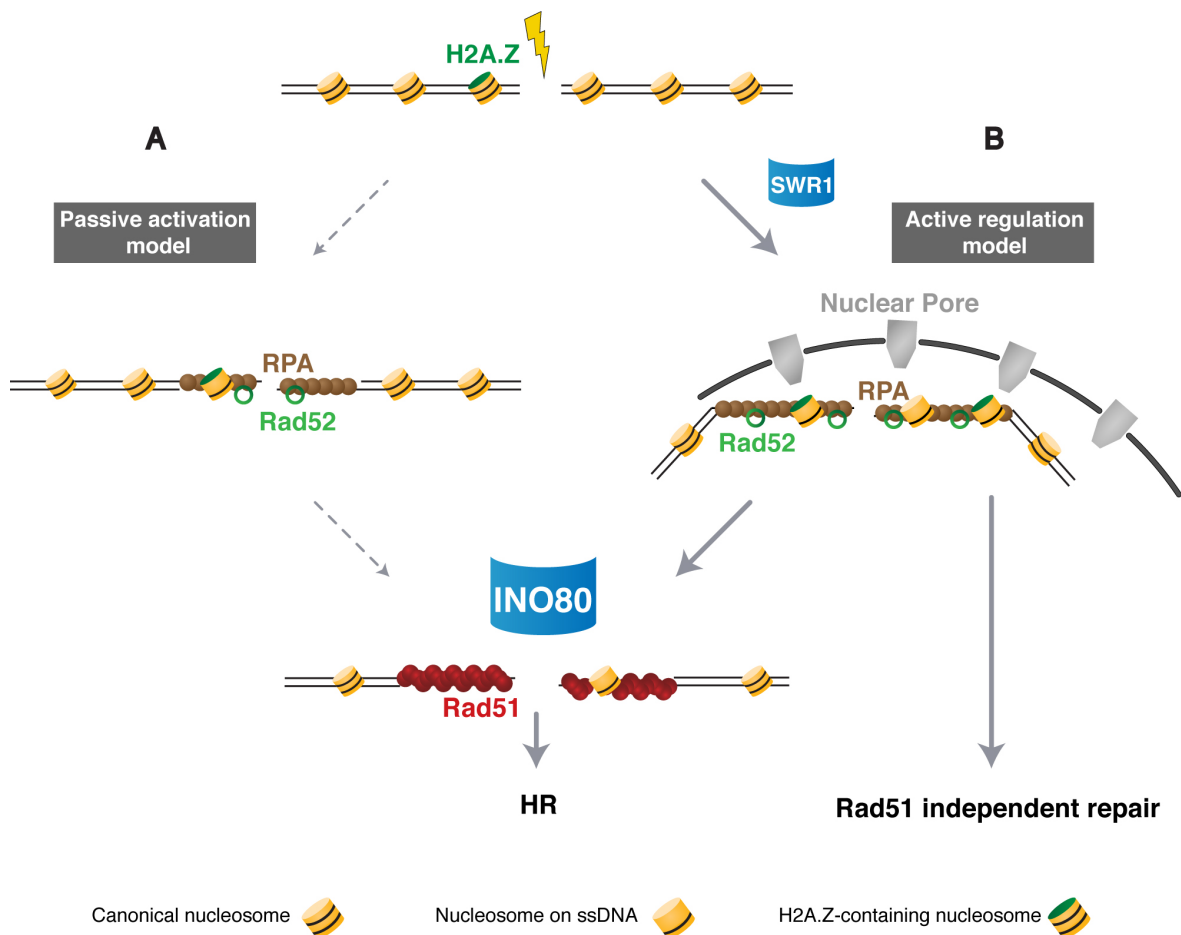


Figure 27 | **A hypothetical model for the function of the INO80-H2A.Z axis during HR**

A DSB is generated at an endogenous locus, flanked by canonical and H2A.Z-containing nucleosomes. **(A)** Intrinsic H2A.Z interferes with Rad51 loading during every HR event and INO80 is required to counteract this inhibition. This passive activation model is unlikely to be true (indicated by dashed arrows). **(B)** Active regulation model: a subset of complex DSBs require more time for their repair. Prolonged resection leads to enhanced incorporation of H2A.Z by SWR1, which fosters relocation of damage sites to the nuclear periphery. Constant suppression of Rad51-mediated HR at the nuclear pore can result in Rad51-independent repair. Alternatively, active regulation of INO80 in this model triggers H2A.Z removal and release of the Rad51 block, allowing completion of canonical HR.

DISCUSSION

Several lines of evidence argue against the passive activation model and support the active regulation model, which I will outline in the following. At first, INO80 is not a *bona fide* recombination factor. It is neither required for mating-type switching in yeast^{126,237} nor for spontaneous sister-chromatid recombination or allelic recombination in diploids^{227,237}. In contrast, the remodeler becomes important when the latter two events are measured after damage induction with MMS²³⁷ or MMC²²⁷, which both induce DSBs at (long-term) stalled replication forks²³⁸. Moreover, this and other studies showed an involvement of INO80 in ectopic recombination^{130,182}. While repair of ectopic donors or collapsed forks can be slow and take several hours, sister chromatid recombination and mating-type switching are rather fast events due to specialized chromosome conformations^{91,191}. Altogether, this speaks for a model in which INO80 function is important for the repair of a subset of “difficult-to-repair” DSBs. In line with the previously proposed mechanistic model of INO80-H2A.Z balancing the targeting of DSBs to the nuclear periphery, it is exactly such DSBs, also at collapsed replication forks, that are anchored at the nuclear pore^{125,129}.

How would the regulation take place at such breaks? One possibility to modulate initial H2A.Z levels is via the incorporation of the histone variant to promote DNA end resection and chromatin opening^{124,125,128}. In agreement, I also found increased levels of H2A.Z next to a DSB in an INO80 mutant following damage induction. Although it will require methods to formally distinguish pre- and post-DSB incorporated H2A.Z molecules to reveal the true source of the inhibitory H2A.Z, at least for mammalian cells it was suggested that failure to remove the post-DSB H2A.Z pool interferes with subsequent repair outcome^{171,227}. Thus, the longer repair takes and the further resection will go²³⁹, the more important the activity of INO80 would become. Cells could then carefully and continuously unleash recombination activity and “buy time” to avoid toxic aberrant recombination events in such scenarios (Figure 27 B). Indeed, INO80 binding to the DSB constantly increases for several hours after induction of irreparable DSBs^{144,194}. Consequently, a lack of the ability to use H2A.Z as a potential recombination constraint should cause negative effects. My preliminary experiments show that expression of a non-acetylatable H2A.Z variant in INO80-defective cells partially rescues ectopic recombination (data not shown). By contrast, the same variant reduces cell survival following prolonged replication fork stalling in absence of INO80 activity, and here, knockout of the recombination promoting H2A.Z de-acetylase is beneficial¹⁶⁴.

In summary, the requirement of INO80 for removal of H2A.Z at DSBs is likely limited to specific types of lesions. H2A.Z might be specifically used to inhibit Rad51

DISCUSSION

filament formation at these sites, possibly by delaying recombination or allowing the usage of an alternative repair pathway. Eventually, this regulation will result in the best condition to promote cellular survival. The development of sophisticated, image-based and detailed repair systems to follow the fate of specific lesions will undoubtedly be essential to our future understanding of this regulation.

After decades of research, HR remains an intriguingly complex and sophisticated pathway to repair DNA breaks and exchange genetic information. This study adds important new insights into the pathway and expands our view on the importance of an adaptation to the variety of complications that it faces inside the nucleus. Future studies will further broaden our horizon, and eventually this will give us better chances to fight the many diseases that have underlying genetic defects in HR.

5 MATERIALS AND METHODS

Unless mentioned differently, materials, chemicals and reagents were purchased from Agilent, BD, Biomol, Bioneer, Bio-Rad, Eppendorf, Eurofins Genomics, GE Healthcare, Life Technologies, Merck, New England Biolabs, PeqLab, Promega, Qiagen, Roth, Roche, Sarstedt, Serva, Sigma or Thermo Fisher Scientific. Flasks, solutions, and de-ionized water were sterilized before use for all the described procedures. Basic microbiological, molecular biological and biochemical techniques followed standard protocols or instructions provided by the manufacturer^{240,241}.

5.1 Microbiology

5.1.1 *Escherichia coli* (*E. coli*) techniques

E. coli strains were cultivated at 37°C either in liquid LB medium or on LB agar plates. Liquid culture density was determined photometrically via absorption at 600 nm (OD₆₀₀).

E. coli strains

Strain	Genotype	Source
XL1-Blue	<i>recA1 endA1 gyrA96 thi-1 hsdR17(r_K⁻m_K⁺) supE44 relA1 lac [F' proAB lacIqZΔM15 Tn10 (Tetr)]</i>	Agilent
Mach1™ T1 ^R	<i>F Φ80(lacZ)ΔM15 ΔlacX74 hsdR(r_K⁻m_K⁺) ΔrecA1398 endA1 tonA</i>	Life Technologies

E. coli media

LB medium/plates

- 1 % (w/v) trypton
- 0.5 % (w/v) yeast extracts
- 1 % (w/v) NaCl
- 1.5 % (w/v) agar (only for plates)
- sterilized by autoclaving

For plasmid selection, 100 µg/ml ampicillin was added to media or plates.

Competent *E. coli* cells

For the preparation of electro-competent *E. coli* cells, 1 l pre-warmed LB medium was inoculated to an OD₆₀₀ of 0.05 from a fresh overnight culture (starting with cells from the commercially available stock) and grown to a final OD₆₀₀ of 0.6-0.8 at 37°C. Subsequently, bacteria were chilled on ice for 30 min and cells were harvested by centrifugation (3000 g,

10 min, 4°C). The bacterial pellet was carefully resuspended in 0.5 l of pre-chilled water and subsequently washed three times with 0.5 l of pre-chilled 10 % (v/v) glycerol. After a final washing step with 50 ml of 10 % (v/v) glycerol, bacteria were resuspended in 3 ml 10 % (v/v) glycerol, 50 μ l aliquots snap-frozen in liquid nitrogen and long-term stored at -80°C.

Transformation of *E. coli* cells

To transform *E. coli* cells via electroporation, 50 μ l cells were thawed on ice immediately before transformation and ~100 ng of plasmid DNA or 8 μ l of a dialyzed ligation reaction (see section 5.2.3) added to the cells. The mixture was transferred to pre-chilled electroporation cuvettes (0.1 cm electrode gap; Bio-Rad) and electroporated with a pulse of 1.8 kV and 25 μ F at a resistance of 200 Ω using a Gene Pulser X-cell (Bio-Rad). Immediately after electroporation, 1 ml warm LB medium was added to the cuvette, cells transferred to a 15 ml tube and incubated for 30 min at 37°C (220 rpm). Successfully transformed cells were eventually selected on LB plates containing Ampicillin via overnight incubation at 37°C.

5.1.2 *Saccharomyces cerevisiae* (*S. cerevisiae*) techniques

All *S. cerevisiae* strains were cultivated at 30°C either in liquid media or on agar plates. Liquid culture density was determined photometrically via absorption at 600 nm (OD₆₀₀) with a value of 1.0 estimated to correspond to a number of 1.5 x 10⁷ cells.

***S. cerevisiae* strains**

All yeast strains were isogenic to either DBY745²⁴² or W303²⁴³. Strains YCL25 and YCL26 were obtained by crossing YCZ173²⁴⁴ with W303 *MAT α* . Strain YCL42 by crossing YCL25 with W303 *MAT α* .

Name	Genotype	Source
JKM179	<i>Δhml::ADE1, MATα, Δhmr::ADE1, ade1, leu2-3,112 lys5, trp1::hisG', ura3-52, ade3::P_{GAL}-HO</i>	Ref. 245
JOR03	JKM179, <i>Δrad54::kanMX6</i>	Ref. 47
JOR05	JKM179, <i>Δrdh54::natNT2</i>	Ref. 47
JOR34	JKM179, <i>Δrad54::kanMX6, Δrdh54::natNT2</i>	Ref. 47
JOR97	YCL26, <i>ChrIV_{491kb}::HOcs-hphNT1</i>	Ref. 47
YCL025	<i>MATα, ade3::P_{GAL}-HO, hmlΔ::pRS-1 hmrΔ::pRS-2</i>	This study
YCL026	<i>MATα, ade3::P_{GAL}-HO, hmlΔ::pRS-1 hmrΔ::pRS-2</i>	This study

MATERIALS AND METHODS

	<i>mathOcsΔ::pBR-1</i>	
YCL042	<i>MATa, ade3::P_{GAL}::HO, hmlΔ::pRS-1 hmrΔ::pRS-2</i>	This study
YCL061	JOR34, <i>RFA1-9myc::hphNT1</i>	This study
YCL063	YCL26, <i>ChrIV_{491kb}::GFPHOcs-hphNT1</i>	This study
YCL072	YCL63, <i>ChrIV_{625kb}::GFPHOinc-kanMX4</i>	This study
YCL076	YCL63, <i>ChrIV_{795kb}::GFPHOinc-kanMX4</i>	This study
YCL078	YCL63, <i>ChrIV_{820kb}::GFPHOinc-kanMX4</i>	This study
YCL080	YCL63, <i>ChrVII_{434kb}::GFPHOinc-kanMX4</i>	This study
YCL081	YCL63, <i>ChrVII_{484kb}::GFPHOinc-kanMX4</i>	This study
YCL083	YCL63, <i>ChrVII_{166kb}::GFPHOinc-kanMX4</i>	This study
YCL084	YCL26, <i>ChrIV_{625kb}::GFPHOinc-kanMX4</i>	This study
YCL085	YCL26, <i>ChrIV_{795kb}::GFPHOinc-kanMX4</i>	This study
YCL086	YCL26, <i>ChrIV_{820kb}::GFPHOinc-kanMX4</i>	This study
YCL104	YCL25, <i>ura3::P_{ADH}-HED1-URA3</i>	This study
YCL110	JOR97, <i>Δarp8::kanMX6</i>	This study
YCL112	YCL72, <i>Δrad54::natNT2</i>	This study
YCL115	YCL76, <i>Δarp8::natNT2</i>	This study
YCL119	JOR97, <i>Δrad54::kanMX6, Δrdh54::natNT2</i>	This study
YCL124	YCL25, <i>ura3::P_{ADH}-hed1^{T131P}-URA3</i>	This study
YCL134	YCL76, <i>ura3::P_{GAL}-RAD54-URA3</i>	This study
YCL157	YCL76, <i>ura3::P_{ADH}-RAD54-URA3</i>	This study
YCL179	JOR97, <i>Δsgs1::kanMX6, Δexo1::natNT2</i>	This study
YCL201	YCL26, <i>ChrIV_{491kb}::HOcs-natNT2</i>	This study
YCL208	YCL201, <i>hta1^{S129}A::kanMX6, hta2^{S129A}::hphNT1</i>	This study
YCL246	YCL201, <i>htb1^{T129}A::kanMX6, htb2^{T129A}::hphNT1</i>	This study
YCL248	JOR97, <i>Δhtz1::natNT2</i>	This study
YCL252	JOR97, <i>Δswr1::natNT2</i>	This study
YCL260	JOR97, <i>Δarp8::kanMX6, Δswr1::natNT2</i>	This study
YCL261	JOR97, <i>Δarp8::kanMX6, Δhtz1::natNT2</i>	This study
YCL344	YCL76, <i>Δarp8::natNT2, Δhtz1::CaURA3</i>	This study
YCL345	YCL76, <i>Δarp8::natNT2, Δswr1::CaURA3</i>	This study
YCL353	<i>MATa, ade3::P_{GAL}-HO, hmlΔ::pRS-1 hmrΔ::pRS-2</i> <i>mathOcsΔ::pBR-1, Δura3, Δtrp1</i>	This study
YCL451	YCL76, <i>Δhtz1::natNT2</i>	This study
YCL458	YCL353, <i>Δhtz1::TRP1</i>	This study
YCL505	<i>MATa, ChrIV_{491kb}::HOcs-hphNT1, Δhta1htb1::LEU2,</i> <i>Δhta2htb2::TRP1, YC33-HTA1-HTB1</i>	This study
YCL506	<i>MATa, ChrIV_{491kb}::HOcs-hphNT1, Δhta1htb1::LEU2,</i> <i>Δhta2htb2::TRP1, YC33-hta1^{S129A}-htb1^{T129A}</i>	This study
YCL513	JOR97, <i>RAD55-6HA::natNT2</i>	This study
YCL514	YCL110, <i>RAD55-6HA::natNT2</i>	This study
YCL515	JOR97, <i>RAD57-6HA::natNT2</i>	This study
YCL517	YCL110, <i>RAD57-6HA::natNT2</i>	This study
YCL537	YCL76, <i>Δswr1::natNT2</i>	This study
YCL584	JOR97, <i>HTZ1-3HA::TRP1</i>	This study
YCL587	JOR97, <i>HTZ1-3HA::TRP1, INO80-9myc::natNT2</i>	This study

MATERIALS AND METHODS

YCL588	YCL110, <i>HTZ1-3HA::TRP1</i>	This study
YCL601	JOR97, <i>INO80-9myc::natNT2</i>	This study
YCL602	YCL76 x YCL458	This study
YCL609	YCL602, <i>Δino80::natNT2</i>	This study
YCL618	YCL80, <i>Δhtz1::natNT2</i>	This study
YCL619	YCL81, <i>Δhtz1::natNT2</i>	This study
YCL626	YCL76, <i>Δies5::natNT2</i>	This study
YCL627	YCL76, <i>Δies5::natNT2, Δhtz1::TRP1</i>	This study
YCL734	YCL76, <i>Δnhp10::natNT2</i>	This study
YCL735	YCL76, <i>Δnhp10::natNT2, Δhtz1::TRP1</i>	This study

S. cerevisiae vectors

Type	Name (Marker)	Purpose	Source
Centromeric	<i>YC33 (URA3)</i>	Expression of protein of interest under URA3 marker	Ref. 246
Integrative	<i>Ylplac-P_{ADH}-T_{ADH} (URA3)</i>	Expression of protein of interest under the ADH promotor at the URA3 locus	Ref. 246
	<i>Ylplac-P_{GAL}-T_{ADH} (URA3)</i>	Expression of protein of interest under the GAL promotor at the URA3 locus	Ref. 246

S. cerevisiae plasmids

Name	Plasmid (Marker)	Source
D4137	<i>HOcs (natNT2)</i>	J. Renkawitz, unpublished
pCL02	<i>Ylplac128-P_{ADH}-RAD54 (URA3)</i>	This study
pCL09	<i>Ylplac128-P_{ADH}-HED1 (URA3)</i>	This study
pCL15	<i>GFPHOcs (hphNT1)</i>	This study
pCL17	<i>GFPHOinc (kanMX6)</i>	This study
pCL22	<i>Ylplac128-P_{GAL}-RAD54 (URA3)</i>	This study
pCL31	<i>Ylplac128-P_{ADH}-hed1^{T131P} (URA3)</i>	This study
pCL41	<i>YCplac33-HTA1-HTB1 (URA3)</i>	This study
pCL44	<i>YCplac33-hta1^{S129A}-htb1^{T129A} (URA3)</i>	This study

S. cerevisiae media and buffers

YPD/YP-Gal/YP-Raff	1 % (w/v) yeast extract 2 % (w/v) bacto-peptone 2 % (w/v) carbon source (glucose, galactose, raffinose) 2 % (w/v) agar (only for plates) sterilized by autoclaving
--------------------	--

MATERIALS AND METHODS

YP-lactate	1 % (w/v) yeast extract 2 % (w/v) bacto-peptone 3 % (w/v) lactic acid adjusted to pH 5.5 with NaOH (ca. 12 g/l final) sterilized by autoclaving
YPD G418/Nat/Hyg plates	after autoclaving, YPD medium with 2 % agar was cooled to 50°C and 200 mg/l G418 (geneticine disulphate, PAA Laboratories), 100 mg/l Nat (nourseothricin, HK Jena) or 500 mg/l Hyg (hygromycin B, PAA Laboratories) was added.
SC-media	0.67 % (w/v) yeast nitrogen base 0.2 % (w/v) amino acid drop out mix (except amino acids selected for by auxotrophy markers) 2 % (w/v) Glucose 2 % agar (w/v) (for plates) sterilized by autoclaving
Drop out amino acid mix	20 mg Ade, Ura, Trp, His 30 mg Arg, Tyr, Leu, Lys 50 mg Phe 100 mg Glu, Asp 150 mg Val 200 mg Thr 400 mg Ser
SORB	100 mM LiOAc 10 mM Tris-HCl, pH 8.0 1 mM EDTA, pH 8.0 1 M sorbitol sterilized by filtration
PEG	100 mM LiOAc 10 mM Tris-HCl, pH 8.0 1 mM EDTA, pH 8.0 40 % (w/v) PEG-3350 sterilized by filtration, stored at 4°C

Storage and cultivation of *S. cerevisiae*

For long-term storage, single yeast colonies were inoculated overnight, mixed with 50 % (v/v) glycerol (final concentration 15 %) and frozen at -80°C. For each experiment, cells were freshly streaked from glycerol stocks onto agar plates using a sterile toothpick or

glass pipette. Liquid cultures were inoculated from pre-cultures to an OD₆₀₀ of 0.1. In case of experiments using YP-lactate, cells were passed through two sequential pre-culture steps to fully inhibit glucose metabolism. Main cultures were then grown under constant shaking (150-250 rpm on a shaking platform) to mid-log phase (OD₆₀₀ = 0.5-0.8) density and further processed according to the experimental regimen.

Preparation of competent *S. cerevisiae* cells

Competent *S. cerevisiae* cells were generated from a 50 ml YPD culture grown to mid-log phase. Cells were harvested by centrifugation (500 g, 5 min, RT) and washed with 5 ml SORB buffer. After resuspension in 360 µl SORB buffer, 50 µl carrier DNA (hering sperm DNA, Invitrogen, 10mg/ml, heat-denatured at 99°C for 10 min) was added and cells either used directly for transformation or stored in aliquots at -80°C.

Transformation of *S. cerevisiae* cells

For transformation, competent *S. cerevisiae* cells were mixed with DNA (10 µl cells + ~100 ng DNA in case of plasmids, 50 µl cells + ~500 ng DNA in case of linearized plasmids and 50 µl cells + 15 µl PCR product in case of PCR-amplified DNA (see section 5.2.2)) and six volumes of PEG buffer. The mixture was incubated at RT for 30 min and subsequently heat-shocked in a waterbath for 15 min at 42°C. Cells were then harvested by centrifugation (500 g, 2 min, RT) and recovered in YPD medium for 2 h prior to plating on selective plates (recovery only in case of antibiotic selection markers). Selection was carried out for 2-3 days at 30°C.

Genetic manipulation of *S. cerevisiae*

Genes were deleted, replaced or tagged using selection cassettes generated by a PCR-based strategy^{172,173}. In brief, selection cassettes containing different marker genes (*kanMX4/6*, *hphNT1*, *natNT2*, *CaURA3*²⁴⁷, *TRP1*²⁴⁸) were amplified using gene specific overhangs, leading to their integration at the endogenous locus, thereby replacing the original gene. Correct cassette integration was generally determined by yeast colony PCR (see below) and chromosomal taggings were additionally confirmed by immunoblotting (see section 5.3.1).

Marker-free seamless deletion of *ura3* and *trp1* alleles to enhance the efficiency of targeted integration using cassettes containing the URA3 or TRP1 markers was achieved as described previously²⁴⁹. In brief, the endogenous locus chosen for seamless deletion was replaced by a construct bearing the URA3 ORF that is flanked upstream by a 40 bp repeat of the endogenous sequence downstream of the integration site. Counter-selection

of the URA3 marker on plates containing 5-Fluoroorotic acid (5'FOA) results in deletion of the URA3 marker by intra-chromosomal recombination between the 40 bp repeats.

Endogenous mutations S129A of H2A alleles and T129A of H2B alleles were generated using PCR cassettes with overhangs carrying the destined mutations and harboring an *ADH1* terminator to maintain proper expression. The presence of mutations was additionally confirmed by DNA sequencing (see section 5.2.1).

For construction of yeast strains harboring site-specific *HO_{cs}* or *GFP-HO_{cs}*, a 36 bp HO endonuclease recognition sequence (5'-AGTTTCAGCTTTCCGCAACAGTATAATT TTATAAAC-3')²⁵⁰ was cloned via oligonucleotide annealing (see section 5.2.3) next to a marker gene in the pFA6a backbone or inside the GFP ORF of pYM25, respectively, and this construct used for PCR amplification with site-specific overhangs for the destined integration site. In case of *GFP-HO_{inc}*, a similar approach was undertaken, but with a mutated HO endonuclease recognition site (5'-AGTTTCAGCTTTCCaCAAtAGTATAATTT TATAAAC-3', mutations in lowercase)¹⁷⁵ flanked by a unique 23 bp sequence (5'-CTAGCTGACGAAATGGCAAACAA-3') cloned into the GFP-encoding sequence of pYM12.

Mating, sporulation and tetrad analysis

For mating, freshly streaked strains of opposing mating types were mixed in 300 μ l YPD and 50 μ l of this mixture was subsequently spotted on warm YPD plates. Plates were incubated for at least 4 h at 30°C, followed by streaking of cells on double-selection plates. In case of auxotrophy/antibiotic double-selection, antibiotics (G418, NAT or HYG) were dissolved in 150 μ l water and spread onto SC selection plates.

After 2-3 days incubation at 30°C, single colonies of diploid cells were inoculated overnight and 500 μ l harvested by centrifugation (500 g, 2 min, RT). For sporulation, cells were washed four times in sterile water prior to resuspension in 3 ml sporulation medium (2 % (w/v) KAc, sterilized by autoclaving) and incubation on a rotating shaker for at least 3 days at 25°C.

For tetrad dissection, sporulated diploid cells were mixed 1:1 with zymolase 100T (1 mg/ml in de-ionized water) and incubated for 5 min at RT. Tetrads were then dissected on YPD plates using a micromanipulator (Singer MSM Systems) and incubated for 2-3 days. Genotype and mating type of each spore were determined by replicating on selection and mating type tester plates.

Mating type analysis of haploid yeast cells

To determine unknown mating types, a large toothpick of each of two mating type tester strain was resuspended in 500 μ l sterile water and this solution (250 μ l in case of RH448) mixed with 50 ml 1 % agarose (dissolved in water, precooled to 42°C). The agarose containing the tester strains was then poured on top of pre-warmed YPD plates (~5 ml per plate) and after cool-down strains with unknown mating type were replicaplated on the tester plates. Because of the sensitivity of the tester strains RC757 (*MATa*) and RH448 (*MATa*) to cells of the opposing mating type, a halo (a region without growth) will form around the streaked strain on one of the two tester plates.

Cell cycle arrest

To arrest cells in G2/M-phase, early- to mid-log phase cells (OD_{600} 0.3-0.5) were treated with the microtubule poison nocodazole (Sigma) at a concentration of 5 μ g/ml. Cells were typically allowed to arrest for one generation time (2-4 h depending on the genetic background) and the arrest confirmed microscopically and later also by flow cytometry (see below).

Cell cycle analysis by flow cytometry

To monitor cell cycle stage, cell amounts corresponding to 1 OD_{600} were harvested from cultures by centrifugation, immediately fixed in 1 ml 70 % ethanol, 50 mM Tris-HCl, pH 7.8 and stored at 4°C until further processing (up to a few weeks). Cells were then washed once in 1 ml Tris buffer (50 mM Tris-HCl pH 7.8) and subjected to RNA digestion by addition of 520 μ l RNAase solution (500 μ l Tris buffer + 20 μ l RNAse A (10 mg/ml in 10 mM Tris-HCl pH 7.5, DNase inactivated by boiling for 10 min)). After incubation on a rotating platform at 37°C for 4 h cells were harvested by centrifugation and resuspended in 220 μ l proteinase K solution (200 μ l Tris buffer + 10 μ l Proteinase K (20 mg/ml in 10 mM Tris-HCl, pH 7.5)). Proteinase K digestion was then performed at 50°C for 30 min cells, followed by centrifugation and resuspension of the cells in 500 μ l Tris buffer. After sonication of all samples (5 s, 50 % cycle, minimum power using a Bandelin SONOPLUS device), 25 μ l of each sample were mixed with 500 μ l SYTOX solution (999 μ l Tris buffer + 1 μ l SYTOX green, Life Technologies). Fluorescence of SYTOX stained cells was finally detected in the FL1 channel of a MACSQuant® Analyzer 10 flow cytometer (Miltenyi Biotec).

Yeast colony PCR

For yeast colony PCR, a small toothpick of cells was dissolved in 20 μ l 0.2 M NaOH and the mixture boiled for 10 min at 95°C in a PCR machine. Subsequently, 40 μ l de-ionized water were added and the cell debris pelleted by a quick spin in a small benchtop centrifuge. 4 μ l of the supernatant were subsequently taken as input DNA for the following PCR reaction (see section 5.2.2).

Induction of single DSBs in vivo

To induce single and site-specific DSB by HO-endonuclease, yeast strains expressing the HO endonuclease gene under control of the GAL promoter¹⁷⁴ have been modified with site-specific HO recognition sites (see above). Strains were then grown in YP-lactate medium to avoid any repressive effects of glucose metabolism on the activation of GAL promoter-driven expression. HO expression was typically induced at mid-log phase (OD_{600} 0.5-0.8) by the addition of galactose to the lactate medium at a final concentration of 2 % (w/v).

Recombination survival assay

To measure recombination via cell survival, strains were streaked directly from glycerol stocks onto YP-Raffinose plates. After 3 days at 30°C, cells were serially diluted in water to an OD of 10^{-5} and 100 μ l or 200 μ l were subsequently plated onto YPD or YP-GAL plates, respectively. After a sufficient growth time (2-4 days), single colonies were counted and the ratio between YP-GAL and YPD taken as recombination efficiency.

Real-time recombination assay

To measure recombination in real-time, cells were inoculated in YP-lactate medium and 2 % galactose added at mid-log phase ($OD_{600} = 0.5-0.8$). At time points of interest, a cell amount corresponding to 1 OD_{600} was taken from the culture, harvested by centrifugation (1000 g, 1 min, RT) and immediately snap-frozen in liquid nitrogen. Cells were either stored short-term at -80°C or directly processed. Genomic DNA was then isolated using the MasterPure™ Yeast DNA Purification Kit (Epicentre) according to the manufacturer's instructions including an extra 5 min incubation at 37°C prior to elution to remove any traces of ethanol. The DNA was eluted in 100 μ l of de-ionized water and 2 μ l were used for analysis by quantitative real-time PCR (see section 5.2.2).

5.2 Molecular biology techniques

5.2.1 DNA isolation, purification and sequencing

Isolation of plasmid DNA from *E. coli*

Plasmid DNA was propagated in and isolated from *E. coli* using the AccuPrep® Plasmid Mini Extraction Kit (Bioneer) according to the manufacturer's instructions.

Purification of linear DNA fragments

To purify linear DNA fragments generated by PCR amplification, the QIAquick PCR Purification Kit (Qiagen) was used according to the manufacturer's instructions.

Purification of DNA fragments from agarose gels

DNA fragments separated by gel electrophoresis were purified using the QIAquick Gel Extraction Kit (Qiagen) according to the manufacturer's instructions.

Isolation of genomic DNA from *S. cerevisiae*

Isolation of genomic DNA from *S. cerevisiae* (e.g. as template for the amplification of specific genes or chromosomal elements by PCR) was performed using the MasterPure™ Yeast DNA Purification Kit (Epicentre) according to the manufacturer's instructions.

Purification of plasmid DNA from *S. cerevisiae*

Isolation of DNA plasmids from yeast was performed using the AccuPrep® Plasmid Mini Extraction Kit (Bioneer) according to the manufacturer's instructions, with the following changes: strains YKH124/127-129¹⁹² (expressing HTA and HTB variants from their endogenous promoter) were grown overnight, 1.5 ml of this culture harvested and resuspended in 250 μ l buffer P1 supplemented with an equal volume of glass beads (\emptyset 500 μ m; Roth). Cells were then lysed for 4 min using a cell disruptor (Disruptor Genie, Scientific Industries) at maximum speed and following the addition of buffer P2 the standard protocol was followed.

Measurement of DNA concentration

DNA concentration was determined photometrically using a NanoDrop ND-1000 spectrophotometer (PeqLab). The absorbance at a wavelength of 260 nm (A₂₆₀) was used for DNA quantification with a value of 1 equaling a concentration of 50 μ g/ml double-stranded DNA.

Separation of DNA fragments by agarose gel electrophoresis

For analytical and preparative separation of DNA fragments, 0.5-1.5 % (w/v) gels containing ultra-pure agarose in TBE buffer (89 mM Tris, 89 mM boric acid, 2 mM EDTA) were prepared. Ethidium bromide was added shortly before the gel was poured (final concentration 1 $\mu\text{g/ml}$) to allow visualization of the DNA using an UV transilluminator (Raytest). DNA samples were mixed with 0.2 volumes of 5 x DNA loading buffer (25 % Glycerol, 10 mM EDTA, Orange G) and electrophoretically separated at 110 volts (12 V/cm) in TBE buffer. The size of DNA fragments was estimated with a standard size marker (1kB ladder, Invitrogen) migrating on the same gel.

DNA sequencing

Sequencing analysis of plasmid DNA or purified PCR products was performed by the core facility of the MPI of Biochemistry using an ABI 3730 DNA analyzer (Applied Biosystems) and ABI Big Dye 3.1 sequencing chemistry. Alternatively, samples were sequenced as value reads at Eurofins Genomics.

5.2.2 DNA amplification by polymerase chain reaction (PCR)

Amplification of genomic DNA fragments

Amplification of genomic or plasmid DNA for subsequent molecular cloning (see section 5.2.3) was performed using the high fidelity Phusion polymerase (Thermo). Specifically, a 50 μl reaction consisted of 200 ng DNA, 0.6 μM of each primer, 0.8 mM dNTP-Mix, 1 x Phusion HF buffer and 2 units of Phusion polymerase. Amplification was performed in a Veriti® Thermal Cycler (Applied Biosystems) with an initial 1 min denaturation step at 98°C, followed by 25 cycles of 20 s 98°C denaturation, 20 s 60°C primer annealing and an amplification-length adjusted extension time (15 s/kb for plasmid DNA, 30 s/kb for genomic DNA plus an additional 20 s) at 72°C. Following a final extension at 72°C for 7 min samples were stored at 4°C or -20°C.

Amplification of marker cassettes for genetic manipulation of yeast

Amplification of marker cassettes was performed using a mixture of Taq and Vent polymerases as described previously^{172,173} with the only change that the PCR amplification program was not adjusted for cassettes bearing the natNT2 marker.

Amplification of DNA for yeast colony PCR

For yeast colony PCR, the DNA template was generated as described above and amplified using Taq polymerase (in-house made by the MPI core facility). Specifically, a 50 μ l reaction consisted of 4 μ l template DNA, 0.64 μ M of each primer, 1.4 mM dNTP-Mix, 1 x ThermoPol Reaction Buffer (New England Biolabs) and 2 units of Taq polymerase. Amplification was performed in a Veriti® Thermal Cycler (Applied Biosystems) with an initial 5 min denaturation step at 94°C, followed by 30 cycles each consisting of 30 s 94°C denaturation, 30 s 55°C primer annealing and an amplification-length adjusted extension time (90 s/kb) at 72°C. Following a final extension at 72°C for 5 min samples were stored at 4°C or -20°C prior to analysis by gel electrophoresis.

Quantitative real-time PCR

Quantitative real-time PCR (qPCR) was performed using the LightCycler 480 system (Roche). For ChIP experiments (see section 5.3.2), SYBR Green-based chemistry either consisted of the LightCycler 480 SYBR Green I Master Mix (Roche, “RocheMix”) or the KAPA SYBR® FAST qPCR kit (Kapa Biosystems, “KAPAMix”). Specifically, a 20 μ l reaction contained 2 μ l of ChIP (undiluted) or input DNA (1:10 dilution), 10 μ l SYBR Green Master Mix and either 0.6 μ M or 0.2 μ M of each primer (see table below) in case of “RocheMix” or “KAPAMix”, respectively. All reactions were performed in technical triplicates in 384-well plates with pipetting conducted by a CAS-1200 PCR setup robot (Corbett Lifescience). Quantification was then achieved via the “second-derivative maximum” method using the LightCycler 480 software. Relative concentrations of the template DNA were determined by fitting these values with a primer-specific standard curve that was generated by a dilution series of one input sample (1:5, 1:50, 1:500 and 1:5000) measured with every primer pair. As quality control, samples clearly differing within technical triplicates, as well as those showing multiple products in a melting curve analysis performed at end of the amplification reaction, were removed from the analysis. For data presentation the IP/input ratios were calculated and, if not indicated differently, normalized to the IP/input ratios of a control primer pair on chromosome X (see table qPCR primer).

In case of measuring FAIRE samples (see section 5.3.2) or analyzing real-time recombination (see section 5.1.2), exclusively the “RocheMix” was used as described for ChIP DNA. Notably, for recombination experiments standard curves were measured with DNA from the latest time point (1:1, 1:10, 1:100 and 1:1000), as recombination products

MATERIALS AND METHODS

are only then robustly detectable. As in case of ChIP DNA, concentrations were normalized to a control locus on chromosome X.

LightCycler programs

	RocheMix, ChIP	KAPAMix, ChIP	Recombination
Initial Denaturation	95°C, 10 min	95°C, 3 min	95°C, 10 min
Amplification/Detection	45 x	40 x	45 x
	95°C, 10 s	95°C, 10 s	95°C, 10 s
	57°C, 10 s	57°C, 20 s	58°C, 10 s
	72°C, 16 s	72°C, 1 s	72°C, 20 s
Melting Curve Analysis	95°C, 30 s	95°C, 5 s	95°C, 30 s
	65°C, 30 s	65°C, 1 min	65°C, 30 s
	65°C-95°C 0.11°C/s, 5 acquisitions/°C	65°C-97°C, 0.11°C/s, 5 acquisitions/°C	65°C-95°C 0.11°C/s, 5 acquisitions/°C
Cool-Down	4°C, ∞	4°C, ∞	4°C, ∞

qPCR primer

Name	Sequence	Genomic Position	Usage
BA069	CAATGGACGAGGAAACAAGAGCGATT	ChrIV_509kb	ChIP_filament
BA070	ACCATACCAGACCTTTTCCAGTCTGT	ChrIV_509kb	ChIP_filament
CL_154	CATACTGTCTCACTCGCTTGGGA	ChrIV, 491 kb	RT-recombination
CL_156	TTGTTTGCCATTTTCGTGCTAG	GFPHOinc	RT-recombination
CL_166	TGGGAATCGTTTTATCCTTGTTTCGC	ChrIV_625kb	ChIP_Donor
CL_167	GTGAAGCAACCAACATAATGCCAGAT	ChrIV_625kb	ChIP_Donor
CL_169	AACCTGATTCTATACAAGCAGCCAA	ChrIV_795kb	ChIP_Donor
CL_170	AATTGGAATGCCCGAGATTCTCAAAC	ChrIV_795kb	ChIP_Donor
CL_175	TCGAGTGGAGATATTTGGGAGAAAGA	ChrIV_820kb	ChIP_Donor
CL_176	TCTGGCAAAGCTTCTATGCTTCTGAT	ChrIV_820kb	ChIP_Donor
CL_226	ATTCCAGGCCAACCCAAGTAAGTC	ChrIV_491kb	ChIP_DSB
CL_227	CTTCCTAGGAGGAGGAAAGCCCAT	ChrIV_491kb	ChIP_DSB
CL_277	GCCACCAATAAGGGTCCATTAGCA	ChrIV_445kb	ChIP_search
CL_278	CCTGATTCGTATCACAGCCAGAA	ChrIV_445kb	ChIP_search
CL_279	CTCTAACGCCACGGTCATGAAGAA	ChrIV_451kb	ChIP_search
CL_280	TCCTAACGGTCTCGGTATTCCTCC	ChrIV_451kb	ChIP_search
CL_303	CACATGTCCAAAGGCTGCTGATGA	ChrIV_421kb	ChIP_search
CL_304	GTTGCTCATTGGGTGGACCAAGTA	ChrIV_421kb	ChIP_search
CL_305	TTGTGAAGTTTTCAAGTTGGCGAGC	ChrIV_421.5kb	ChIP_search
CL_306	AGGGAGAAGAGGCCAAAACAACAGG	ChrIV_421.5kb	ChIP_search
CL_307	AAGTGCAGAGCTGCTGATATTGCT	ChrIV_422kb	ChIP_search

MATERIALS AND METHODS

CL_308	AGTCAATCCGCATTACAGGCAAGA	ChrIV_422kb	ChIP_search
CL_309	AGAAACGTCACTTCAGCTCTGTCA	ChrIV_422.5kb	ChIP_search
CL_310	ATGAGCTGCGCTCAAATTGCCATA	ChrIV_422.5kb	ChIP_search
CL_311	TCTTGTGCTGTGCTTTACCACCAT	ChrIV_423kb	ChIP_search
CL_312	ACGCTAACTCCGGAATTGACTGT	ChrIV_423kb	ChIP_search
CL_323	ACTGCAACAAGACCTTCACTCAACT	ChrXV_536kb	ChIP_alt.control
CL_324	GCAGGATGGTTTTCTGGTGAGGA	ChrXV_536kb	ChIP_alt.control
CL_325	CTAAACGTGGCCGCATTTGGTAAG	ChrVI_242kb	ChIP_alt.control
CL_326	ATCATCGCCGATTGGATAAGGGTG	ChrVI_242kb	ChIP_alt.control
CL_327	TGATAGCTTCTGCAATCGTAGGGC	ChrV_358kb	ChIP_alt.control
CL_328	TGGATCACGGTGCTAAGGAGGTTA	ChrV_358kb	ChIP_alt.control
CL_329	TGGTCTGAGTTTCCAGTTCTTTGGT	Chrl_55kb	ChIP_alt.control
CL_330	AGCGTCCAAACTAAATGAGCAGTCT	Chrl_55kb	ChIP_alt.control
CL_494	TGGGATAATGGTAGTACTGGGCGT	ChrIV_500kb	ChIP_filament
CL_495	CAGCTGCTCCGAAACCAATTTTGA	ChrIV_500kb	ChIP_filament
CL_496	GTATACCTGACGGGCAGTCCTTTT	ChrIV_505kb	ChIP_filament
CL_497	GCAGTGACGGTTCAAGATCTCCTT	ChrIV_505kb	ChIP_filament
CterYJL112Win	GCGTGCCTGGTCACAGGTTACATACGAC	ChrX_207kb	Standard control
CterYJL112Wr	TCATACGGCCCAAATATTTACGTCCC	ChrX_207kb	Standard control
HO-100check	GAGCATATTA CTACAGTTTGGCTC	ChrIII_200kb	DSB induction
HO+0.2kb In	CCTGGTTTTGGTTTTGTAGAGTGG	ChrIII_201kb	ChIP_DSB
HO+0.2kb re	GAGCAAGACGATGGGGAGTTTC	ChrIII_201kb	ChIP_DSB
HO +190re	GGATAGCTATACTGACAACATTCAG	ChrIII_200kb	DSB induction
JOR053	CCCAAGCTCACAAATTAATATGGC	ChrIII_275kb	ChIP_search
JOR054	GCATCTGTAGTACCACTGCTCTTTG	ChrIII_275kb	ChIP_search
JOR238	TACACATAAGAGGCTCATTAGGGC	ChrIV_540kb	ChIP_search
JOR239	CCAGCGTAATTATAGGATTGCCA	ChrIV_540kb	ChIP_search
JOR324	GTTTCCCCAGCTTTCCGTGT	ChrIV_492kb	ChIP_filament
JOR325	TTGCTTCTTG CAGAAGTGGAGA	ChrIV_492kb	ChIP_filament
JOR330	AGGGCCAACACCTAGTCCAA	ChrIV_496kb	ChIP_filament
JOR331	AGGCGAAGTTAGTGCTGAACA	ChrIV_496kb	ChIP_filament

5.2.3 Molecular cloning

Restriction digest

For sequence-specific restriction digestion of PCR amplified DNA or plasmid DNA, enzymes (New England Biolabs) were used according to the manufacturer's instructions. Typically, 1.5 μ g of plasmid DNA or the amount of a purified 50 μ l PCR reaction (see section 5.2.2) were taken as input. In case the digestion reaction generated side products with a length > 100 bp or not, the reaction was purified either via gel extraction or column-based purification, respectively (see section 5.2.1).

De-phosphorylation of linearized plasmid DNA

De-phosphorylation of the free 5'-ends of the vector backbone was performed using 1.5 μg of digested and purified vector DNA incubated with 2 units of rAPid Alkaline Phosphatase (Roche) in the provided reaction buffer for 1 h at 37°C. Alkaline Phosphatase was subsequently heat-inactivated by incubation at 75°C for 5 min prior to ligation.

Oligonucleotide annealing

To generate DNA inserts with a size of less than 120 bp, oligonucleotide annealing instead of PCR amplification was used. To this end, complementary oligonucleotides with overhangs specific to the restriction enzymes of choice were ordered and dissolved at a concentration of 100 μM in 50 mM Tris-HCl, pH 8.0, 100 mM NaCl, 1 mM EDTA. 10 μl of each oligonucleotide were then mixed in a PCR reaction tube and denatured in a Veriti® Thermal Cycler (Applied Biosystems) at 95°C for 90 s. Subsequently, the temperature was gradually decreased at a rate of 1°C per 20 s until reaching 4°C and 2 μl of the reaction used as input for DNA ligation.

DNA ligation

For DNA ligation, linearized and de-phosphorylated vector DNA and digested PCR product were mixed in a ratio of 1:5 in a 20 μl ligation reaction containing 1 x T4 DNA ligase buffer and 400 units of T4 DNA ligase (New England Biolabs). The reaction was subsequently incubated for 15 min at 25°C, followed by heat-inactivation of DNA ligase at 65°C for 10 min. The sample was then dialyzed for 20 min against de-ionized water using a nitrocellulose filter (pore size 0.05 μm , Millipore) and 8 μl were used for transformation into electro-competent *E. coli* cells.

Site-directed mutagenesis

Introduction of specific point mutations, as well as small insertions or deletions into plasmid DNA were achieved using the PCR-based QuickChange® Site-Directed Mutagenesis Kit (Agilent Technologies). Briefly, complementary oligonucleotides bearing the mutation of interest were designed with at least 20-25 nucleotides flanking the mutation on each side. PCR amplification was then performed using Pfu Turbo polymerase and 10 ng plasmid DNA as starting material. Dam-methylated, non-mutagenized input DNA was removed from the reaction following PCR amplification by addition of 10 units of the DpnI restriction endonuclease (New England Biolabs) and incubation at 37°C for 1.5-3 h. After dialysis (see above), 8 μl of the reaction were

transformed into electro-competent *E. coli* cells. Finally, extracted plasmid DNA was analyzed for the presence of desired and absence of undesired mutations by DNA sequencing.

5.3 Biochemical and cell biological techniques

5.3.1 Protein techniques

Buffers and solutions

HU sample buffer	200 mM Tris-HCl, pH 6.8 8 M urea 5 % (w/v) SDS 1 mM EDTA 0.1 % (w/v) bromophenol blue 100mM DTT (freshly added before use)
MOPS running buffer	50 mM MOPS 50 mM Tris base 3.5 mM SDS 1 mM EDTA
Blotting buffer (self-made)	250 mM Tris base 1.92 M glycine 0.1 % (w/v) SDS 20 % (v/v) methanol
Swift blotting buffer	5 % (v/v) 20 x Swift buffer (G-Bioscience) 10 % (v/v) Methanol
TBS-T solution	25 mM Tris-HCl, pH 7.5 137 mM NaCl 2.6 mM KCl 0.1 % (v/v) Tween 20
PBS	10 mM phosphate, pH 7.4 137 mM NaCl 2.7 mM KCl
IP lysis buffer	50 mM Tris-HCl, pH 7.5 150 mM NaCl 10 % (v/v) glycerol 2 mM MgCl ₂ 0.5 % (v/v) NP-40

Preparation of denatured protein extracts (TCA precipitation)

For the generation of denatured protein extracts, a cell amount corresponding to one OD₆₀₀ was harvested by centrifugation and immediately frozen in liquid nitrogen. After thawing, cells were lysed by resuspension in 150 µl 1.85 M NaOH, 7.5 % beta-mercaptoethanol and incubated for 15 min on ice. Proteins were then precipitated from the lysate by addition of 150 µl ice-cold 55 % TCA and incubation for 15 min on ice. After centrifugation (20000 g, 15 min, 4°C) and complete removal of TCA supernatant protein pellets were resuspended in HU buffer and incubated for 10 min at 65°C prior to analysis by SDS-PAGE (see below).

SDS-polyacrylamide gel electrophoresis (SDS-PAGE)

Proteins samples were loaded on pre-cast 4-12 % NuPAGE Bis-Tris gels (Thermo Fisher Scientific). Gel electrophoresis was performed in MOPS buffer at a constant voltage of 120V until the bromphenol blue front reached the end of the gel.

Immunoblot analysis

For immunoblot (western blot) analysis, proteins separated by SDS-PAGE were subsequently transferred to polyvinylidene fluoride (PVDF) membranes (ImmobilionP, Millipore) using wet blotting in an electric tank blotter (Hoefer) at a constant voltage of 70 V for 90 min at 4°C. Blotting efficiency was determined by transfer of the Precision Plus Protein All Blue Standard (Bio-Rad). Membranes were then quickly washed with TBS-T, blocked for 30-60 min in TBS-T + 5 % milk powder at RT and incubated with primary antibodies diluted in TBS-T + 5 % milk powder (see table “antibodies” below) overnight at 4°C. Membranes were then placed at RT, washed three times with TBS-T (5-10 min each), incubated 1-1.5 h with a horseradish peroxidase (HRP)-coupled secondary antibody (Dianova) and washed again three times with TBS-T (5-10 min each). Signal detection was performed using chemiluminescence kits ECL, ECL-plus or ECL advanced (GE Healthcare) and exposure of the membranes to chemiluminescence sensitive films (Amersham Hyperfilm ECL, GE Healthcare) with variable exposure times and subsequent automated film development.

Determination of protein interactions by immunoprecipitation

For immunoprecipitation experiments native yeast extracts were prepared. To avoid protein degradation, all steps were performed at 4°C and the IP lysis buffer was freshly supplemented with protease inhibitors (1 x EDTA-free complete cocktail and 1 mg/ml Pefabloc SC (Roche)). Briefly, 150 OD₆₀₀ of yeast cells were harvested from cultures at

MATERIALS AND METHODS

desired time points, washed once in ice-cold PBS and transferred to 2 ml reaction tubes. Cell pellets were either snap-frozen in liquid nitrogen and short-term stored at -80°C or directly processed for cell extract preparation. To this end, pellets were resuspended in 800 μ l of IP lysis buffer, an equal volume of zirconia/silica beads (BioSpec Inc.) added and lysis performed on a multi-tube bead-beater (MM301, Retsch GmbH) in 6 intervals of 1 min shaking (frequency 30/s) and 4 min pausing for cool-down (bead-beater was used in a 4°C room). Lysed samples were then separated from the beads and collected in a fresh tube by piggyback elution. To enrich protein interactions that occur in the chromatin environment, the lysate was subsequently sonicated for 10 min in ice-water (output 200W; 10 cycles with 30 s sonication and 30 s break) using the Bioruptor UCD-200 sonication system (Diagenode). Cell debris was then removed by centrifugation (4000 g, 10 min, 4°C) and the supernatant added to 1 ml of IP lysis buffer. 25 μ l HA affinity matrix (Roche) were washed twice with IP lysis buffer and incubated with 800 μ l of the lysate for 3 h at 4°C on a rotating wheel. Next, the beads were pelleted by centrifugation (500 g, 1 min, 4°C), the supernatant removed by aspiration and the beads washed 3 x with 500 μ l of IP lysis buffer. The immunoprecipitated material was eluted from the beads by addition of 40 μ l of HU buffer and incubation at 65°C for 10 min in a shaking thermomixer (1400 rpm). As input control, 20 μ l of the lysate were mixed with 60 μ l of HU buffer and similarly incubated at 65°C. Both the input material and the immunoprecipitated material were subsequently analyzed by SDS-PAGE and immunoblot analysis (see above).

Antibodies

Antibody	Type	Use	Source
Arp5 (ab12099)	primary (rabbit IgG)	ChIP (2 μ l)	Abcam
c-myc (A-14)	primary (rabbit IgG)	Blot (1:2500)	Santa Cruz
Dpm1	primary (mouse IgG)	Blot (1:500)	Thermo Fisher
γ H2A	primary (rabbit IgG)	ChIP (3 μ l)	Upstate
H2A	primary (rabbit IgG)	ChIP (3 μ l)	Active Motif
H2B	primary (rabbit IgG)	ChIP (3 μ l)	Active Motif
H3 c-terminal	primary (rabbit IgG)	ChIP (6 μ l)	Active Motif
HA (ab9110)	primary (rabbit IgG)	ChIP (3 μ l)	Abcam
HA (F-7)	primary (mouse IgG)	Blot (1:1000)	Sana Cruz
HRP-coupled α -mouse	Secondary (goat IgG)	Blot (1:5000)	Dianova
HRP-coupled α -rabbit	Secondary (goat IgG)	Blot (1:5000)	Dianova
Htz1	primary (rabbit IgG)	Blot (1:750) ChIP (3 μ l)	ActiveMotif
Pgk1	primary (mouse IgG)	Blot (1:2000)	Thermo Fisher
Rad51 (ab63798)	primary (rabbit IgG)	Blot (1:5000)	Abcam
Rad51 (y-180)	primary (rabbit IgG)	ChIP (4 μ l)	Santa Cruz

MATERIALS AND METHODS

Rad52	primary (rabbit IgG)	Blot (1:2000) ChIP (3 μ l)	Ref. 251
RPA (RFA)	primary (rabbit IgG)	ChIP (1.5 μ l)	Agrisera

5.3.2 Chromatin techniques

Buffers and solutions

FA lysis buffer

- 50 mM Hepes-KOH, pH 7.5
- 150 mM NaCl
- 1 mM EDTA
- 1 % (v/v) Triton X-100
- 0.1 % (w/v) Deoxycholic acid, Na-salt
- 0.1 % (w/v) SDS

FA lysis buffer 500 (high salt)

- 50 mM Hepes-KOH, pH 7.5
- 500 mM NaCl
- 1 mM EDTA
- 1 % (v/v) Triton X-100
- 0.1 % (w/v) Deoxycholic acid, Na-salt
- 0.1 % (w/v) SDS

ChIP wash buffer

- 10 mM Tris-HCl, pH 8
- 250 mM LiCl
- 1 mM EDTA
- 0.5 % (v/v) NP-40
- 0.5 % (w/v) Deoxycholic acid, Na-salt

TE

- 10 mM Tris-HCl, pH 8
- 1 mM EDTA

ChIP elution buffer

- 50 mM Tris-HCl, pH 7.5
- 10 mM EDTA
- 1 % (w/v) SDS

Chromatin immunoprecipitation

Chromatin immunoprecipitation (ChIP) was essentially performed as described previously^{47,252}. For all ChIP experiments in this study, 200 ml cultures of cells were cross-linked by addition of Formaldehyde (37 % solution, Roth) to a final concentration of 1 % (v/v) and incubation for 16 min under moderate shaking at RT prior to the addition of 2.5 M Glycine to terminate the reaction. Cross-linked cultures were then allowed to shake another minimum of 15 min before 140 OD₆₀₀ were harvested by centrifugation (3500 g,

MATERIALS AND METHODS

5 min, 4°C), washed with ice-cold PBS and transferred to 2 ml reaction tubes. Cell pellets were immediately snap-frozen in liquid nitrogen and stored at -80°C (up to a few weeks) until further processing. Although proteases were likely inactivated during cross-linking, subsequent cell lysis was performed at 4°C and the FA lysis buffer freshly supplemented with protease inhibitors (1x EDTA-free complete cocktail and 1 mg/ml Pefabloc SC (Roche)). Pellets were then resuspended in 800 µl of FA lysis buffer, an equal volume of zirconia/silica beads (BioSpec Inc.) added and lysis performed on a multi-tube bead-beater (MM301, Retsch GmbH) in 6 intervals of 3 min shaking (frequency 30/s) and 3 min pausing for cool-down (bead-beater was used in a 4°C room). Lysed samples were separated from the beads and collected in a fresh tube by piggyback elution. The chromatin fraction was subsequently enriched by centrifugation (20000 g, 15 min, 4°C), followed by resuspension of the pellet in 1 ml FA lysis buffer and transferred to hard plastic 15 ml TPX tubes (Diagenode). 40 cycles of sonication were then conducted (output 200 W; each cycle 30 s sonication and 30 s break) using the Bioruptor UCD-200 sonication system (Diagenode), with the aim to shear the DNA to an average length of 250-500 bp (occasionally controlled by phenol-chloroform purification and subsequent agarose gel electrophoresis of input DNA). After every 10 cycles, 200 ml water of the sonication bath were exchanged for an equal volume of ice to constantly maintain low temperatures. An additional ml of FA lysis buffer was then added to the sheared chromatin and cell debris removed by centrifugation (6150 g, 30 min, 4°C). 20 µl of chromatin lysate were taken aside as input reference and 800 µl used for immunoprecipitation. To this end, the lysate supplemented with a primary antibody of choice (see table “antibodies” in section 5.3.1) was incubated for 1.5 h at RT on a rotating wheel, followed by addition of 20 µl Protein A Sepharose CL-4B (GE Healthcare), pre-swollen in 80 µl of lysis buffer, and another 30 min of incubation. Next, the beads were pelleted by centrifugation (500 g, 1 min, RT), the supernatant removed by aspiration and the beads consecutively washed 3 x with FA lysis buffer and 1 x each with FA lysis buffer 500, ChIP wash buffer and TE. The immunoprecipitated material was eluted from the beads by addition of 110 µl ChIP elution buffer and incubation at 65°C for 10 min in a shaking thermomixer (1400 rpm). The eluate was separated from the sepharose beads by centrifugation (8000 g, 2 min, RT) and 100 µl transferred to a 0.5 ml reaction tube. Both eluate and input samples were subjected to Proteinase K (Sigma, final concentration 2mg/ml) digestion in a volume of 200 µl with a final SDS concentration of 0.5 % for 2 h at 42°C, and subsequently cross-links were reversed by incubation at 65°C for 6 h. All samples were finally purified using the QIAquick PCR purification kit (Qiagen) with input

DNA eluted in 50 μ l and ChIP DNA eluted in 100 μ l EB buffer. Thereafter, samples were either subjected to qPCR (see section 5.2.2), whole genome amplification for ChIP-chip analysis (see below) or next-generation sequencing library amplification for ChIP-seq analysis (see below).

ChIP-chip analysis

ChIP-chip analysis to detect protein binding to DNA on a genome-wide level was performed as described previously^{47,125}. Briefly, ChIP-samples were RNase A-digested (10 mg/ml in 10 mM Tris-HCl pH 7.5, DNase-inactivated by boiling for 10 min, final concentration 0.1 mg/ml) and again purified using the QIAquick PCR purification system (Qiagen). DNA was then amplified in two rounds of 14 cycles using the GenomePlex Whole Genome Amplification (WGA) and reamplification kits (Sigma) as described in the Farnham Lab protocol for WGA amplification of DNA²⁵³. Subsequent labeling of input and IP samples (using Cy3 or Cy5 fluorescent dyes), hybridization to custom-made high-density arrays covering the whole *S. cerevisiae* genome (NimbleGen), array scanning as well as raw data extraction were performed by SourceBioSource. NimbleGen custom arrays were specified by 84 base pairs median genomic probe spacing and only unique oligonucleotides. ChIP-chip experiments were performed in duplicates, involving a hybridization dye-swap of input and IP material.

ChIP-seq analysis

ChIP coupled to next-generation sequencing was performed to detect protein binding to DNA on a genome-wide level following official cessation of the NimbleGen microarray service. Briefly, ChIP DNA was prepared as described above with the exception of an RNase A digestion step (final concentration 0.2 mg/ml) for 1 h at 37°C prior to the addition of Proteinase K. Sequencing libraries were then generated using the MicroPlex library preparation kit v2 including 48 indices (Diagenode) as described by the manufacturer's instructions. Specifically, DNA concentrations were determined using the QuantiT™ PicoGreen® dsDNA assay kit (Thermo Fisher Scientific) together with an Infinite M1000 Pro microplate reader (Tecan) and the DNA then typically amplified for 4+9 cycles (input, 2 ng starting material) or 4+14 cycles (IP, 200 pg starting material), aiming at a final concentration of 10 ng/ μ l. Subsequent determination of sample molarity using an Agilent 2100 Bioanalyzer (Agilent Genomics), and sequencing of 50 bp single-end reads on an Illumina HiSeq sequencer (Illumina) at an average of 3 million reads per sample were performed by the sequencing core facility of the LMU Munich (LAFUGA). ChIP-seq experiments were typically performed in duplicates and to avoid technical fluctuations,

duplicates of all samples in one experiment were typically amplified together and, using 48-index multiplexing, sequenced together on a single lane.

Determination of protein binding to chromatin (chromatin binding assay)

For the analysis of histone removal from chromatin following DNA damage induction, cell extracts were prepared and separated into chromatin-bound and soluble protein fractions using a sucrose cushion. Briefly, cells were nocodazole-arrested (see section 5.1.2) in YPD and subsequently subjected to DNA damage by addition of Phleomycin (InvivoGen, final concentration 50 $\mu\text{g}/\text{ml}$). Cell amounts of 25 OD₆₀₀ were collected from the culture immediately prior to DNA damage induction as well as 30, 60 and 120 min afterwards. At each time point, cells were harvested by centrifugation (1000 g, 2 min, 4°C) and ATP-dependent processes were immediately blocked by resuspension in STOP buffer (150 mM NaCl, 1 mM NaN₃, 50 mM NaF, 10 mM EDTA, pH 8.0) until all samples were collected. Pellets were then sequentially washed with de-ionized water and 1.2 M sorbitol, resuspended in 1 ml CB1 buffer (50 mM sodium citrate, 1.2M sorbitol, 40 mM EDTA, pH 8.0) and spheroblased by addition of 138 μl spheroblast solution (125 μl 2xCB1 buffer, 8 μl zymolyase Z100T (50mg/ml), 5 μl β -Me) and 30 min incubation at 30°C. Spheroblasts were collected by centrifugation (290 g, 4 min, 4°C), resuspended in 425 μl 1.2 M Sorbitol and lysed by addition of 50 μl 10 x lysis buffer (500 mM KAc, 20 mM MgCl₂, 200 mM Hepes-KOH, pH 7.9, freshly supplemented with protease inhibitors) as well as 50 μl 10 % TX-100 and incubation at 4°C for 5 min. Aliquots of total cell extracts were collected, 250 μl of the remaining material applied on 125 μl of a sucrose cushion (50 mM Hepes/KOH pH7.5, 100 mM KCl, 2.5 mM MgCl₂, 0.4 M Sorbitol, 0.25 % T-X100, 30 % Sucrose, freshly supplemented with 1mM DTT and protease inhibitors) and chromatin and soluble fractions separated by centrifugation (20000 g, 5 min, 4°C). Proteins in total extracts and soluble fractions were TCA-precipitated and the resulting protein pellets together with the chromatin pellets incubated in HU buffer for 10 min at 65°C prior to analysis via SDS-PAGE (see section 5.3.1).

Detection of open chromatin using FAIRE

Formaldehyde-associated isolation of responsive elements (FAIRE) was essentially performed as described previously¹⁹⁰ and used to identify open chromatin during homology search. Briefly, yeast cells were treated as for ChIP (see above), with the only difference that 50 OD₆₀₀ of cells were harvested. Also cell lysis was performed as indicated for ChIP, yet directly sonicating the whole cell lysate without enriching the chromatin fraction by centrifugation. To distinguish open from condensed chromatin,

sonicated samples were subsequently divided in two halves, each mixed with an equal volume of Phenol-Chloroform-Isoamylalcohol (PCI, 25:24:1, Roth) and nucleosomal DNA precipitated by centrifugation (20000 g, 15 min, 4°C). The nucleosome-free DNA in the aqueous phase was then purified via ethanol precipitation by adding 0.1 volumes of 3 M NaOAc and 2.5 volumes of ice-cold EtOH and subsequent centrifugation (20000 g, 15 min, 4°C). After a washing step with 70 % ice-cold EtOH, pellets were dried for 5 min at 50°C, eluted in 40 µl of TE and corresponding samples re-pooled. RNA was digested using RNase A (final concentration 0.25 µg/ml) for 30 min at 37°C and the remaining DNA purified using the QIAquick PCR purification kit (Qiagen). DNA was eventually analyzed by qPCR as indicated above.

5.4 Bioinformatics

5.4.1 ChIP-chip analysis

Quality controls, normalization and data analysis of ChIP-chip experiments were performed using the R software tool²⁵⁴ (www.Rproject.org) as described previously²⁵⁵ (Tobias Straub Epigenome project PROT43, <http://www.epigenesys.eu/>). Despite array normalization and mean-averaging two independent experiments, the depicted data represent raw data. Consequently, single spikes correspond to single oligonucleotides and are hybridization artifacts. All ChIP-chip data are normalized to the input and the corresponding 0 h data set.

5.4.2 ChIP-seq analysis

Multiplexed raw data files generated on the Illumina HiSeq sequencer were initially de-multiplexed using the Illumina De-Multiplex application available on the Galaxy web platform hosted by the sequencing core facility of the LMU Munich. De-multiplexed raw data was subsequently further processed by Tobias Straub (Bioinformatics Core Facility, LMU Munich) and Assa Yeroslaviz (Bioinformatics Core Facility, MPI of Biochemistry) using the R software tool²⁵⁶.

Briefly, raw data quality was analyzed using the FastQC tool (<http://www.bioinformatics.babraham.ac.uk/projects/fastqc/>). The fastq raw files were then mapped to the *S. cerevisiae* genome (genome built R-64-1-1) downloaded from Ensembl using the bowtie1 aligner²⁵⁷ with standard parameters except -m=1, indicating that reads mapping to the genome more than once were filtered from the analysis. The genome was

split into non-overlapping windows with a size of 500 bp and all successfully mapped reads (generally > 70 %) assigned to their corresponding window(s) using the GenomicRanges R package²⁵⁸ (a read was considered to map to two neighboring windows as soon as a single base overlapped between those two). For a statistical comparison of input with IP samples the window counts were TMM-normalized²⁵⁹, the dispersion was estimated²⁶⁰ and a negative binomial generalized log-linear model was fitted using a generalized linear model²⁶¹ using the edgeR²⁶² R package. Normalized IP/input values were then written to wig files for visualization using publicly available genome browsers^{263,264}. In case of the centromere analysis depicted in Figure 24 A, BEDtools²⁶⁵ was used to generate a saf file containing 500 bp windows of the regions surrounding all centromeres ± 90 kb, except CenIV. Reads in the respective windows were then counted from the mapped files using featureCounts²⁶⁶ and the subsequently calculated normalized IP/input ratios of corresponding windows with similar linear distances averaged over all chromosomes. The ratios were plotted as a locally weighted regression using the geom_smooth function of the ggplot2 R package²⁶⁷.

All data depicted present log₂ enrichments and were normalized to the corresponding 0 h time point.

5.4.3 Statistical analysis

ChIP-qPCR data and recombination assay data typically represent the mean of three independent biological replicates with the error bars corresponding to their standard deviation (SD), if not indicated differently. All ChIP-chip and ChIP-seq data are depicted on log₂ scales as the mean of two biological replicates (with error bars corresponding to the standard error of the mean (SEM)). Statistical significance was tested via Student's t-test analysis, typically for unpaired samples, but paired in case where mutant strains have been normalized to their corresponding wild type. One asterisk indicates $p < 0.05$, two asterisks indicate $p < 0.01$ and three asterisks indicate $p < 0.001$.

5.4.4 Online resources and computer programs

S. cerevisiae genomic sequence and protein information was derived from the Saccharomyces Genome Database (www.yeastgenome.org) and UniProt Consortium (<http://www.uniprot.org>), DNA and protein sequence manipulation as well as Sanger sequencing analysis performed using DNA-Star software (DNA Star Inc.).

ChIP-chip and ChIP-seq data were generally visualized and presented using the Integrated Genome Browser²⁶⁴ (<http://bioviz.org/igb/index.html>) and Matlab was used to segment ChIP-chip data into windows of certain kb ranges for data presented in Figure 11, Figure 12 and Figure 13.

Data depicted in diagrams, including their statistical analysis, were generated with the help of GraphPad Prism software (www.graphpad.com/scientific-software/prism/) and immunoblots were cropped as well as level- and contrast-adjusted using Adobe Photoshop (Adobe Systems Inc.).

Figures and illustrations were arranged and designed using Adobe Illustrator (Adobe Systems Inc.) and general text and table generation done via the Microsoft Office software package (Microsoft Corp.).

For literature review, databases integrated into the National Center of Biotechnology Information (www.ncbi.nlm.nih.gov) and Papers 3 (<http://papersapp.com/mac/>) were used.

6 REFERENCES

1. Crick, F. The double helix: a personal view. *Nature* **248**, 766–769 (1974).
2. Hoeijmakers, J. H. DNA damage, aging, and cancer. *N Engl J Med* **361**, 1475–1485 (2009).
3. Lindahl, T. Instability and decay of the primary structure of DNA. *Nature* **362**, 709–715 (1993).
4. Lindahl, T. The Intrinsic Fragility of DNA (Nobel Lecture). *Angew. Chem. Int. Ed. Engl.* **55**, 8528–8534 (2016).
5. Friedberg, E. C. DNA damage and repair. *Nature* **421**, 436–440 (2003).
6. Barnes, D. E. & Lindahl, T. Repair and genetic consequences of endogenous DNA base damage in mammalian cells. *Annu. Rev. Genet.* **38**, 445–476 (2004).
7. Nospikel, T. DNA repair in mammalian cells : Nucleotide excision repair: variations on versatility. *Cell. Mol. Life Sci.* **66**, 994–1009 (2009).
8. Jiricny, J. The multifaceted mismatch-repair system. *Nat Rev Mol Cell Biol* **7**, 335–346 (2006).
9. San Filippo, J., Sung, P. & Klein, H. Mechanism of eukaryotic homologous recombination. *Annu. Rev. Biochem.* **77**, 229–257 (2008).
10. Harper, J. W. & Elledge, S. J. The DNA damage response: ten years after. *Mol Cell* **28**, 739–745 (2007).
11. Hoeijmakers, J. H. Genome maintenance mechanisms for preventing cancer. *Nature* **411**, 366–374 (2001).
12. Vilenchik, M. M. & Knudson, A. G. Endogenous DNA double-strand breaks: production, fidelity of repair, and induction of cancer. *Proc. Natl. Acad. Sci. U.S.A.* **100**, 12871–12876 (2003).
13. Mehta, A. & Haber, J. E. Sources of DNA double-strand breaks and models of recombinational DNA repair. *Cold Spring Harb Perspect Biol* **6**, a016428–a016428 (2014).
14. Ensminger, M. *et al.* DNA breaks and chromosomal aberrations arise when replication meets base excision repair. *J. Cell Biol.* **206**, 29–43 (2014).
15. Huang, L. C., Clarkin, K. C. & Wahl, G. M. Sensitivity and selectivity of the DNA damage sensor responsible for activating p53-dependent G1 arrest. *Proc. Natl. Acad. Sci. U.S.A.* **93**, 4827–4832 (1996).
16. Bennett, C. B., Lewis, A. L., Baldwin, K. K. & Resnick, M. A. Lethality induced by a single site-specific double-strand break in a dispensable yeast plasmid. *Proc. Natl. Acad. Sci. U.S.A.* **90**, 5613–5617 (1993).
17. Helleday, T., Petermann, E., Lundin, C., Hodgson, B. & Sharma, R. A. DNA repair pathways as targets for cancer therapy. *Nat. Rev. Cancer* **8**, 193–204 (2008).
18. de Massy, B. Initiation of meiotic recombination: how and where? Conservation and specificities among eukaryotes. *Annu. Rev. Genet.* **47**, 563–599 (2013).
19. Haber, J. E. Mating-type genes and MAT switching in *Saccharomyces cerevisiae*. *Genetics* **191**, 33–64 (2012).
20. Alt, F. W., Zhang, Y., Meng, F.-L., Guo, C. & Schwer, B. Mechanisms of programmed DNA lesions and genomic instability in the immune system. *Cell* **152**, 417–429 (2013).
21. Lieber, M. R. The mechanism of double-strand DNA break repair by the nonhomologous DNA end-joining pathway. *Annu. Rev. Biochem.* **79**, 181–211 (2010).
22. Daley, J. M., Palmboos, P. L., Wu, D. & Wilson, T. E. Nonhomologous end joining in yeast. *Annu. Rev. Genet.* **39**, 431–451 (2005).
23. Milne, G. T., Jin, S., Shannon, K. B. & Weaver, D. T. Mutations in two Ku homologs define a DNA end-joining repair pathway in *Saccharomyces cerevisiae*.

REFERENCES

- Mol. Cell. Biol.* **16**, 4189–4198 (1996).
24. Feldmann, H. & Winnacker, E. L. A putative homologue of the human autoantigen Ku from *Saccharomyces cerevisiae*. *J Biol Chem* **268**, 12895–12900 (1993).
 25. Boulton, S. J. & Jackson, S. P. *Saccharomyces cerevisiae* Ku70 potentiates illegitimate DNA double-strand break repair and serves as a barrier to error-prone DNA repair pathways. *EMBO J* **15**, 5093–5103 (1996).
 26. Walker, J. R., Corpina, R. A. & Goldberg, J. Structure of the Ku heterodimer bound to DNA and its implications for double-strand break repair. *Nature* **412**, 607–614 (2001).
 27. Stracker, T. H. & Petrini, J. H. The MRE11 complex: starting from the ends. *Nat Rev Mol Cell Biol* **12**, 90–103 (2011).
 28. Teo, S. H. & Jackson, S. P. Lif1p targets the DNA ligase Lig4p to sites of DNA double-strand breaks. *Curr Biol* **10**, 165–168 (2000).
 29. Wilson, T. E., Grawunder, U. & Lieber, M. R. Yeast DNA ligase IV mediates non-homologous DNA end joining. *Nature* **388**, 495–498 (1997).
 30. Chen, L., Trujillo, K., Ramos, W., Sung, P. & Tomkinson, A. E. Promotion of Dnl4-catalyzed DNA end-joining by the Rad50/Mre11/Xrs2 and Hdf1/Hdf2 complexes. *Molecular Cell* **8**, 1105–1115 (2001).
 31. Graham, T. G. W., Walter, J. C. & Loparo, J. J. Two-Stage Synapsis of DNA Ends during Non-homologous End Joining. *Mol Cell* **61**, 850–858 (2016).
 32. Wilson, T. E. & Lieber, M. R. Efficient processing of DNA ends during yeast nonhomologous end joining. Evidence for a DNA polymerase beta (Pol4)-dependent pathway. *J Biol Chem* **274**, 23599–23609 (1999).
 33. Wu, X., Wilson, T. E. & Lieber, M. R. A role for FEN-1 in nonhomologous DNA end joining: the order of strand annealing and nucleolytic processing events. *Proc. Natl. Acad. Sci. U.S.A.* **96**, 1303–1308 (1999).
 34. Tseng, H.-M. & Tomkinson, A. E. Processing and joining of DNA ends coordinated by interactions among Dnl4/Lif1, Pol4, and FEN-1. *J Biol Chem* **279**, 47580–47588 (2004).
 35. Sfeir, A. & Symington, L. S. Microhomology-Mediated End Joining: A Back-up Survival Mechanism or Dedicated Pathway? *Trends in Biochemical Sciences* **40**, 701–714 (2015).
 36. Cannavó, E. & Cejka, P. Sae2 promotes dsDNA endonuclease activity within Mre11-Rad50-Xrs2 to resect DNA breaks. *Nature* **514**, 122–125 (2014).
 37. Lee, K. & Lee, S. E. *Saccharomyces cerevisiae* Sae2- and Tel1-dependent single-strand DNA formation at DNA break promotes microhomology-mediated end joining. *Genetics* **176**, 2003–2014 (2007).
 38. Mateos-Gomez, P. A. *et al.* Mammalian polymerase θ promotes alternative NHEJ and suppresses recombination. *Nature* **518**, 254–257 (2015).
 39. Heyer, W. D., Ehmsen, K. T. & Liu, J. Regulation of homologous recombination in eukaryotes. *Annu. Rev. Genet.* **44**, 113–139 (2010).
 40. Venkitaraman, A. R. Cancer Suppression by the Chromosome Custodians, BRCA1 and BRCA2. *Science* **343**, 1470–1475 (2014).
 41. Huertas, P., Cortes-Ledesma, F., Sartori, A. A., Aguilera, A. & Jackson, S. P. CDK targets Sae2 to control DNA-end resection and homologous recombination. *Nature* **455**, 689–692 (2008).
 42. Zhu, Z., Chung, W.-H., Shim, E. Y., Lee, S. E. & Ira, G. Sgs1 helicase and two nucleases Dna2 and Exo1 resect DNA double-strand break ends. *Cell* **134**, 981–994 (2008).
 43. Mimitou, E. P. & Symington, L. S. Sae2, Exo1 and Sgs1 collaborate in DNA double-strand break processing. *Nature* **455**, 770–774 (2008).
 44. Deng, S. K., Gibb, B., de Almeida, M. J., Greene, E. C. & Symington, L. S. RPA antagonizes microhomology-mediated repair of DNA double-strand breaks. *Nat*

REFERENCES

- Struct Mol Biol* **21**, 405–412 (2014).
45. Shinohara, A. & Ogawa, T. Stimulation by Rad52 of yeast Rad51-mediated recombination. *Nature* **391**, 404–407 (1998).
 46. New, J. H., Sugiyama, T., Zaitseva, E. & Kowalczykowski, S. C. Rad52 protein stimulates DNA strand exchange by Rad51 and replication protein A. *Nature* **391**, 407–410 (1998).
 47. Renkawitz, J., Lademann, C. A., Kalocsay, M. & Jentsch, S. Monitoring homology search during DNA double-strand break repair in vivo. *Mol Cell* **50**, 261–272 (2013).
 48. Wright, W. D. & Heyer, W.-D. Rad54 functions as a heteroduplex DNA pump modulated by its DNA substrates and Rad51 during D loop formation. *Mol Cell* **53**, 420–432 (2014).
 49. Sarbajna, S. & West, S. C. Holliday junction processing enzymes as guardians of genome stability. *Trends in Biochemical Sciences* **39**, 409–419 (2014).
 50. Wu, L. & Hickson, I. D. The Bloom's syndrome helicase suppresses crossing over during homologous recombination. *Nature* **426**, 870–874 (2003).
 51. Malkova, A. & Ira, G. Break-induced replication: functions and molecular mechanism. *Curr. Opin. Genet. Dev.* **23**, 271–279 (2013).
 52. Saini, N. *et al.* Migrating bubble during break-induced replication drives conservative DNA synthesis. *Nature* **502**, 389–392 (2013).
 53. Kanaar, R., Wyman, C. & Rothstein, R. Quality control of DNA break metabolism: in the 'end', it's a good thing. *EMBO J* **27**, 581–588 (2008).
 54. Zelensky, A., Kanaar, R. & Wyman, C. Mediators of homologous DNA pairing. *Cold Spring Harb Perspect Biol* **6**, a016451–a016451 (2014).
 55. Lisby, M., Barlow, J. H., Burgess, R. C. & Rothstein, R. Choreography of the DNA damage response: spatiotemporal relationships among checkpoint and repair proteins. *Cell* **118**, 699–713 (2004).
 56. Wolner, B., van Komen, S., Sung, P. & Peterson, C. L. Recruitment of the recombinational repair machinery to a DNA double-strand break in yeast. *Mol Cell* **12**, 221–232 (2003).
 57. Sugawara, N., Wang, X. & Haber, J. E. In vivo roles of Rad52, Rad54, and Rad55 proteins in Rad51-mediated recombination. *Mol Cell* **12**, 209–219 (2003).
 58. Sung, P. Yeast Rad55 and Rad57 proteins form a heterodimer that functions with replication protein A to promote DNA strand exchange by Rad51 recombinase. *Genes & Development* **11**, 1111–1121 (1997).
 59. Liu, J. *et al.* Rad51 paralogues Rad55-Rad57 balance the antirecombinase Srs2 in Rad51 filament formation. *Nature* **479**, 245–248 (2011).
 60. Gaines, W. A. *et al.* Promotion of presynaptic filament assembly by the ensemble of *S. cerevisiae* Rad51 paralogues with Rad52. *Nat Commun* **6**, 7834 (2015).
 61. Bernstein, K. A. *et al.* The Shu complex, which contains Rad51 paralogues, promotes DNA repair through inhibition of the Srs2 anti-recombinase. *Molecular Biology of the Cell* **22**, 1599–1607 (2011).
 62. Godin, S. *et al.* The Shu complex interacts with Rad51 through the Rad51 paralogues Rad55-Rad57 to mediate error-free recombination. *Nucleic Acids Res.* **41**, 4525–4534 (2013).
 63. Taylor, M. R. G. *et al.* Rad51 Paralogs Remodel Pre-synaptic Rad51 Filaments to Stimulate Homologous Recombination. *Cell* **162**, 271–286 (2015).
 64. Daley, J. M., Gaines, W. A., Kwon, Y. & Sung, P. Regulation of DNA pairing in homologous recombination. *Cold Spring Harb Perspect Biol* **6**, a017954–a017954 (2014).
 65. Veaute, X. *et al.* The Srs2 helicase prevents recombination by disrupting Rad51 nucleoprotein filaments. *Nature* **423**, 309–312 (2003).
 66. Krejci, L. *et al.* DNA helicase Srs2 disrupts the Rad51 presynaptic filament.

REFERENCES

- Nature* **423**, 305–309 (2003).
67. Pfander, B., Moldovan, G.-L., Sacher, M., Hoege, C. & Jentsch, S. SUMO-modified PCNA recruits Srs2 to prevent recombination during S phase. *Nature* **436**, 428–433 (2005).
 68. Ceballos, S. J. & Heyer, W.-D. Functions of the Snf2/Swi2 family Rad54 motor protein in homologous recombination. *Biochim Biophys Acta* **1809**, 509–523 (2011).
 69. Spies, J. *et al.* Nek1 Regulates Rad54 to Orchestrate Homologous Recombination and Replication Fork Stability. *Mol Cell* **62**, 903–917 (2016).
 70. Psakhye, I. & Jentsch, S. Protein group modification and synergy in the SUMO pathway as exemplified in DNA repair. *Cell* **151**, 807–820 (2012).
 71. Renkawitz, J., Lademann, C. A. & Jentsch, S. Mechanisms and principles of homology search during recombination. *Nat Rev Mol Cell Biol* **15**, 369–383 (2014).
 72. Mazin, A. V. & Kowalczykowski, S. C. The specificity of the secondary DNA binding site of RecA protein defines its role in DNA strand exchange. *Proc. Natl. Acad. Sci. U.S.A.* **93**, 10673–10678 (1996).
 73. Cloud, V., Chan, Y.-L., Grubb, J., Budke, B. & Bishop, D. K. Rad51 is an accessory factor for Dmc1-mediated joint molecule formation during meiosis. *Science* **337**, 1222–1225 (2012).
 74. Mazin, A. V. & Kowalczykowski, S. C. The function of the secondary DNA-binding site of RecA protein during DNA strand exchange. *EMBO J* **17**, 1161–1168 (1998).
 75. De Vlaminck, I. *et al.* Mechanism of homology recognition in DNA recombination from dual-molecule experiments. *Mol Cell* **46**, 616–624 (2012).
 76. Folta-Stogniew, E., O'Malley, S., Gupta, R., Anderson, K. S. & Radding, C. M. Exchange of DNA base pairs that coincides with recognition of homology promoted by *E. coli* RecA protein. *Mol Cell* **15**, 965–975 (2004).
 77. Rangunathan, K., Liu, C. & Ha, T. RecA filament sliding on DNA facilitates homology search. *Elife* **1**, e00067 (2012).
 78. Forget, A. L. & Kowalczykowski, S. C. Single-molecule imaging of DNA pairing by RecA reveals a three-dimensional homology search. *Nature* **482**, 423–427 (2012).
 79. Qi, Z. *et al.* DNA sequence alignment by microhomology sampling during homologous recombination. *Cell* **160**, 856–869 (2015).
 80. Chen, Z., Yang, H. & Pavletich, N. P. Mechanism of homologous recombination from the RecA-ssDNA/dsDNA structures. *Nature* **453**, 489–484 (2008).
 81. Aylon, Y. & Kupiec, M. DSB repair: the yeast paradigm. *DNA repair* **3**, 797–815 (2004).
 82. Aylon, Y., Liefshitz, B., Bitan-Banin, G. & Kupiec, M. Molecular dissection of mitotic recombination in the yeast *Saccharomyces cerevisiae*. *Mol. Cell. Biol.* **23**, 1403–1417 (2003).
 83. Inbar, O. & Kupiec, M. Homology search and choice of homologous partner during mitotic recombination. *Mol. Cell. Biol.* **19**, 4134–4142 (1999).
 84. Haber, J. E. & Leung, W. Y. Lack of chromosome territoriality in yeast: promiscuous rejoining of broken chromosome ends. *Proc. Natl. Acad. Sci. U.S.A.* **93**, 13949–13954 (1996).
 85. Lichten, M. & Haber, J. E. Position effects in ectopic and allelic mitotic recombination in *Saccharomyces cerevisiae*. *Genetics* **123**, 261–268 (1989).
 86. White, R. R. *et al.* Double-strand break repair by interchromosomal recombination: an in vivo repair mechanism utilized by multiple somatic tissues in mammals. *PLoS ONE* **8**, e84379 (2013).
 87. Cavalli, G. & Misteli, T. Functional implications of genome topology. *Nat Struct Mol Biol* **20**, 290–299 (2013).

REFERENCES

88. Zimmer, C. & Fabre, E. Principles of chromosomal organization: lessons from yeast. *J. Cell Biol.* **192**, 723–733 (2011).
89. Wong, H. *et al.* A predictive computational model of the dynamic 3D interphase yeast nucleus. *Curr Biol* **22**, 1881–1890 (2012).
90. Branzei, D. & Foiani, M. Maintaining genome stability at the replication fork. *Nat Rev Mol Cell Biol* **11**, 208–219 (2010).
91. Nasmyth, K. & Haering, C. H. Cohesin: its roles and mechanisms. *Annu. Rev. Genet.* **43**, 525–558 (2009).
92. Loidl, J. The hidden talents of SPO11. *Developmental Cell* **24**, 123–124 (2013).
93. Hoang, M. L. *et al.* Competitive repair by naturally dispersed repetitive DNA during non-allelic homologous recombination. *PLoS Genet* **6**, e1001228 (2010).
94. Argueso, J. L. *et al.* Double-strand breaks associated with repetitive DNA can reshape the genome. *Proc. Natl. Acad. Sci. U.S.A.* **105**, 11845–11850 (2008).
95. Neumann, F. R. *et al.* Targeted INO80 enhances subnuclear chromatin movement and ectopic homologous recombination. *Genes Dev* **26**, 369–383 (2012).
96. Dion, V., Kalck, V., Horigome, C., Towbin, B. D. & Gasser, S. M. Increased mobility of double-strand breaks requires Mec1, Rad9 and the homologous recombination machinery. *Nature Cell Biology* **14**, 502–509 (2012).
97. Miné-Hattab, J. & Rothstein, R. Increased chromosome mobility facilitates homology search during recombination. *Nature Cell Biology* **14**, 510–517 (2012).
98. Seeber, A., Dion, V. & Gasser, S. M. Checkpoint kinases and the INO80 nucleosome remodeling complex enhance global chromatin mobility in response to DNA damage. *Genes Dev* **27**, 1999–2008 (2013).
99. Cho, N. W., Dilley, R. L., Lampson, M. A. & Greenberg, R. A. Interchromosomal Homology Searches Drive Directional ALT Telomere Movement and Synapsis. *Cell* **159**, 108–121 (2014).
100. Lottersberger, F., Karssemeijer, R. A., Dimitrova, N. & de Lange, T. 53BP1 and the LINC Complex Promote Microtubule-Dependent DSB Mobility and DNA Repair. *Cell* **163**, 880–893 (2015).
101. Dion, V. & Gasser, S. M. Chromatin movement in the maintenance of genome stability. *Cell* **152**, 1355–1364 (2013).
102. Strecker, J. *et al.* DNA damage signalling targets the kinetochore to promote chromatin mobility. *Nature Cell Biology* **18**, 281–290 (2016).
103. Muers, M. Chromatin: Evolutionary insights into nucleosomes. *Nat Rev Genet* **14**, 78 (2013).
104. Jiang, C. & Pugh, B. F. Nucleosome positioning and gene regulation: advances through genomics. *Nat Rev Genet* **10**, 161–172 (2009).
105. Kornberg, R. D. Chromatin structure: a repeating unit of histones and DNA. *Science* **184**, 868–871 (1974).
106. Luger, K., Mäder, A. W., Richmond, R. K., Sargent, D. F. & Richmond, T. J. Crystal structure of the nucleosome core particle at 2.8 Å resolution. *Nature* **389**, 251–260 (1997).
107. Ransom, M., Dennehey, B. K. & Tyler, J. K. Chaperoning histones during DNA replication and repair. *Cell* **140**, 183–195 (2010).
108. Patterton, H. G., Landel, C. C., Landsman, D., Peterson, C. L. & Simpson, R. T. The biochemical and phenotypic characterization of Hho1p, the putative linker histone H1 of *Saccharomyces cerevisiae*. *J Biol Chem* **273**, 7268–7276 (1998).
109. Andrews, A. J. & Luger, K. Nucleosome structure(s) and stability: variations on a theme. *Annu Rev Biophys* **40**, 99–117 (2011).
110. Smerdon, M. J. DNA repair and the role of chromatin structure. *Curr Opin Cell Biol* **3**, 422–428 (1991).
111. Soria, G., Polo, S. E. & Almouzni, G. Prime, Repair, Restore: The Active Role of

REFERENCES

- Chromatin in the DNA Damage Response. *Molecular Cell* **46**, 722–734 (2012).
112. Peterson, C. L. & Almouzni, G. Nucleosome dynamics as modular systems that integrate DNA damage and repair. *Cold Spring Harb Perspect Biol* **5**, a012658–a012658 (2013).
113. Maze, I., Noh, K.-M., Soshnev, A. A. & Allis, C. D. Every amino acid matters: essential contributions of histone variants to mammalian development and disease. *Nat Rev Genet* **15**, 259–271 (2014).
114. Talbert, P. B. & Henikoff, S. Histone variants--ancient wrap artists of the epigenome. *Nat Rev Mol Cell Biol* **11**, 264–275 (2010).
115. Malik, H. S. & Henikoff, S. Phylogenomics of the nucleosome. *Nat. Struct. Biol.* **10**, 882–891 (2003).
116. Faast, R. *et al.* Histone variant H2A.Z is required for early mammalian development. *Curr Biol* **11**, 1183–1187 (2001).
117. Mizuguchi, G. *et al.* ATP-driven exchange of histone H2AZ variant catalyzed by SWR1 chromatin remodeling complex. *Science* **303**, 343–348 (2004).
118. Billon, P. & Côté, J. Precise deposition of histone H2A.Z in chromatin for genome expression and maintenance. *Biochim Biophys Acta* **1819**, 290–302 (2013).
119. Wu, W.-H. *et al.* Swc2 is a widely conserved H2AZ-binding module essential for ATP-dependent histone exchange. *Nat Struct Mol Biol* **12**, 1064–1071 (2005).
120. Fan, J. Y., Rangasamy, D., Luger, K. & Tremethick, D. J. H2A.Z alters the nucleosome surface to promote HP1 α -mediated chromatin fiber folding. *Molecular Cell* **16**, 655–661 (2004).
121. Jiang, Y. *et al.* Local generation of fumarate promotes DNA repair through inhibition of histone H3 demethylation. *Nature Cell Biology* **17**, 1158–1168 (2015).
122. Suto, R. K., Clarkson, M. J., Tremethick, D. J. & Luger, K. Crystal structure of a nucleosome core particle containing the variant histone H2A.Z. *Nat. Struct. Biol.* **7**, 1121–1124 (2000).
123. Redon, C. *et al.* Histone H2A variants H2AX and H2AZ. *Curr. Opin. Genet. Dev.* **12**, 162–169 (2002).
124. Xu, Y. *et al.* Histone H2A.Z controls a critical chromatin remodeling step required for DNA double-strand break repair. *Mol Cell* **48**, 723–733 (2012).
125. Kalocsay, M., Hiller, N. J. & Jentsch, S. Chromosome-wide Rad51 spreading and SUMO-H2A.Z-dependent chromosome fixation in response to a persistent DNA double-strand break. *Mol Cell* **33**, 335–343 (2009).
126. Papamichos-Chronakis, M., Krebs, J. E. & Peterson, C. L. Interplay between Ino80 and Swr1 chromatin remodeling enzymes regulates cell cycle checkpoint adaptation in response to DNA damage. *Genes & Development* **20**, 2437–2449 (2006).
127. van Attikum, H., Fritsch, O. & Gasser, S. M. Distinct roles for SWR1 and INO80 chromatin remodeling complexes at chromosomal double-strand breaks. *EMBO J* **26**, 4113–4125 (2007).
128. Adkins, N. L., Niu, H., Sung, P. & Peterson, C. L. Nucleosome dynamics regulates DNA processing. *Nat Struct Mol Biol* **20**, 836–842 (2013).
129. Nagai, S. *et al.* Functional targeting of DNA damage to a nuclear pore-associated SUMO-dependent ubiquitin ligase. *Science* **322**, 597–602 (2008).
130. Horigome, C. *et al.* SWR1 and INO80 chromatin remodelers contribute to DNA double-strand break perinuclear anchorage site choice. *Mol Cell* **55**, 626–639 (2014).
131. Sarma, K. & Reinberg, D. Histone variants meet their match. *Nat Rev Mol Cell Biol* **6**, 139–149 (2005).
132. Baldi, S. & Becker, P. B. The variant histone H2A.V of *Drosophila*--three roles, two guises. *Chromosoma* **122**, 245–258 (2013).
133. Falck, J., Coates, J. & Jackson, S. P. Conserved modes of recruitment of ATM,

REFERENCES

- ATR and DNA-PKcs to sites of DNA damage. *Nature* **434**, 605–611 (2005).
134. Altmeyer, M. *et al.* Liquid demixing of intrinsically disordered proteins is seeded by poly(ADP-ribose). *Nat Commun* **6**, 8088 (2015).
135. Iacovoni, J. S. *et al.* High-resolution profiling of gammaH2AX around DNA double strand breaks in the mammalian genome. *EMBO J* **29**, 1446–1457 (2010).
136. Renkawitz, J., Lademann, C. A. & Jentsch, S. γ H2AX spreading linked to homology search. *Cell Cycle* **12**, 2526–2527 (2013).
137. Stewart, G. S., Wang, B., Bignell, C. R., Taylor, A. M. R. & Elledge, S. J. MDC1 is a mediator of the mammalian DNA damage checkpoint. *Nature* **421**, 961–966 (2003).
138. Mailand, N. *et al.* RNF8 ubiquitylates histones at DNA double-strand breaks and promotes assembly of repair proteins. *Cell* **131**, 887–900 (2007).
139. Kinner, A., Wu, W., Staudt, C. & Iliakis, G. Gamma-H2AX in recognition and signaling of DNA double-strand breaks in the context of chromatin. *Nucleic Acids Res.* **36**, 5678–5694 (2008).
140. Downs, J. A., Lowndes, N. F. & Jackson, S. P. A role for *Saccharomyces cerevisiae* histone H2A in DNA repair. *Nature* **408**, 1001–1004 (2000).
141. Unal, E. *et al.* DNA damage response pathway uses histone modification to assemble a double-strand break-specific cohesin domain. *Mol Cell* **16**, 991–1002 (2004).
142. Strom, L., Lindroos, H. B., Shirahige, K. & Sjogren, C. Postreplicative recruitment of cohesin to double-strand breaks is required for DNA repair. *Mol Cell* **16**, 1003–1015 (2004).
143. Downs, J. A. *et al.* Binding of chromatin-modifying activities to phosphorylated histone H2A at DNA damage sites. *Mol Cell* **16**, 979–990 (2004).
144. Bennett, G., Papamichos-Chronakis, M. & Peterson, C. L. DNA repair choice defines a common pathway for recruitment of chromatin regulators. *Nat Commun* **4**, 2084 (2013).
145. Thorslund, T. *et al.* Histone H1 couples initiation and amplification of ubiquitin signalling after DNA damage. *Nature* **527**, 389–393 (2015).
146. Price, B. D. & D'Andrea, A. D. Chromatin Remodeling at DNA Double-Strand Breaks. *Cell* **152**, 1344–1354 (2013).
147. Kouzarides, T. Chromatin modifications and their function. *Cell* **128**, 693–705 (2007).
148. Murr, R. *et al.* Histone acetylation by Trrap-Tip60 modulates loading of repair proteins and repair of DNA double-strand breaks. *Nat Cell Biol* **8**, 91–99 (2006).
149. Clapier, C. R. & Cairns, B. R. The biology of chromatin remodeling complexes. *Annu. Rev. Biochem.* **78**, 273–304 (2009).
150. Flaus, A., Martin, D. M. A., Barton, G. J. & Owen-Hughes, T. Identification of multiple distinct Snf2 subfamilies with conserved structural motifs. *Nucleic Acids Res.* **34**, 2887–2905 (2006).
151. Eisen, J. A., Sweder, K. S., Hanawalt, P. C. Evolution of the SNF2 family of proteins: subfamilies with distinct sequences and functions. *Nucleic Acids Res.* **23**, 2715–2723 (1995).
152. Downs, J. A., Nussenzweig, M. C. & Nussenzweig, A. Chromatin dynamics and the preservation of genetic information. *Nature* **447**, 951–958 (2007).
153. Shim, E. Y. *et al.* RSC mobilizes nucleosomes to improve accessibility of repair machinery to the damaged chromatin. *Mol. Cell. Biol.* **27**, 1602–1613 (2007).
154. Chen, X. *et al.* The Fun30 nucleosome remodeler promotes resection of DNA double-strand break ends. *Nature* **489**, 576–580 (2012).
155. Eapen, V. V., Sugawara, N., Tsabar, M., Wu, W.-H. & Haber, J. E. The *Saccharomyces cerevisiae* Chromatin Remodeler Fun30 Regulates DNA End Resection and Checkpoint Deactivation. *Mol. Cell. Biol.* **32**, 4727–4740 (2012).

REFERENCES

156. Costelloe, T. *et al.* The yeast Fun30 and human SMARCAD1 chromatin remodellers promote DNA end resection. *Nature* **489**, 581–584 (2012).
157. Sinha, M. & Peterson, C. L. A Rad51 presynaptic filament is sufficient to capture nucleosomal homology during recombinational repair of a DNA double-strand break. *Mol Cell* **30**, 803–810 (2008).
158. Tsukuda, T. *et al.* INO80-dependent chromatin remodeling regulates early and late stages of mitotic homologous recombination. *DNA repair* **8**, 360–369 (2009).
159. Chai, B., Huang, J., Cairns, B. R. & Laurent, B. C. Distinct roles for the RSC and Swi/Snf ATP-dependent chromatin remodelers in DNA double-strand break repair. *Genes Dev* **19**, 1656–1661 (2005).
160. Hicks, W. M., Yamaguchi, M. & Haber, J. E. Real-time analysis of double-strand DNA break repair by homologous recombination. *Proc. Natl. Acad. Sci. U.S.A.* **108**, 3108–3115 (2011).
161. Sinha, M., Watanabe, S., Johnson, A., Moazed, D. & Peterson, C. L. Recombinational repair within heterochromatin requires ATP-dependent chromatin remodeling. *Cell* **138**, 1109–1121 (2009).
162. Gerhold, C. B. & Gasser, S. M. INO80 and SWR complexes: relating structure to function in chromatin remodeling. *Trends Cell Biol* **24**, 619–631 (2014).
163. Shen, X., Mizuguchi, G., Hamiche, A. & Wu, C. A chromatin remodelling complex involved in transcription and DNA processing. *Nature* **406**, 541–544 (2000).
164. Papamichos-Chronakis, M., Watanabe, S., Rando, O. J. & Peterson, C. L. Global regulation of H2A.Z localization by the INO80 chromatin-remodeling enzyme is essential for genome integrity. *Cell* **144**, 200–213 (2011).
165. Li, Q. *et al.* Acetylation of histone H3 lysine 56 regulates replication-coupled nucleosome assembly. *Cell* **134**, 244–255 (2008).
166. Chen, C.-C. *et al.* Acetylated lysine 56 on histone H3 drives chromatin assembly after repair and signals for the completion of repair. *Cell* **134**, 231–243 (2008).
167. Kim, J. A. & Haber, J. E. Chromatin assembly factors Asf1 and CAF-1 have overlapping roles in deactivating the DNA damage checkpoint when DNA repair is complete. *Proc. Natl. Acad. Sci. U.S.A.* **106**, 1151–1156 (2009).
168. Heo, K. *et al.* FACT-mediated exchange of histone variant H2AX regulated by phosphorylation of H2AX and ADP-ribosylation of Spt16. *Mol Cell* **30**, 86–97 (2008).
169. Luk, E. *et al.* Chz1, a nuclear chaperone for histone H2AZ. *Mol Cell* **25**, 357–368 (2007).
170. Obri, A. *et al.* ANP32E is a histone chaperone that removes H2A.Z from chromatin. *Nature* **505**, 648–653 (2014).
171. Gursoy-Yuzugullu, O., Ayrapetov, M. K. & Price, B. D. Histone chaperone Anp32e removes H2A.Z from DNA double-strand breaks and promotes nucleosome reorganization and DNA repair. *Proc. Natl. Acad. Sci. U.S.A.* **112**, 7507–7512 (2015).
172. Knop, M. *et al.* Epitope tagging of yeast genes using a PCR-based strategy: more tags and improved practical routines. *Yeast* **15**, 963–972 (1999).
173. Janke, C. *et al.* A versatile toolbox for PCR-based tagging of yeast genes: new fluorescent proteins, more markers and promoter substitution cassettes. *Yeast* **21**, 947–962 (2004).
174. Sugawara, N. & Haber, J. E. Monitoring DNA recombination initiated by HO endonuclease. *Methods Mol. Biol.* **920**, 349–370 (2012).
175. Nickoloff, J. A., Singer, J. D. & Heffron, F. In vivo analysis of the *Saccharomyces cerevisiae* HO nuclease recognition site by site-directed mutagenesis. *Mol. Cell. Biol.* **10**, 1174–1179 (1990).
176. Haber, J. E. Mating-type gene switching in *Saccharomyces cerevisiae*. *Annu. Rev. Genet.* **32**, 561–599 (1998).

REFERENCES

177. Lee, C.-S. *et al.* Chromosome position determines the success of double-strand break repair. *Proc. Natl. Acad. Sci. U.S.A.* **113**, E146–54 (2016).
178. Burgess, S. M. & Kleckner, N. Collisions between yeast chromosomal loci in vivo are governed by three layers of organization. *Genes & Development* **13**, 1871–1883 (1999).
179. Agmon, N., Pur, S., Liefshitz, B. & Kupiec, M. Analysis of repair mechanism choice during homologous recombination. *Nucleic Acids Res.* **37**, 5081–5092 (2009).
180. Jin, Q. W., Fuchs, J. & Loidl, J. Centromere clustering is a major determinant of yeast interphase nuclear organization. *J. Cell. Sci.* **113 (Pt 11)**, 1903–1912 (2000).
181. Duan, Z. *et al.* A three-dimensional model of the yeast genome. *Nature* **465**, 363–367 (2010).
182. Agmon, N., Liefshitz, B., Zimmer, C., Fabre, E. & Kupiec, M. Effect of nuclear architecture on the efficiency of double-strand break repair. *Nature Cell Biology* **15**, 694–699 (2013).
183. Heyer, W.-D., Li, X., Rolfmeier, M. & Zhang, X.-P. Rad54: the Swiss Army knife of homologous recombination? *Nucleic Acids Res.* **34**, 4115–4125 (2006).
184. Klein, H. L. RDH54, a RAD54 homologue in *Saccharomyces cerevisiae*, is required for mitotic diploid-specific recombination and repair and for meiosis. *Genetics* **147**, 1533–1543 (1997).
185. Busygina, V. *et al.* Hed1 regulates Rad51-mediated recombination via a novel mechanism. *Genes & Development* **22**, 786–795 (2008).
186. Brown, M. S. & Bishop, D. K. DNA strand exchange and RecA homologs in meiosis. *Cold Spring Harb Perspect Biol* **7**, a016659 (2015).
187. Busygina, V. *et al.* Novel attributes of Hed1 affect dynamics and activity of the Rad51 presynaptic filament during meiotic recombination. *Journal of Biological Chemistry* **287**, 1566–1575 (2012).
188. Alexeev, A., Mazin, A. & Kowalczykowski, S. C. Rad54 protein possesses chromatin-remodeling activity stimulated by the Rad51-ssDNA nucleoprotein filament. *Nat. Struct. Biol.* **10**, 182–186 (2003).
189. Jaskelioff, M., van Komen, S., Krebs, J. E., Sung, P. & Peterson, C. L. Rad54p is a chromatin remodeling enzyme required for heteroduplex DNA joint formation with chromatin. *J Biol Chem* **278**, 9212–9218 (2003).
190. Simon, J. M., Giresi, P. G., Davis, I. J. & Lieb, J. D. Using formaldehyde-assisted isolation of regulatory elements (FAIRE) to isolate active regulatory DNA. *Nat Protoc* **7**, 256–267 (2012).
191. Belton, J.-M. *et al.* The Conformation of Yeast Chromosome III Is Mating Type Dependent and Controlled by the Recombination Enhancer. *Cell Reports* **13**, 1855–1867 (2015).
192. Lee, C.-S., Lee, K., Legube, G. & Haber, J. E. Dynamics of yeast histone H2A and H2B phosphorylation in response to a double-strand break. *Nat Struct Mol Biol* **21**, 103–109 (2014).
193. Shen, X., Ranallo, R., Choi, E. & Wu, C. Involvement of actin-related proteins in ATP-dependent chromatin remodeling. *Mol Cell* **12**, 147–155 (2003).
194. van Attikum, H., Fritsch, O., Hohn, B. & Gasser, S. M. Recruitment of the INO80 complex by H2A phosphorylation links ATP-dependent chromatin remodeling with DNA double-strand break repair. *Cell* **119**, 777–788 (2004).
195. Klopff, E. *et al.* Cooperation between the INO80 complex and histone chaperones determines adaptation of stress gene transcription in the yeast *Saccharomyces cerevisiae*. *Mol. Cell. Biol.* **29**, 4994–5007 (2009).
196. Tsukuda, T., Fleming, A. B., Nickoloff, J. A. & Osley, M. A. Chromatin remodelling at a DNA double-strand break site in *Saccharomyces cerevisiae*. *Nature* **438**,

REFERENCES

- 379–383 (2005).
197. Szostak, J. W., Orr-Weaver, T. L., Rothstein, R. J. & Stahl, F. W. The double-strand-break repair model for recombination. *Cell* **33**, 25–35 (1983).
 198. Symington, L. S. End resection at double-strand breaks: mechanism and regulation. *Cold Spring Harb Perspect Biol* **6**, a016436–a016436 (2014).
 199. Chaumeil, J. *et al.* The RAG2 C-terminus and ATM protect genome integrity by controlling antigen receptor gene cleavage. *Nat Commun* **4**, 2231 (2013).
 200. Rocha, P. P., Chaumeil, J. & Skok, J. A. Molecular biology. Finding the right partner in a 3D genome. *Science* **342**, 1333–1334 (2013).
 201. Roukos, V. *et al.* Spatial dynamics of chromosome translocations in living cells. *Science* **341**, 660–664 (2013).
 202. Smeenk, G. & van Attikum, H. The chromatin response to DNA breaks: leaving a mark on genome integrity. *Annu. Rev. Biochem.* **82**, 55–80 (2013).
 203. Papamichos-Chronakis, M. & Peterson, C. L. Chromatin and the genome integrity network. *Nat Rev Genet* **14**, 62–75 (2013).
 204. Aymard, F. *et al.* Transcriptionally active chromatin recruits homologous recombination at DNA double-strand breaks. *Nat Struct Mol Biol* **21**, 366–374 (2014).
 205. Danilowicz, C. *et al.* The differential extension in dsDNA bound to Rad51 filaments may play important roles in homology recognition and strand exchange. *Nucleic Acids Res.* **42**, 526–533 (2014).
 206. Zhang, Z., Fan, H. Y., Goldman, J. A. & Kingston, R. E. Homology-driven chromatin remodeling by human RAD54. *Nat Struct Mol Biol* **14**, 397–405 (2007).
 207. Kwon, Y. *et al.* ATP-dependent chromatin remodeling by the *Saccharomyces cerevisiae* homologous recombination factor Rdh54. *J Biol Chem* **283**, 10445–10452 (2008).
 208. Prasad, T. K. *et al.* A DNA-translocating Snf2 molecular motor: *Saccharomyces cerevisiae* Rdh54 displays processive translocation and extrudes DNA loops. *J. Mol. Biol.* **369**, 940–953 (2007).
 209. Amitani, I., Baskin, R. J. & Kowalczykowski, S. C. Visualization of Rad54, a chromatin remodeling protein, translocating on single DNA molecules. *Mol Cell* **23**, 143–148 (2006).
 210. Cozzarelli, N. R., Cost, G. J., Nöllmann, M., Viard, T. & Stray, J. E. Giant proteins that move DNA: bullies of the genomic playground. *Nat Rev Mol Cell Biol* **7**, 580–588 (2006).
 211. Fulconis, R., Mine, J., Bancaud, A., Dutreix, M. & Viovy, J.-L. Mechanism of RecA-mediated homologous recombination revisited by single molecule nanomanipulation. *EMBO J* **25**, 4293–4304 (2006).
 212. van der Heijden, T. *et al.* Homologous recombination in real time: DNA strand exchange by RecA. *Mol Cell* **30**, 530–538 (2008).
 213. Petukhova, G., Stratton, S. & Sung, P. Catalysis of homologous DNA pairing by yeast Rad51 and Rad54 proteins. *Nature* **393**, 91–94 (1998).
 214. Petukhova, G., Sung, P. & Klein, H. Promotion of Rad51-dependent D-loop formation by yeast recombination factor Rdh54/Tid1. *Genes Dev* **14**, 2206–2215 (2000).
 215. Nimonkar, A. V., Amitani, I., Baskin, R. J. & Kowalczykowski, S. C. Single molecule imaging of Tid1/Rdh54, a Rad54 homolog that translocates on duplex DNA and can disrupt joint molecules. *J Biol Chem* **282**, 30776–30784 (2007).
 216. Clever, B., Schmuckli-Maurer, J., Sigrist, M., Glassner, B. J. & Heyer, W. D. Specific negative effects resulting from elevated levels of the recombinational repair protein Rad54p in *Saccharomyces cerevisiae*. *Yeast* **15**, 721–740 (1999).
 217. Aymard, F. & Legube, G. A TAD closer to ATM. *Mol Cell Oncol* **3**, e1134411 (2016).

REFERENCES

218. Savic, V. Do chromatin changes around a nascent double strand DNA break spread spherically into linearly non-adjacent chromatin? *Front Genet* **4**, 139 (2013).
219. Thiriet, C. & Hayes, J. J. Replication-independent core histone dynamics at transcriptionally active loci in vivo. *Genes & Development* **19**, 677–682 (2005).
220. Kimura, H. & Cook, P. R. Kinetics of core histones in living human cells: little exchange of H3 and H4 and some rapid exchange of H2B. *J. Cell Biol.* **153**, 1341–1353 (2001).
221. Louters, L. & Chalkley, R. Exchange of histones H1, H2A, and H2B in vivo. *Biochemistry* **24**, 3080–3085 (1985).
222. Xu, M. *et al.* Partitioning of histone H3-H4 tetramers during DNA replication-dependent chromatin assembly. *Science* **328**, 94–98 (2010).
223. Burgess, R. J. & Zhang, Z. Histone chaperones in nucleosome assembly and human disease. *Nat Struct Mol Biol* **20**, 14–22 (2013).
224. Li, A. *et al.* Phosphorylation of histone H2A.X by DNA-dependent protein kinase is not affected by core histone acetylation, but it alters nucleosome stability and histone H1 binding. *Journal of Biological Chemistry* **285**, 17778–17788 (2010).
225. Bauerschmidt, C. *et al.* Cohesin phosphorylation and mobility of SMC1 at ionizing radiation-induced DNA double-strand breaks in human cells. *Exp Cell Res* **317**, 330–337 (2011).
226. Scully, R. & Xie, A. Double strand break repair functions of histone H2AX. *Mutat. Res.* **750**, 5–14 (2013).
227. Alatwi, H. E. & Downs, J. A. Removal of H2A.Z by INO80 promotes homologous recombination. *EMBO Rep* **16**, 986–994 (2015).
228. Wu, L. & Hickson, I. D. DNA helicases required for homologous recombination and repair of damaged replication forks. *Annu. Rev. Genet.* **40**, 279–306 (2006).
229. Ira, G., Malkova, A., Liberi, G., Foiani, M. & Haber, J. E. Srs2 and Sgs1-Top3 suppress crossovers during double-strand break repair in yeast. *Cell* **115**, 401–411 (2003).
230. Horigome, C. *et al.* PolySUMOylation by Siz2 and Mms21 triggers relocation of DNA breaks to nuclear pores through the Slx5/Slx8 STUbL. *Genes Dev* **30**, 931–945 (2016).
231. Clarkson, M. J., Wells, J. R., Gibson, F., Saint, R. & Tremethick, D. J. Regions of variant histone His2AvD required for *Drosophila* development. *Nature* **399**, 694–697 (1999).
232. Li, W., Nagaraja, S., Delcuve, G. P., Hendzel, M. J. & Davie, J. R. Effects of histone acetylation, ubiquitination and variants on nucleosome stability. *Biochemical Journal* **296 (Pt 3)**, 737–744 (1993).
233. Abbott, D. W., Ivanova, V. S., Wang, X., Bonner, W. M. & Ausió, J. Characterization of the stability and folding of H2A.Z chromatin particles: implications for transcriptional activation. *J Biol Chem* **276**, 41945–41949 (2001).
234. Park, Y.-J., Dyer, P. N., Tremethick, D. J. & Luger, K. A new fluorescence resonance energy transfer approach demonstrates that the histone variant H2AZ stabilizes the histone octamer within the nucleosome. *J Biol Chem* **279**, 24274–24282 (2004).
235. Zhang, H., Roberts, D. N. & Cairns, B. R. Genome-wide dynamics of Htz1, a histone H2A variant that poises repressed/basal promoters for activation through histone loss. *Cell* **123**, 219–231 (2005).
236. Zlatanova, J. & Thakar, A. H2A.Z: view from the top. *Structure* **16**, 166–179 (2008).
237. Kawashima, S. *et al.* The INO80 complex is required for damage-induced recombination. *Biochem. Biophys. Res. Commun.* **355**, 835–841 (2007).
238. Zeman, M. K. & Cimprich, K. A. Causes and consequences of replication stress.

REFERENCES

- Nature Cell Biology* **16**, 2–9 (2014).
239. Symington, L. S. & Gautier, J. Double-strand break end resection and repair pathway choice. *Annu. Rev. Genet.* **45**, 247–271 (2011).
240. Ausubel, F. M. *Current Protocols in Molecular Biology*. (John Wiley & Sons, 2010).
241. Sambrook, J., Fritsch, E. F. & Maniatis, T. *Molecular Cloning: A Laboratory Manual*. (Cold Spring Harbor Laboratory Press, 1989).
242. Rudin, N. & Haber, J. E. Efficient repair of HO-induced chromosomal breaks in *Saccharomyces cerevisiae* by recombination between flanking homologous sequences. *Mol. Cell. Biol.* **8**, 3918–3928 (1988).
243. Thomas, B. J. & Rothstein, R. Elevated recombination rates in transcriptionally active DNA. *Cell* **56**, 619–630 (1989).
244. Zierhut, C. & Diffley, J. F. X. Break dosage, cell cycle stage and DNA replication influence DNA double strand break response. *EMBO J* **27**, 1875–1885 (2008).
245. Lee, S. E. *et al.* *Saccharomyces* Ku70, mre11/rad50 and RPA proteins regulate adaptation to G2/M arrest after DNA damage. *Cell* **94**, 399–409 (1998).
246. Gietz, R. D. & Sugino, A. New yeast-*Escherichia coli* shuttle vectors constructed with in vitro mutagenized yeast genes lacking six-base pair restriction sites. *Gene* **74**, 527–534 (1988).
247. Goldstein, A. L., Pan, X. & McCusker, J. H. Heterologous URA3MX cassettes for gene replacement in *Saccharomyces cerevisiae*. *Yeast* **15**, 507–511 (1999).
248. Longtine, M. S. *et al.* Additional modules for versatile and economical PCR-based gene deletion and modification in *Saccharomyces cerevisiae*. *Yeast* **14**, 953–961 (1998).
249. Akada, R. *et al.* PCR-mediated seamless gene deletion and marker recycling in *Saccharomyces cerevisiae*. *Yeast* **23**, 399–405 (2006).
250. Paques, F. & Haber, J. E. Two pathways for removal of nonhomologous DNA ends during double-strand break repair in *Saccharomyces cerevisiae*. *Mol. Cell. Biol.* **17**, 6765–6771 (1997).
251. Sacher, M., Pfander, B., Hoegge, C. & Jentsch, S. Control of Rad52 recombination activity by double-strand break-induced SUMO modification. *Nat Cell Biol* **8**, 1284–1290 (2006).
252. Aparicio, O. *et al.* Chromatin immunoprecipitation for determining the association of proteins with specific genomic sequences in vivo. *Curr Protoc Mol Biol* **Chapter 21**, Unit 21.3 (2005).
253. O'Geen, H., Nicolet, C. M., Blahnik, K., Green, R. & Farnham, P. J. Comparison of sample preparation methods for ChIP-chip assays. *BioTechniques* **41**, 577–580 (2006).
254. R Core Team. *R: A language and environment for statistical computing*. *R Foundation for Statistical Computing, Vienna, Austria*. 2013. (2014).
255. Prestel, M., Feller, C., Straub, T., Mitlöhner, H. & Becker, P. B. The activation potential of MOF is constrained for dosage compensation. *Mol Cell* **38**, 815–826 (2010).
256. R Core Team. *R: A language and environment for statistical computing*. *R Foundation for Statistical Computing, Vienna, Austria*. 2015. (2015).
257. Langmead, B., Trapnell, C., Pop, M. & Salzberg, S. L. Ultrafast and memory-efficient alignment of short DNA sequences to the human genome. *Genome Biol.* **10**, R25 (2009).
258. Lawrence, M. *et al.* Software for computing and annotating genomic ranges. *PLoS Comput. Biol.* **9**, e1003118 (2013).
259. Robinson, M. D. & Oshlack, A. A scaling normalization method for differential expression analysis of RNA-seq data. *Genome Biol.* **11**, R25 (2010).
260. Chen, Y., Lun, A. & Smyth, G. K. Differential expression analysis of complex

REFERENCES

- RNA-seq experiments using edgeR. ... *analysis of next generation sequencing data* (2014). doi:10.1007/978-3-319-07212-8_3
261. McCarthy, D. J., Chen, Y. & Smyth, G. K. Differential expression analysis of multifactor RNA-Seq experiments with respect to biological variation. *Nucleic Acids Res.* **40**, 4288–4297 (2012).
262. Robinson, M. D., McCarthy, D. J. & Smyth, G. K. edgeR: a Bioconductor package for differential expression analysis of digital gene expression data. *Bioinformatics* **26**, 139–140 (2010).
263. Robinson, J. T. *et al.* Integrative genomics viewer. *Nat Biotechnol* **29**, 24–26 (2011).
264. Nicol, J. W., Helt, G. A., Blanchard, S. G., Raja, A. & Loraine, A. E. The Integrated Genome Browser: free software for distribution and exploration of genome-scale datasets. *Bioinformatics* **25**, 2730–2731 (2009).
265. Quinlan, A. R. & Hall, I. M. BEDTools: a flexible suite of utilities for comparing genomic features. *Bioinformatics* **26**, 841–842 (2010).
266. Liao, Y., Smyth, G. K. & Shi, W. featureCounts: an efficient general purpose program for assigning sequence reads to genomic features. *Bioinformatics* **30**, 923–930 (2014).
267. Wickham, H. *ggplot2: elegant graphics for data analysis.* (2009).

7 ABBREVIATIONS

3D	Three-dimensional
BIR	Break-induced replication
bp	Base-pairs
BRCA2	Breast cancer type 2 susceptibility protein
CDK	Cyclin-dependent kinase
Cen	Centromere
ChIP	Chromatin immunoprecipitation
Chr	Chromosome
D-loop	Displacement loop
DDR	DNA damage response
dHJ	Double-Holliday junction
DNA	Desoxyribonucleic acid
dNTP	Desoxynucleoside triphosphate
DSB	DNA double-strand break
dsDNA	Double-stranded DNA
DTT	Dithiothreitol
e.g.	Exempli gratia, for example
EDTA	Ethylenediaminetetraacidic acid
FACT	Facilitates chromatin transcription
<i>g</i>	Centrifugational G-force
Gal	Galactose
h	Hour(s)
H1	Histone H1
H2A	Histone H2A
H2A.Z	Histone H2A variant Z
H2AX	Histone H2A variant X
H2B	Histone H2B
H3	Histone H3
H4	Histone H4
HA	Hemagglutinin epitope
HML	Hidden MAT left, silent mating-type locus
HMR	Hidden MAT right, silent mating-type locus
HO	Homothallic switching endonuclease
HOcs	HO recognition site
HOinc	Mutated (incleavable) HO recognition site
HR	Homologous recombination
i.e.	Id est, that is/that means
INO80	Inositol requiring 80
kb	Kilobase pairs
Log	Logarithmic
MAT	Mating-type locus
MATa	MAT locus containing a information
MAT α	MAT locus containing α information
min	Minute

ABBREVIATIONS

MMC	Mitomycin C
MMEJ	Microhomology-mediated end joining
MMS	Methyl methanesulfonate
Myc	Epitope derived from c-myc
NHEJ	Non-homologous end joining
NP-40	Nonidet p-40
nt	Nucleotide(s)
ODx	Optical density at x nm
ORF	Open reading frame
p-value	Probability value
PAGE	Polyacrylamide gel electrophoresis
PBS	Phosphate buffered saline
PCR	Polymerase chain reaction
PEG	Polyethylene glycol
Pgk1	Phospho-glycerate kinase 1
PVDF	Polyvinylidene fluoride
qPCR	Quantitative real-time PCR
Raf	Raffinose
RE	Recombination enhancer element
RNA	Ribonucleic acid
RNAPII	RNA polymerase II
RPA	Replication protein A
rpm	Revolutions per minute
RSC	Chromatin structure remodeling
RT	Room temperature
s	Second(s)
SD	Standard deviation
SDS	Sodium dodecylsulfate
SDSA	Synthesis-dependent strand annealing
SEM	Standard error of the mean
SSA	Single-strand annealing
SSB	Single-strand break
ssDNA	Single-stranded DNA
SUMO	Small ubiquitin-like modifier
SWI/SNF	Switching defective/sucrose non-fermentable
TBE	Tris, boric acid, EDTA
TBS-T	Tris-buffered saline with Tween-20
TCA	Trichloro acetic acid
Tel	Telomere
VDJ	Variable, diversity and joining genes
WT	Wild type
YPD	Yeast bactopectone dextrose
β-ME	β-mercaptoethanol

8 ACKNOWLEDGEMENT

Without the support of many people, this thesis would not have been possible.

First of all, I would like to express my sincere gratitude to my supervisor, Stefan Jentsch. Thank you Stefan for the conceptual biological thinking that you taught, the outstanding scientific freedom that I experienced in your lab, and the great personal support that you continuously provide. It was such a great time that I had in your lab and I owe a lot of this valuable experience to you.

Many thanks go to Peter Becker, for agreeing to act as a co-referee for this thesis and even more for his support and scientific input as part of my thesis advisory committee. Similar thanks also go to my second TAC member, Christian Biertümpfel.

I am very grateful to the sequencing core facility of the LMU Munich (LAFUGA) and especially to Stefan Krebs for sequencing my various ChIP libraries. The same holds true for Tobias Straub and Assa Yeroslaviz, who both analyzed numerous ChIP-seq experiments and were patient enough to explain all the bioinformatic details to me.

Many thanks go to the staff of the MCB department who allowed me to focus so well on the science, because of their hard work “behind the scenes”. I would like to especially thank Massimo for providing endless support of YP-lactate, always on time!

Thanks to the people who acted as guinea pigs with regards to my own supervision talents: Sven, for your precise technical assistance, Christoph and Gregor, for being brave enough to work on somewhat risky side projects. It was a great experience with all of you.

One person largely shaped my scientific development and thinking during the first half of this thesis and I still benefit a lot from this time today. Thank you, Jörg, for providing tremendous help, for fantastic scientific discussions, for successfully shared work and for overall becoming a good friend.

If there is one thing in the department that might even be a bit better than the science, it is the people! All of you here generate such a fantastic working atmosphere, are open-minded for discussions on science and non-science related subjects and make things just so much easier especially during the hard times. In particular, this holds true for my former and current (extended) lab members Alex, André, Ben, Irina, Jörg, Markus, Matias, Max, Sean and Sven, but also the “outsiders” Julian, FloP and FloW. In times of shrinking DNA repair expertise in our own group, I am also very grateful for the support from the second floor, especially mentioning Boris and Susi here. Special thanks also to my sports buddies: Alex for good running sessions, FloP for great battles on the tennis courts, and Neysan for bringing me back to a nice football pitch. All much appreciated! Particular thanks also to André, Ben, FloW, Markus and Matias for critical reading of this thesis.

Zum Schluss möchte ich noch einigen Menschen danken, die zwar nicht immer verstehen was ich genau mache (☺), ohne die ich aber niemals so weit gekommen wäre. Danke Papa und Karlin, dafür, dass ich immer auf euch zurückkommen kann und dafür, dass ihr mich immer unterstützt. Mama, ich weiß du wärst stolz auf mich!

Mein größter Dank gilt Katharina. Dafür, dass du Teil meines Lebens bist und dafür, dass du es soviel besser machst.

9 CURRICULUM VITAE

Claudio Lademann

Education

- Since 08/2011 **PhD studies** at the Max Planck Institute of Biochemistry, Department of Molecular Cell Biology, Martinsried, Germany
PhD Thesis: “*Homologous recombination within a chromatin environment*”
- 09/2009 – 07/2011 **Master’s degree (M. Sc. ETH)** in Biology with a Major in Cell Biology at the ETH Zurich, Switzerland
Master Thesis: “*Insights into macromolecular organization and post-translational modification of the FANCD2/FANCI-associated nuclease 1*”
- 10/2006 – 06/2009 **Bachelor’s degree (B. Sc.)** in Molecular Cell Biology at the Heidelberg University, Germany
Bachelor Thesis: “*Characterization of the glycosylation machinery in the endoplasmic reticulum*”
- 03/2006 **Abitur** (Secondary School Leaving Examination) at the Hohenstaufen Gymnasium Kaiserslautern, Germany

Publications

- Renkawitz J*, **Lademann CA***, Jentsch S. 2014. *Mechanisms and principles of homology search during recombination*. Nat Rev Mol Cell Biol. Jun;15(6):369-83. *: equal contribution
- Renkawitz J, **Lademann CA**, Jentsch S. 2013. *γH2AX spreading linked to homology search*. Cell Cycle. Aug 15;12(16):2526-7.
- Renkawitz J, **Lademann CA**, Kalocsay M, Jentsch S. 2013. *Monitoring homology search during DNA double-strand break repair in vivo*. Mol Cell. Apr 25;50(2):261-72.
- Kratz K, Schöpf B, Kaden S, Sendoel A, Eberhard R, **Lademann C**, Cannavó E, Sartori AA, Hengartner MO, Jiricny J. 2010. *Deficiency of FANCD2-Associated Nuclease KIAA1018/FAN1 Sensitizes Cells to Interstrand Crosslinking Agents*. Cell. June 9;142(1):77-88.

Awards and Honors

- Fellowship of the International Max Planck Research School for Molecular and Cellular Life Sciences
- Merck Innovation Cup 2016: Runner-Up with the Team Oncology